

2011

Oxygen Diffusion Characterization of FRP Composites Used in Concrete Repair and Rehabilitation

Chandra K. Khoe

University of South Florida, chandrakhoe@verizon.net

Follow this and additional works at: <http://scholarcommons.usf.edu/etd>

 Part of the [American Studies Commons](#), [Chemical Engineering Commons](#), [Civil Engineering Commons](#), and the [Materials Science and Engineering Commons](#)

Scholar Commons Citation

Khoe, Chandra K., "Oxygen Diffusion Characterization of FRP Composites Used in Concrete Repair and Rehabilitation" (2011). *Graduate Theses and Dissertations*.
<http://scholarcommons.usf.edu/etd/3181>

This Dissertation is brought to you for free and open access by the Graduate School at Scholar Commons. It has been accepted for inclusion in Graduate Theses and Dissertations by an authorized administrator of Scholar Commons. For more information, please contact scholarcommons@usf.edu.

Oxygen Diffusion Characterization of FRP Composites Used in Concrete
Repair and Rehabilitation

by

Chandra K. Khoe

A dissertation submitted in partial fulfillment
of the requirements for the degree of
Doctor of Philosophy
Department of Civil and Environmental Engineering
College of Engineering
University of South Florida

Co-Major Professor: Rajan Sen, Ph.D.
Co-Major Professor: Venkat Bhethanabotla, Ph.D.
Autar Kaw, Ph.D.
Gray Mullins, Ph.D.
Kandethody M. Ramachandran, Ph.D.

Date of Approval:
March 22, 2011

Keywords: Corrosion, Permeability, Epoxy, Carbon, Glass, Diffusion Cell

Copyright © 2011, Chandra K. Khoe

Dedication

Dedicated to my father, Hendra K. Khoe.

Acknowledgements

My deepest gratitude to my advisors, Dr. Rajan Sen, and Dr. Venkat Bhethanabotla for their excellent support, patience, and guidance for the most academic challenges that I ever had. Their integrity, wisdom, knowledge and commitment to the highest standards inspired and motivated me for my future career. It would have been next to impossible to write this Dissertation without their help and motivation. I would like to thank my defense committee: Dr. Autar Kaw, Dr. Gray Mullins, and Dr. Kandethody M. Ramachandran for their time, efforts and valuable suggestions in my proposal defense. I also want to thank Dr. Jose Porteiro as my Committee Chair.

It is a pleasure to thank those who made this Dissertation possible, such as my friends and colleagues, Dr. Stefan Cular, Dr. Sanchari Chowdhury, Dr. Kingsley Lau, Dr. Mouchir Chenouda for their great help, advice, and support. I also would like to thank the engineering shops (Robert Smith and Tom Gage), Justin Dodson, Mathew Farrell, Steve Tozier, Matthew Durshimer, Purvik Patel, Madelyn Rubin, Wayne Wilson, Ranzo Taylor, Walter F. Hunziker, Jorge Rivas, Oscar Gomez, Himat Solanki, and Roy Wilber for their helped with experimental works, and friendships. My special thanks to my former supervisor, William

Geers, P.E., whose encouragement, supervision, and support from the beginning have enabled me to take a first step enrollment in graduate degree program.

My thanks and appreciation to the National Science Foundation (NSF) for providing a necessary financial support under Grant No. CMS-0409401. I acknowledge that the experimental works would not be completed without help from Nanomaterial and Nanomanufacturing Research Center (NNRC), Sensors Research Laboratory, and Structural Research Laboratory.

Last, I want to thank my wife (Natalia Sugiharto) and my kids (Sasha and Shannon Sugiharto) for their support, patience, and love.

Table of Contents

List of Tables	iv
List of Figures	vi
Abstract	x
Chapter 1 Introduction	1
1.1 Background	1
1.2 Aim and Motivation	2
1.3 Organization	4
Chapter 2 Development of Diffusion Cell	7
2.1 Introduction	7
2.2 Background	7
2.3 Existing Test Methods	8
2.3.1 ASTM F1307	9
2.3.2 ASTM D3985	10
2.3.3 Gas Chromatography	12
2.3.4 CSIRO	13
2.4 Development of New Diffusion Cell	15
2.5 Concentration Gradient	17
2.6 Leak Proofing	17
2.7 Data Collection	18
2.8 Testing Procedure	19
2.9 Time for Test	20
2.10 Summary and Conclusions	20
Chapter 3 Measurement of Oxygen Permeability of Epoxy Polymers	22
3.1 Introduction	22
3.2 Research Significance	23
3.3 Definitions	24
3.4 Existing Methods	24
3.5 Objectives	26
3.6 Experimental Program	26

3.7	Diffusion Cell	27
3.8	Oxygen Sensor	29
3.9	Sensor Oxygen Consumption	31
3.10	Sample Preparation	34
3.11	Calibration Specimens	34
3.12	Epoxy Specimens	35
3.13	Test Details	37
3.14	Corrected Data	37
3.15	Extraction of Permeation Constants	37
3.16	Results	40
	3.16.1 Epoxy Results	41
3.17	Discussion	47
3.18	Application to Concrete	48
3.19	Simplified Analysis	48
3.20	Numerical Example	50
3.21	Solution	50
3.22	Calculation of Corrosion Rate	51
3.23	Summary and Conclusions	52
Chapter 4	Oxygen Permeability of Fiber Reinforced Laminates	53
4.1	Introduction	53
4.2	Objectives	55
4.3	Diffusion Basics	56
4.4	Measuring Permeability Constants	57
4.5	Diffusion Cell	58
4.6	Oxygen Sensor.....	59
4.7	Sensor Oxygen Consumption	59
4.8	Experimental Program	60
4.9	Sample Preparation	64
4.10	Test Details	65
4.11	Corrected Data	67
4.12	Results	68
4.13	Discussion	72
4.14	Summary and Conclusions	78
Chapter 5	Oxygen Permeability of FRP-Concrete Repair Systems	80
5.1	Introduction	80
5.2	Scope	81
5.3	Background	81
5.4	Measuring Permeability	83
5.5	Diffusion Cell	83
5.6	Experimental Program	86
	5.6.1 Concrete Specimen – Type 1	89
	5.6.2 Epoxy-Concrete – Type 2	90

5.6.3	FRP-Concrete – Types 3-4	90
5.7	Test Details	92
5.8	Corrected Data	94
5.9	Results	95
5.9.1	Concrete	98
5.9.2	Comparison with Published Values	98
5.9.3	Epoxy-Concrete	101
5.9.4	FRP-Concrete	101
5.10	Discussion	102
5.10.1	Equivalent Thickness for FRP-Concrete Systems	102
5.11	Summary and Conclusions	105
Chapter 6	Design of Optimal FRP Corrosion Repair	107
6.1	Introduction	107
6.2	Results	107
6.2.1	Comments on Results	109
6.3	Discussion	109
6.3.1	Equivalent FRP Thickness	110
6.3.2	Numerical Example	110
6.4	Parametric Study	111
Chapter 7	Contributions and Recommendations	114
7.1	Introduction	114
7.2	Contributions	114
7.3	Recommendations for Future Work	115
References	118
Appendices	124
Appendix I	Computer Software MATLAB Program	125
Appendix II	Volume Fiber Fraction Calculation	129
Appendix III	Scanning Electron Micrograph (SEM) for CFRP Specimens	132
Appendix IV	Scanning Electron Micrograph (SEM) for GFRP Specimens	134
Appendix V	Scanning Electron Micrograph (SEM) for Concrete Specimens	136
Appendix VI	Sample Calculation	138
Appendix VII	Dry vs. Wet Concrete.....	141
About the Author	End Page

List of Tables

Table 3-1	Epoxy Specimens Properties (Fyfe Co 2003, Sika 2003, Air Products 2008, West System 2008)	35
Table 3-2	Teflon and PET Mylar Results	40
Table 3-3	Permeation Results for Epoxy Polymers Tested	42
Table 4-1	Epoxy Materials Property	60
Table 4-2	FRP Fabric Material Property	62
Table 4-3	Oxygen Permeation Constant Values for Epoxy and FRP Laminates	67
Table 4-4	Oxygen Permeation Constant Values for Randomly Oriented FRP Laminates	68
Table 4-5	Void Ratios in CFRP Laminates	73
Table 5-1	Concrete Mix Design (FDOT 2010)	86
Table 5-2	Epoxy Details (Fyfe Co 2003, BASF 2007)	88
Table 5-3	FRP Fabric Properties (Fyfe Co 2003, BASF 2007)	88
Table 5-4	Oxygen Permeation Constant for Concrete with Different w/c Ratios	98
Table 5-5	Oxygen Permeation Constant for Epoxy-Concrete Systems A & B in mol.m ² /m ³ .atm.sec.	99
Table 5-6	Oxygen Permeation Constant for FRP-Concrete Systems A & B in mol.m ² /m ³ .atm.sec.	100

Table 6-1	Equivalent FRP Thickness	111
Table 6-2	Variation in Corrosion Depth in Steel Reinforcement in Concrete Slab	112
Table 6-3	Comparative Effect of Corrosion Repair	112
Table II-1	Volume Fiber Fraction Average for System A to D.....	131
Table VII-1	Properties of Concrete	141
Table VII-2	Concrete Data Measurement	142
Table VII-3	Oxygen Permeation Constant for Dry and Wet Concrete (units in mol.m ² /m ³ .atm.sec)	143

List of Figures

Figure 2-1	Typical Method for Attaching Plastic Bottle/ Tub	9
Figure 2-2	Typical Method for Flexible Pouches	9
Figure 2-3	Practical Arrangement of Component ASTM D3985	11
Figure 2-4	Gas Chromatography Diffusion Cell	13
Figure 2-5	CSIRO Schematic of Diffusion Apparatus (Trefry 2001)	14
Figure 2-6	Diffusion Cell Partially Disassembled: A. Top Cell, B. Bottom Cell, C. Red Rubber Gaskets, and D. 8 Pairs of Bolts, Washers & Nuts	16
Figure 2-7	Prototypes New Diffusion Cell	18
Figure 2-8	Illustration of Components	19
Figure 3-1	Schematic Diagram of the Diffusion Cell	28
Figure 3-2	Aluminum Insert to Reduce Chamber Volume	29
Figure 3-3	Calibration Curves of Sensors	30
Figure 3-4	Consumption Rate Effect for the Sensors in Different O ₂ Concentrations	32
Figure 3-5	Consumption Rate vs. Oxygen Concentration	33
Figure 3-6	Test Specimens Set Up – 1 Control and 3 Test Cells	36
Figure 3-7	Raw and Corrected Data for Teflon Specimen	38
Figure 3-8	Experimental and Fitted Data for Teflon Specimen	43

Figure 3-9 Experimental and Fitted Data for PET Mylar Specimen	44
Figure 3-10 Experimental and Fitted Data for Epoxy A	44
Figure 3-11 Experimental and Fitted Data for Epoxy B	45
Figure 3-12 Experimental and Fitted Data for Epoxy C	45
Figure 3-13 Experimental and Fitted Data for Epoxy D	46
Figure 3-14 Experimental and Fitted Data for Epoxy E	46
Figure 3-15 Steel Layout in Numerical Example	50
Figure 4-1 Schematic Diagram of Diffusion Cell	57
Figure 4-2 Fiber Orientation in Laminates Tested	63
Figure 4-3 Fiber FRP Orientation	64
Figure 4-4 Experiment and Fitted Data for Glass FRP One Layer of Fiber	69
Figure 4-5 Experiment and Fitted Data for Glass FRP Two Layers of Fiber	69
Figure 4-6 Comparison of Normalized Permeation Constant	71
Figure 4-7 Comparison of Normalized Permeation Constant for Random Laminates	72
Figure 4-8 SEM Micrograph One Layer GFRP Specimen.....	75
Figure 4-9 SEM Micrograph Two Layers GFRP Specimen	76
Figure 4-10 SEM Micrograph Bidirectional GFRP Specimen	76
Figure 4-11 SEM Micrograph Random GFRP Specimen.....	77
Figure 5-1 Diffusion Cell for Testing FRP-Concrete Systems.....	84
Figure 5-2 Concrete, Epoxy-Concrete and FRP-Concrete Specimen	87
Figure 5-3 Concrete Specimen	89
Figure 5-4 FRP-Concrete Specimen Preparation.....	91

Figure 5-5 FRP-Concrete Specimen	92
Figure 5-6 Diffusion Test Set Up for FRP-Concrete Systems.....	94
Figure 5-7 Experiment and Fitted Data for Concrete with w/c 0.40	95
Figure 5-8 Experiment and Fitted Data for Epoxy-Concrete System B.....	96
Figure 5-9 Experiment and Fitted Data for CFRP-Concrete One Layer System B	97
Figure 5-10 Experiment and Fitted Data for CFRP-Concrete Two Layer System B	97
Figure 5-11 Diffusion Model for FRP-Concrete Specimen.....	103
Figure 6-1 Average Oxygen Permeation Constant for Concrete Specimens in mol. m ² /m ³ .atm.sec. (Note: 1 mol. m ² /m ³ .atm.sec. = 3.28 mol. ft ² /ft ³ .atm.sec.)	108
Figure 6-2 Average Oxygen Permeation Constant for Epoxy, FRP, and FRP-Concrete Specimens in mol. m ² /m ³ .atm.sec. (Note: 1 mol. m ² /m ³ .atm.sec. = 3.28 mol. ft ² /ft ³ .atm.sec.)	108
Figure 7-1 Figaro Carbon Dioxide Sensor TGS 4161	117
Figure III-1 SEM One Layer CFRP Unidirectional Specimen	132
Figure III-2 SEM Two Layers CFRP Unidirectional Specimen	133
Figure III-3 SEM Random Layer CFRP Specimen	133
Figure IV-1 SEM One Layer GFRP Unidirectional Specimen	134
Figure IV-2 SEM Two Layers GFRP Unidirectional Specimen	135
Figure IV-3 SEM Random Layer GFRP Unidirectional Specimen	135
Figure V-1 SEM for Concrete with w/c Ratio 0.40.....	136
Figure V-2 SEM for Concrete with w/c Ratio 0.45.....	137
Figure V-3 SEM for Concrete with w/c Ratio 0.50.....	137

Figure VII-1 Fitted Data vs. Experimental Data for Dry Concrete Specimen (Note: 1 atm = 0.101 MPa)	142
Figure VII-2 Fitted Data vs. Experimental Data for Wet Concrete Specimen (Note: 1 atm = 0.101 MPa)	143

Abstract

Many independent studies have conclusively demonstrated that fiber reinforced polymers (FRP) slow down chloride-induced corrosion of steel in concrete. The mechanism for this slow down is not well understood but it has been hypothesized that FRP serves as a barrier to the ingress of chloride, moisture, and oxygen that sustain electrochemical corrosion of steel.

This dissertation presents results from an experimental study that determined the oxygen permeation rates of materials used in infrastructure repair. In the study, the oxygen permeation constants for epoxy, carbon and glass fiber laminates, concrete, epoxy-concrete and FRP-concrete systems were determined and a method developed to use these results for designing the corrosion repair of FRP-concrete systems.

A new diffusion cell was developed that could be used to test both thin polymer specimens and much thicker FRP-concrete specimens. Concentration gradients were introduced by exposing one face of the specimen to air and the other face continuously to 100% oxygen for the duration of the test to achieve steady state conditions. Partial pressures on the two surfaces were measured using electronic sensors and oxygen permeation constants extracted from the

data using a quasi-steady state theoretical model based on Fick's law. Results obtained using this system were in agreement with published data for specimens such as Teflon and Polyethylene Terephthalate (PET) Mylar whose oxygen permeation constant is available in the published literature.

Following the successful calibration of the system, oxygen permeation constants for epoxy, Carbon Fiber Reinforced Polymer (CFRP) and Glass Fiber Reinforced Polymer (GFRP) laminates were determined. It was found that the oxygen permeation constant for epoxies was an order of magnitude lower than that for FRP. Furthermore, two layer FRP laminates were found to be more permeable than single layer laminates. This finding had been reported previously in the literature but had been considered anomalous. Scanning electron micrographs showed that this was due to the wet layup process that inevitably trapped air between the multiple FRP layers.

The oxygen permeability of FRP-concrete systems was evaluated for three different water-cementitious ratios of 0.4, 0.45 and 0.50 for both CFRP and GFRP materials. Results showed that the performance of CFRP and GFRP were comparable and the best results were obtained when FRP was used with concrete with the highest water-cementitious ratio. A simple design method is proposed to apply the findings from the research. This uses the concept of an equivalent FRP thickness derived following Fick's law.

The findings from the research can be used to optimize FRP applications in corrosion repair. The experimental set up can easily be adapted to measure

diffusion of carbon dioxide through FRP and other materials. This has potential applications in other disciplines, e.g. climate change.

Chapter 1 – Introduction

1.1 Background

Durable repair of damage caused by chloride-induced corrosion is difficult to achieve. Best practice requires removal of all chloride-contaminated concrete from around the reinforcement, cleaning all exposed steel and introducing concrete that has the same electrochemical and mechanical properties as the original concrete. This repair protocol is not cost effective; the repair and re-repair of corrosion damage is a common and costly problem worldwide.

In recent years, there has been interest in the use of fiber reinforced polymers (FRP) for corrosion repair. FRP are high strength fibers embedded in a resin matrix. Fibers most commonly used are glass and carbon. Glass fiber reinforced polymers (GFRP) typically use vinylester resins while epoxy resins are commonly used with carbon fiber reinforced polymers (CFRP).

FRPs can be unidirectional in which all fibers are in one direction or bidirectional in which they are in placed in orthogonal ($0^{\circ}/90^{\circ}$) directions. FRPs are available as pre-cured laminates or can be prepared on site using a wet layup process. Alternatively, they can be prepregs in which the fibers are

saturated with resin in a factory and sent to the site in hermetically sealed containers.

1.2 Aim and Motivation

Originally, FRPs were used for strengthening and rehabilitating structures. Since the mid-1990s its application has been extended to repair corrosion damage (Tarricone 1995, Restrepol and DeVino 1996, Shiekh et al. 1997, Samaan et al. 1998, Sen et al. 1999, Alampalli 2001, Pantazopolou et al. 2001, Debaiky et al. 2002, Sen 2003, Wang et al. 2004, Badawi and Soudki 2005, Suh et al. 2007 & 2008, Winters et al. 2008). Numerous studies have conclusively demonstrated that while FRPs cannot stop corrosion, it can slow down the corrosion rate (Baiyasi and Harichandran 2001, Berver et al. 2001, Wootton et al. 2003, and Wheat et al. 2005). The precise mechanism responsible for this slow down is not understood; however, it is commonly believed that FRPs are barrier elements. As such, they slow down the ingress of deleterious elements such as oxygen, moisture and chlorides that are responsible for sustaining electro-chemical corrosion of steel in concrete (Emmons 1993, Christopher and Albert 2000, Newman 2001).

Insight into the barrier characteristics of FRP can be assessed by measuring permeation characteristics of deleterious materials through FRP. Since oxygen molecules are the smallest, they diffuse the fastest. Therefore, their characterization is the most relevant. This dissertation describes an experimental

study to determine the oxygen permeation characteristics of FRP and FRP-concrete systems. Though there have been studies to determine the oxygen permeation characteristics of concrete (Lawrence 1984, Gjørsvik et al. 1986, Kobayashi and Shuttah 1991, Omaha et al. 1991, Hansson 1993, Ngala et al. 1995, Lu 1997, Buenfeld and Okundi 1998, Abbas et al. 1999, Castellote et al. 2001, Williamson and Clark 2001, Khan 2003, Shafiq and Cabrera 2006, Tittarelli 2009, Hussain and Ishida 2010) there was only one study relating to FRP (Colin et al. 2005) and none for FRP-concrete systems. This study represents the first comprehensive research project directed towards oxygen permeation characterization of FRP materials used in infrastructure applications.

In the study, several commercially available FRP systems were tested and a steady state model developed to allow extraction of the relevant diffusion or permeation constant. SEM investigations were undertaken to evaluate microstructure and interfacial characteristics. The goal was to gain an understanding on the mechanism by which the use of FRP led to more durable corrosion repairs and also to explain anomalous data reported by researchers (Debaiky et al. 2002, Wootton et al. 2003, and Suh et al. 2007).

Several methods are available (ASTM F1307 2002, ASTM D3985 2005, Trefry 2001, Chowdhury 2010) for determining the oxygen permeation of polymers. However, they are not optimal for evaluating thicker materials typically used in infrastructure applications. Therefore there was a need to develop a new diffusion cell and an appropriate testing protocol.

The main objectives of the study can be summarized as follows:

1. Development of diffusion cell and a steady state model for extracting permeation constants.
2. Verification of correctness of the theoretical model.
3. Determination of the oxygen permeation characteristics of FRP laminates prepared using wet layup system.
4. Determination of the oxygen permeation characteristics of concrete and FRP-concrete systems
5. Application of results in predicting corrosion rate of steel in FRP repaired systems.

1.3 Organization

The objectives listed in the previous section are the subject of several publications (Khoe et al. 2009, 2010, 2011a (in press), 2011b (in press) and 2011c (under review)). These self-standing publications constitute different chapters of the dissertation. Inevitably, this approach leads to repetition. Supplementary information is provided in seven separate appendices.

The following is a brief description of the remaining chapters:

Chapter 2 provides background information on the development of the diffusion cell.

Chapter 3 presents the theoretical model and its calibration through tests carried out on polymers and epoxies. It also describes how results can be applied

to predict corrosion rates in repairs. The MATLAB program developed is included as Appendix I.

Chapter 4 presents results on oxygen permeation characteristics of four different FRP materials widely used in infrastructure applications. Scanning electron micrographs included in this chapter help to explain anomalous findings reported in the literature.

Chapter 5 presents results on the oxygen permeation characteristics of concrete and FRP-concrete systems.

Chapter 6 presents an overview of all the results with a focus on application.

Chapter 7 summarizes the main contributions from the research and avenues for future research.

In addition to the seven chapters, there are seven appendices. These cover the following:

Appendix I presents step-by-step computer MATLAB program calculations for extracting the permeation constant using a quasi steady state model.

Appendix II presents step-by-step volume fiber calculations and summarizes the average volume fiber fraction for all the FRP laminates tested.

Appendix III presents additional scanning electron micrographs (SEM) for CFRP specimens.

Appendix IV presents additional scanning electron micrographs (SEM) for GFRP specimens.

Appendix V presents scanning electron micrographs (SEM) for concrete specimens with three water-cementitious ratios (0.40, 0.45 and 0.50).

Appendix VI provides sample calculations for using the findings from this research to predict metal loss inside a FRP repair.

Appendix VII provides results from a limited study comparing the oxygen permeability of wet and dry concrete.

Chapter 2 – Development of Diffusion Cell

2.1 Introduction

Several methods are available for measuring oxygen diffusion characteristics of polymer materials. However, since they were developed for the food-packaging industry, they can only be used where the material thickness is very small. As such they are unsuitable for measuring the oxygen diffusion characteristics of the much thicker systems used in infrastructure applications where epoxy or FRP is bonded to concrete elements.

This chapter traces the development of a new diffusion cell that is geared towards oxygen diffusion characterization of polymers that are typically used in infrastructure applications. The new diffusion cell can also be used to evaluate the effectiveness of FRP-concrete systems in resisting chloride-induced corrosion.

2.2 Background

The underlying principle governing diffusion of gases is Fick's law. This states that the rate of transfer of diffusing substances is proportional to the concentration gradient measured normal to the section. Thus, test methods rely on setting up concentration gradients that will then promote mass transfer.

If the gas concentrations can be kept constant on both surfaces of a polymer sample, steady-state conditions develop. Steady-state conditions make it possible to develop models that can extract the permeation and diffusion constant from the data if the solubility constant is known. However, the theoretical models developed in this study are outside the scope of this chapter (Crank 1968, Crank 1975, Koros et al. 1981, Vasquez-Borucki et al. 2000, Bird et al. 2002). This chapter focuses exclusively on the development of a new diffusion cell.

Concentration gradients can be achieved by using vacuum and non-vacuum based methods. Since non-vacuum-based methods were deemed to be less complex, these are used in the study and are therefore reviewed in this chapter.

2.3 Existing Test Methods

Four non-vacuum based methods are reviewed. These include two ASTM methods (ASTM F1307 2002, ASTM D3985 2005) developed for the food packaging industry, a CSIRO method developed in Australia (Trefry 2001) and a method using gas chromatography developed earlier at USF that was a precursor for the present study.

2.3.1 ASTM F1307

This ASTM standard covers procedures for determining the steady state rate of transmission of oxygen into packages that enclose a dry environment. Typical elements intended for this test include rigid plastic bottles, tubs or flexible bags or pouches as shown in Figure 2-1 & 2-2.

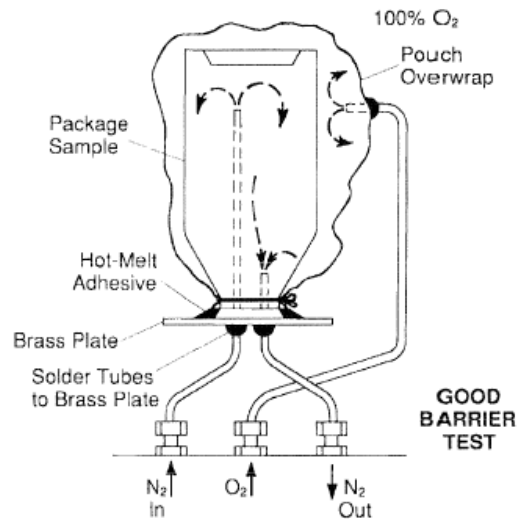


Figure 2-1 Typical Method for Attaching Plastic Bottle/ Tub

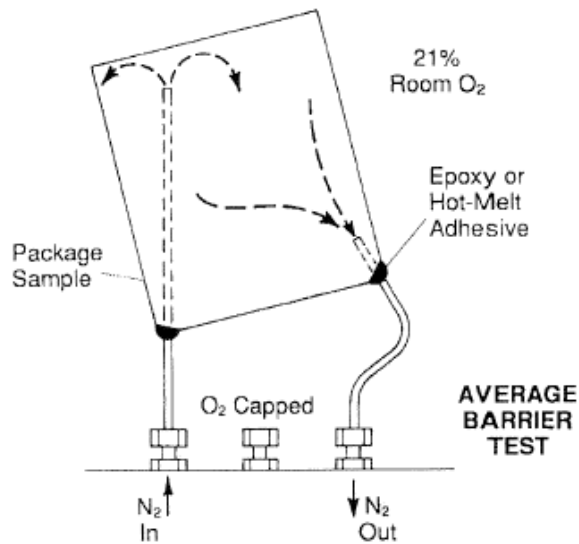


Figure 2-2 Typical Method for Flexible Pouches

In the test, the air inside the package is purged by maintaining a constant flow rate of nitrogen from 30 minutes to several hours depending on the volume of the container. Subsequently, the flow rate is reduced and maintained for the next 30 minutes before the flow of nitrogen (carrier gas) is diverted to coulometric sensors. These can count the number of electrons that enter the sensor (four electrons represent one oxygen molecule). The sensor output increases gradually before reaching a steady state and that may require several hours or days. To expedite testing, the outside of the package can be maintained at 100% oxygen level (see Figure 2-1). This will increase the transmission rate by a ratio of $100/21 = 4.8$.

Because of the dependence of the oxygen transmission rate on temperature (it varies by 3 to 9%/C), tests should be conducted in a draft-free constant temperature environment. ASTM (ASTM D3985 2005 and ASTM F1307 2002) spells out procedures for calculating the oxygen permeance of the specimen.

2.3.2 ASTM D3985

ASTM D3985 (ASTM D3985 2005) standard covers procedures for determining the steady state rate of transmission of oxygen for plastics in the form of film, sheeting, laminates, coextrusions or plastic coated papers or fabrics.

Unlike ASTM F1307 (ASTM F1307 2002) where the specimen itself serves as the diffusion cell, in this set up, the test specimen is placed inside a diffusion cell where it serves as a barrier between the upper and lower parts of the cell. Precise dimensions of the cell are not specified in the standard (ASTM F1307 states that the typical diffusion cell areas are 100 cm^2 and 30 cm^2).

The volumes above and below the test specimen are not deemed to be critical. However, they should be small to allow rapid gas exchange but big enough so that a bulging (or sagging) film is not in contact with the top or bottom surfaces of the cell.

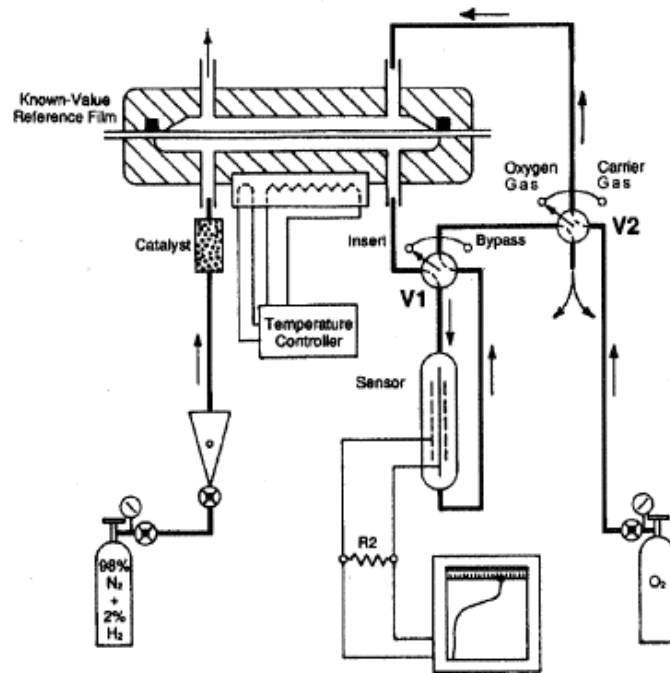


Figure 2-3 Practical Arrangement of Component ASTM D3985

One face of the specimen is exposed to dry oxygen (test gas) while the other is exposed to nitrogen (carrier gas). A neoprene O-ring is placed in a

machined groove to position the specimen on the "oxygen" face. The nitrogen side has a raised flat rim which is critical for sealing the diffusion cell when the test specimen is pressed.

Air is first purged from the upper and lower diffusion cell chambers as shown in Figure 2-3. Thick samples may require several hours to purge or even overnight. After this, a reduced flow rate is maintained for 30 minutes. The sensor is then inserted and base line measurements taken. Subsequently, the test side is connected to an oxygen supply.

An equation is provided that allows the oxygen permeation constant to be extracted. Its unit is in mol/m.s.Pa.

2.3.3 Gas Chromatography

The oxygen diffusion characterization of FRP material may be determined using Gas Chromatography (GC). In an earlier study, a diffusion cell was made from an aluminum tubing (outside diameter 73 mm with a 4.8 mm wall thickness) and 114.3 mm length. An aluminum plate was welded to the bottom of the cell; FRP material was bonded to the top. Inlet and outlet tubes were attached to the bottom (Figure 2-4). The inlet tube was used to fill the chamber with nitrogen. The cell was kept in air where it is exposed to 20.7% oxygen. The outlet tube was used to periodically extract samples (with a 1 ml syringe) of the contents of the chamber. The composition of the extracted sample was determined using gas chromatography. Special techniques are required to

extract the gas sample with the 1 ml syringe from the septum. This method was very cumbersome and error-prone since the readings were taken manually. More importantly, making the system air-tight was problematic.

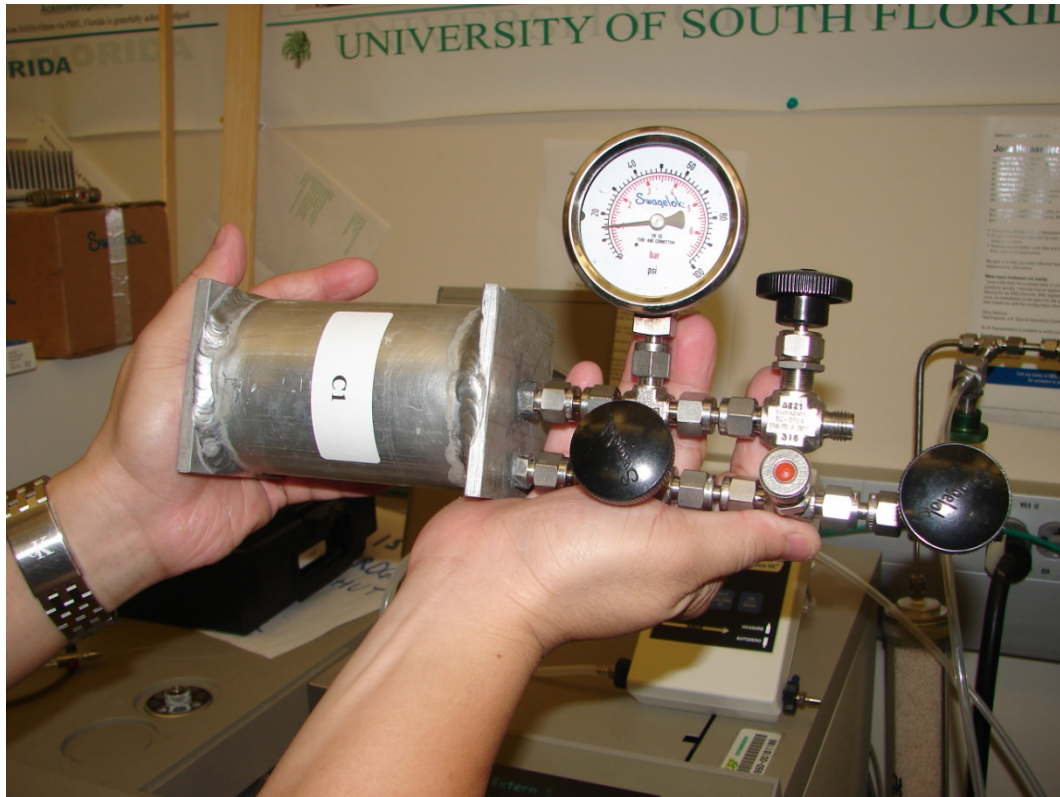


Figure 2-4 Gas Chromatography Diffusion Cell

2.3.4 CSIRO

Commonwealth Scientific and Industrial Research Organization (CSIRO) is Australia's national science agency and is one of the largest and most diverse research agencies in the world. In 2001, they developed a diffusion cell to measure the oxygen characteristic of high density polypropylene membranes. These geo-membranes were used to limit the amount of oxygen that would

reach tailings (residues of extracted metal ores) placed in de-watered soils to prevent them from reacting with the soil and producing undesirable acid sulfate soils.

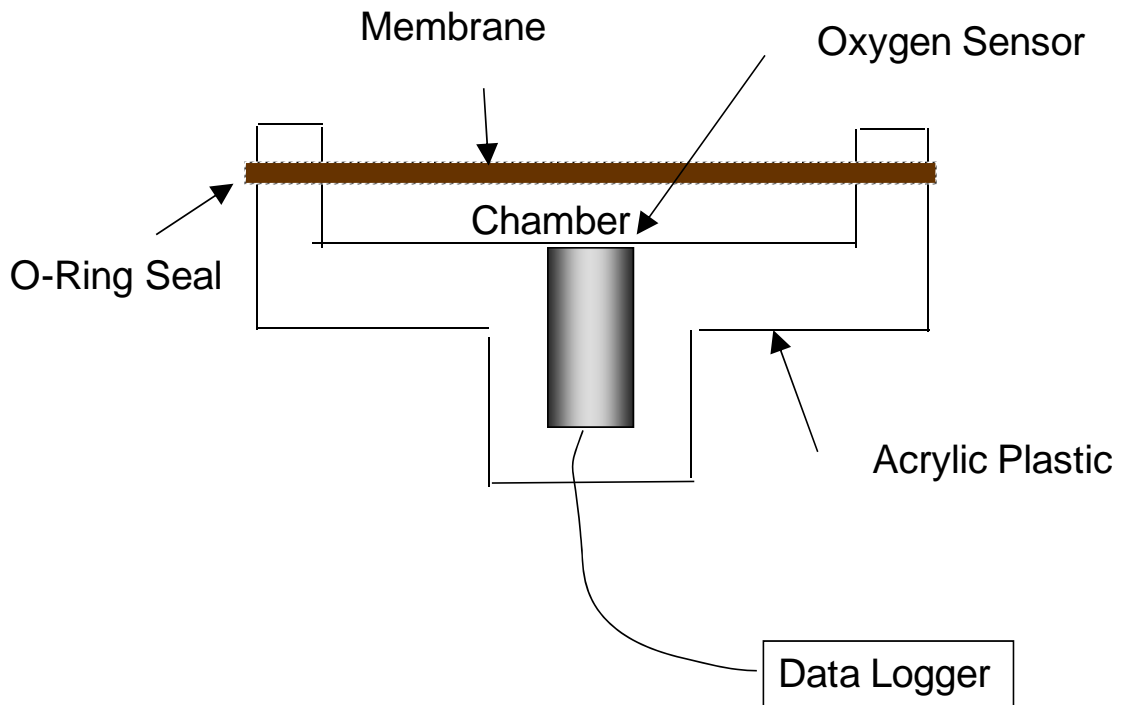


Figure 2-5 – CSIRO Schematic of Diffusion Apparatus (Trefry 2001)

Figure 2-5 is a schematic of the system developed by CSIRO. The cylindrical cell made of acrylic plastic has a volume of 18 cm^3 with a depth of 0.5 cm. As with the GC cell, the test specimen forms the lid of the cell where it is positioned by an O-ring to provide a gas-tight seal. The exposed surface area of the membrane is 39 cm^2 .

The test assembly is conditioned for 1-2 weeks (at room temperature) in an anaerobic environment. Subsequently it is moved to an aerobic environment. Oxygen diffusion through the membrane is measured using a

Figaro oxygen sensor (KE 25, Figaro 2004) that is countersunk with its top flush with the base of the cell.

The Figaro sensor is essentially a lead-oxygen battery. It has a lead anode, and a gold cathode. Oxygen entering the sensor reacts to set up a current that is proportional to the oxygen concentration. Results reported indicate that it took a week for the results to stabilize. Samples tested ranged in thickness from 0.75 mm to 7.2 mm. An analytical model was developed to determine the oxygen diffusion constant.

2.4 Development of New Diffusion Cell

The goal of the present study was to develop a new system that could be used to evaluate the oxygen diffusion characteristics of thicker polymer films used in infrastructure applications.

Previous experience with the development of gas chromatographic technique had indicated the importance of electronic data collection and the avoidance of leaks. Moreover, since a large number of tests had to be conducted, assembly of the cell had to be rapid and simple yet leak proof.

Aluminum had been used for fabricating the diffusion cell developed earlier primarily because of its light weight. However, as leaks were detected in the aluminum weld it was decided that the new cell would be made of stainless steel and would be assembled using bolts.

A pair of blank, round, stainless steel plates was purchased from Nor-Cal. The plates were 12 mm thick and had a 144 mm outside diameter. They were provided with eight bolt holes located symmetrically around the outside perimeter.

The central part of the plates was machined to create 83 mm diameter and 4.5 mm deep recess that constituted the diffusion chamber. In case the time taken to complete the test was inordinate, the volume of this chamber could be reduced by placing appropriately sized aluminum inserts in the opening.

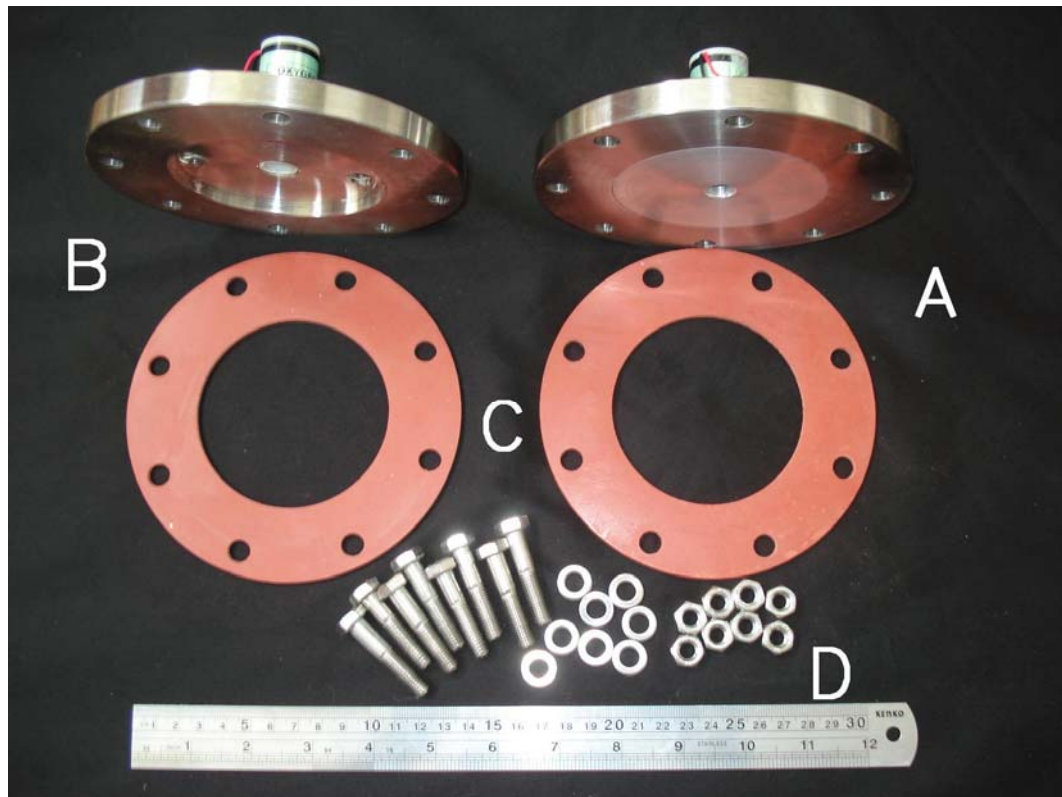


Figure 2-6 Diffusion Cell Partially Disassembled: A. Top Cell, B. Bottom Cell, C. Red Rubber Gaskets, and D. 8 Pairs of Bolts, Washers & Nuts.

The test specimen is positioned between two 144 mm diameter stainless plates. Originally, grooves were cut so that O-rings could be used to make it airtight as was used in the CSIRO diffusion cell. However, after extensive testing it was discovered to be unreliable. The problem was easily overcome by replacing the O-rings by 3 mm thick red rubber gaskets. Ironically, this had been recommended in a doctoral dissertation (Paul 1965) published over 40 years ago.

The diffusion cell is assembled by bolting the two stainless steel plates together using eight stainless steel bolts, nuts and washers (Figure 2-6). A special, calibrated digital torque wrench was used to ensure uniformity in the applied force. As the lengths of the bolts can be varied, it provides a simple yet effective means for testing samples of different thicknesses.

2.5 Concentration Gradient

The diffusion cell was assembled in air and therefore one face of the specimen has the same oxygen concentration as air (20.7% of oxygen). The other face was flushed with 100% concentration oxygen to provide the needed concentration gradient. A similar gradient could also have been created by flushing pure nitrogen instead.

2.6 Leak Proofing

In any cell that is assembled manually, elaborate procedures are needed to ensure that there are no leaks. In this case, threaded inlet and outlet

openings in the bottom plate were made leak proof by using liquid threaded seal Teflon in conjunction with a Swagelok male connector.

2.7 Data Collection

The same Figaro electrochemical oxygen sensor used in the CSIRO was also used in this study. However, all data was corrected to account for oxygen that was consumed by this sensor.

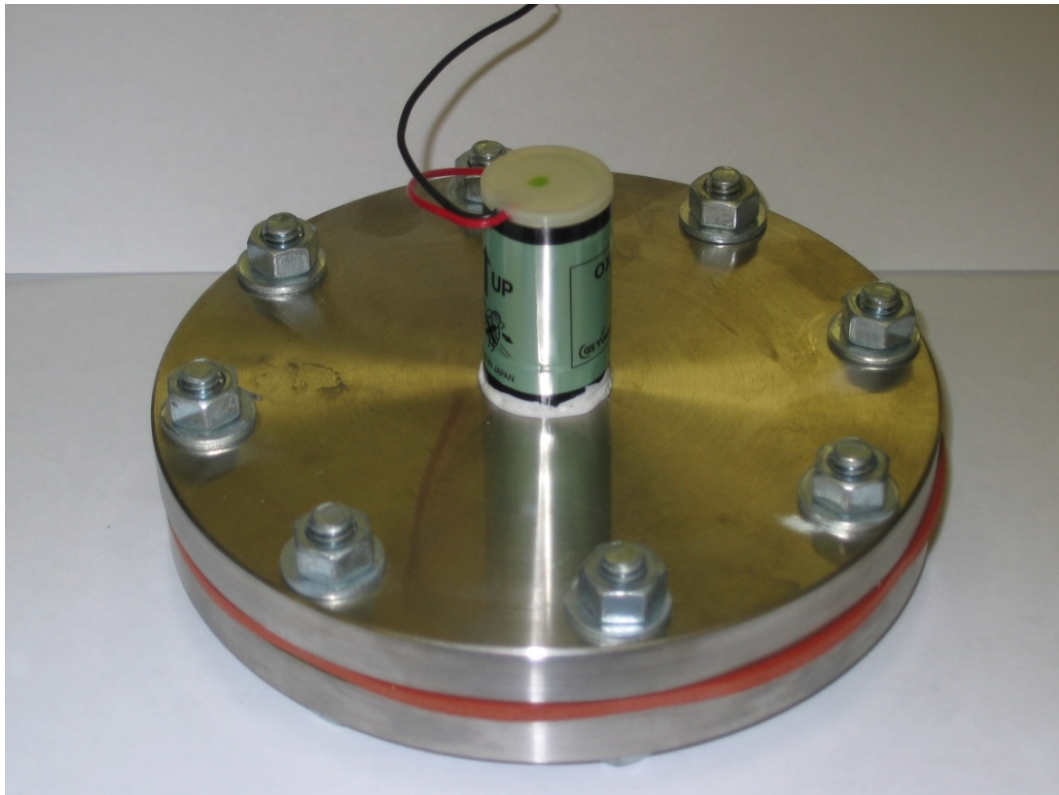


Figure 2-7 Prototypes New Diffusion Cell

The sensor was connected to the Agilent 34970A data acquisition system to allow data to be recorded. Temperature data were also recorded at the same time since the diffusion constant depends on temperature.

Figure 2-7 shows a photograph of a prototype new diffusion cell with the oxygen sensor attached at the top. The bolted assembly and the rubber gasket can be clearly seen. Two cells are shown since in the testing an additional cell with an impermeable material such as steel was tested simultaneously. This set up served as an early warning system for possible leaks.

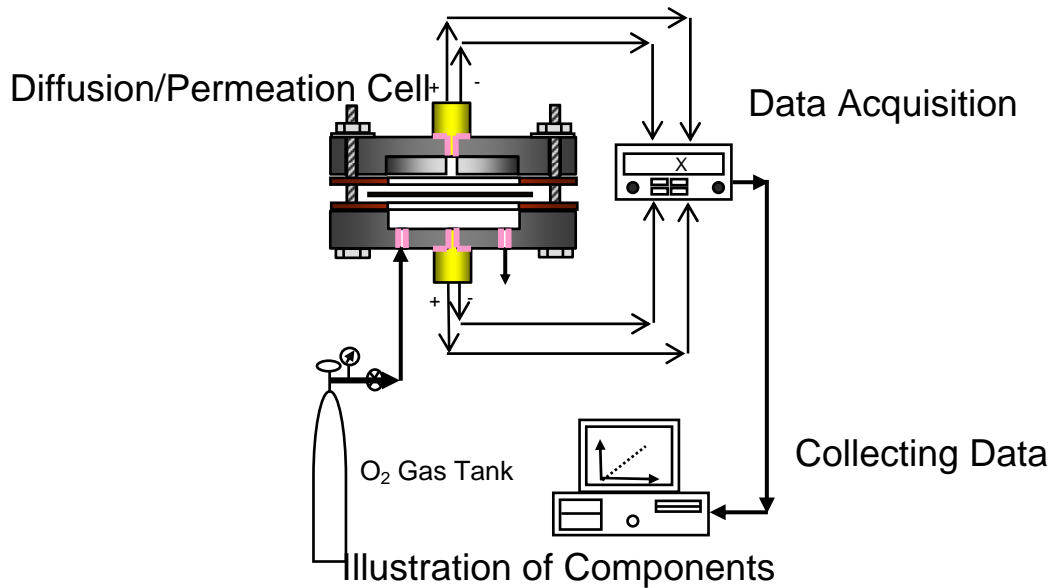


Figure 2-8 Illustration of Components

2.8 Testing Procedure

Following extensive trials, the set up shown in Figure 2-6 was revised to incorporate an additional sensor at the bottom. This permitted the oxygen concentrations on both surfaces of the test specimen to be continuously monitored thereby enabling verification of steady state conditions assumed in the theoretical model. A schematic of the new test set up is shown in Figure 2-8.

To make sure that the data were correctly obtained, four specimens were tested simultaneously. Three contained test specimens; the fourth had a stainless insert where no oxygen was consumed by the sensor. This set up enabled any experimental errors to be readily detected.

2.9 Time for Test

Typically, results were obtained within 24 hours. The theoretical model developed allowed the permeation constant of the specimen to be obtained by numerical solution of the governing differential equation. Results obtained were in good agreement with those in the published literature.

2.10 Summary and Conclusions

Available methods for determining the oxygen diffusion permeation characteristics for thicker polymers used in infrastructure applications are unsuitable. This chapter describes the development of a new diffusion cell suitable for this application. The diffusion cell proposed is relatively simple to construct and since bolts are used its size can be readily altered to accommodate a wide range of specimens.

Calibration tests conducted on thin polymers for which results are available validate the test method and the theoretical model developed in Chapter 3-5. More tests are shown in the next chapters to evaluate different epoxies, fiber reinforced polymers, and fiber reinforced polymers in concrete.

The diffusion cell developed provides a simple method for identifying materials and systems that are most effective for corrosion repair of infrastructure elements. By incorporating these materials, it will become possible to optimize the performance of polymer materials used for corrosion repair and rehabilitation in the future.

Chapter 3 – Measurement of Oxygen Permeability of Epoxy Polymers

3.1 Introduction

Epoxies are commonly used in corrosion repair for sealing cracks in concrete and as coatings on exterior repairs. More recently, they have been used as the resin matrix in fiber reinforced polymers that are increasingly being used in corrosion repair (Sheikh et al. 1997, Debaiky et al. 2002, Sen 2003). In all these applications, the epoxy serves as a barrier element that impedes the ingress of deleterious chemicals that can lead to corrosion of steel in concrete.

Chloride-induced corrosion is by far the most pervasive corrosion in reinforced or pre-stressed concrete elements. Diffusion of chloride ions to the level of the steel reinforcement results in the destruction of the passive layer that normally protects steel from corroding. Following its destruction, the presence of oxygen and moisture allows the electro-chemical reactions to continue unabated resulting in corrosion of steel.

It is evident therefore, that the effectiveness of repairs where epoxies are used is contingent on its ability to keep out both moisture and oxygen. The resistance of epoxies to water is well documented (Newman 2001) and indeed epoxies are used as external coatings for this very reason. However, unlike

water, oxygen is non-polar. Thus, it will not be adsorbed at the polar sites of amine cured epoxies as is the case for water (Christopher and Albert 2000). For this reason, oxygen diffusion through epoxies is likely to be more critical in corrosion repair. As far as it can be ascertained, this has not been the subject of any previous research.

Several methods are available (ASTM F1307 2002, ASTM D3985 2005, Trefry 2001, Chowdhury 2010) for determining the oxygen permeation of polymers. However, as they were not intended for evaluating thicker materials such as fiber reinforced polymers used in infrastructure applications, their utilization will be very time consuming. This chapter describes the development of an experimental technique that allows determination of the oxygen permeation characteristics of polymers that are difficult to prepare as thin films. A quasi-steady state diffusion model is developed to interpret the data and extract the oxygen permeation constants. The validity of this technique was established by comparing results obtained using this technique with published results. Subsequently, it was utilized to obtain the oxygen permeation constant for five different commercially available epoxies used in marine applications and as the matrix for fiber reinforced polymers.

3.2 Research Significance

Epoxies are widely used as coatings and for repairing cracks in reinforced concrete. Knowledge of the oxygen permeability through epoxies is therefore

important in material selection for preventing corrosion. The new diffusion cell developed in this work enables oxygen characterization of polymer elements used for infrastructure repair for which available test methods are not optimal. The development of a quasi-steady-state model provides a simple means for interpreting data and extracting oxygen permeation constants.

3.3 Definitions

Two commonly used terms, diffusion and permeation, need to be differentiated: *Diffusion* refers to the rate of transfer of molecules through unit area per time. It has units of m^2/sec [ft^2/sec]; the *permeation* constant is a derived quantity defined as the product of the diffusion constant and solubility. It has units of $\text{mol m}^2/\text{m}^3 \text{ atm. sec}$ [$\text{mol ft}^2/\text{ft}^3\text{-atm. sec}$].

Permeation constants are often more valuable in practical applications as they provide permeation rates of the diffusing molecule directly. In this work, these are extracted directly from the developed quasi-steady-state model.

3.4 Existing Methods

Oxygen diffusion characterization of polymers is important in disciplines as diverse as food packaging, medicine, mining and petroleum refining. As a result, several techniques have evolved over the years to meet the special requirements of these particular industries. These use vacuum or non-vacuum based methods for establishing the required concentration gradients. Since non-vacuum based

methods like ASTM F1307 2002, ASTM D3985 2005 and CSIRO (Trefry 2001) are simpler to set up and are more amenable for testing brittle materials; these were the focus of this study.

Two ASTM standards were developed for the food packaging industry: ASTM F1307 is for testing plastic containers that also serve as the diffusion cell. As such, it is unsuitable for this study. On the other hand, ASTM D3985 is more suitable since it is used for testing plastics in the form of film, sheeting, laminates, co-extrusions or plastic-coated papers.

ASTM D3985 uses a diffusion cell though no dimensions are specified in the standard. The test specimen is placed inside this cell where it serves as a barrier between the upper and lower portions. One face of the specimen is exposed to oxygen while the other is exposed to nitrogen to achieve steady state conditions. Coulometric sensors are used to measure the oxygen that diffuses through the test specimen. These count the number of electrons that enter the sensor (four electrons represent one oxygen molecule). The oxygen permeability constant is calculated by dividing the oxygen transmission rate under steady state conditions by the partial pressure inside the test chamber.

CSIRO developed a diffusion cell for determining the oxygen diffusion characteristics of high density polypropylene membranes used by the mining industry. The cell was made of acrylic plastic and had a volume of 18 cm^3 [1.1 in^3] with a depth of 0.5 cm [0.2 in]. Oxygen diffusion through the membrane was measured using a Figaro oxygen sensor (KE 25, Figaro 2004) that was

located at the base of the cell. An analytical model was developed to determine the oxygen diffusion constant.

3.5 Objectives

The goal of this study was to develop an efficient experimental and analytical technique geared towards the determination of the oxygen permeation characterization of thicker polymer films such as epoxies used for concrete repair. This requires:

1. Design of a suitable diffusion cell
2. Development of an analytical technique that allows interpretation of data and also extraction of oxygen permeability constants.
3. Validation of the proposed technique by comparison with results published in the literature.
4. Determination of oxygen permeation constants for representative epoxies.

3.6 Experimental Program

The new method developed is based in part on both the ASTM and CSIRO designs to characterize the oxygen permeability of thicker polymer films. The basic components of these systems, namely the diffusion cell and sensors were retained. However, modifications were made to the design of the diffusion cell so that it was optimal for testing thicker elements, such as fiber reinforced polymers and concrete specimens. Thus, the dimensions of the diffusion cell could be

altered to accommodate different sized specimens and the volume of the diffusion chamber adjustable. Additionally, an analytical technique was developed to allow the oxygen permeation constants to be extracted from the experimental data.

3.7 Diffusion Cell

Figure 3-1 shows the diffusion cell developed for the study. It consists of two 12 mm [0.472 in] thick circular stainless steel plates 145 mm [5.709 in.] (outside diameter). The plates were purchased from Nor-Cal as "blanks" excepting for eight symmetrically located 9.119 mm [0.359 in.] diameter bolt holes. The central part of both these blanks was machined to create a diffusion chamber for the test specimen. Its volume is $1.7617 \times 10^{-5} \text{ m}^3$ [1.08 in³]. However, this could be reduced by inserting specially machined aluminum pieces (Figure 3-2).

The specimen is positioned between two 145 mm [5.709 in.] diameter 3 mm [0.12 in.] thick red rubber gaskets selected to provide an airtight seal (Paul 1965). The two stainless steel plates are bolted together using eight stainless steel bolts, nuts and washers. A special, calibrated digital torque wrench was used to ensure uniformity in the applied force. As the lengths of the bolts can be varied, it provides a simple means for testing samples of different thicknesses.

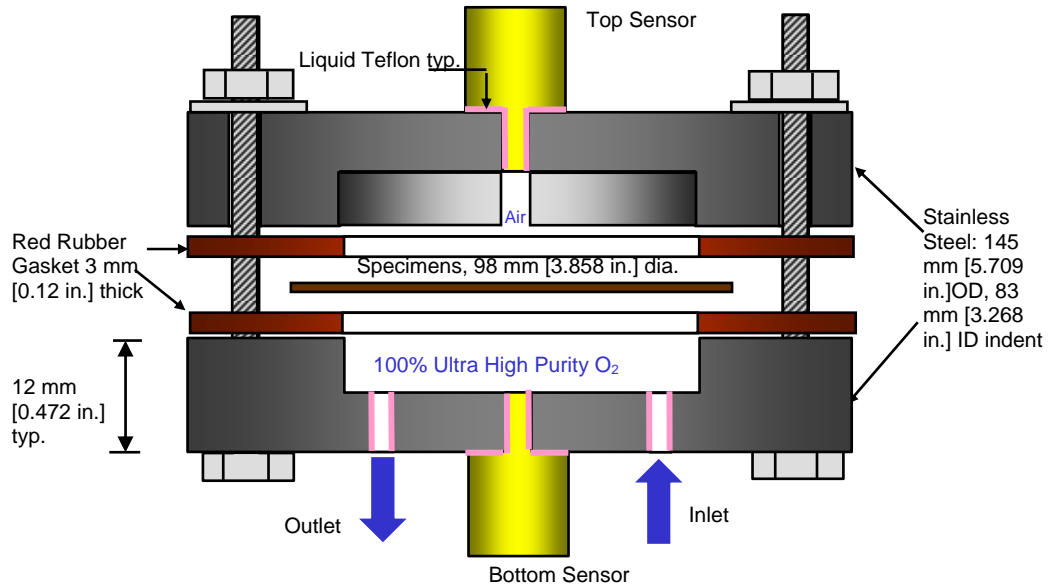


Figure 3-1 Schematic Diagram of the Diffusion Cell

The diffusion cell was assembled in air and therefore one face of the specimen has the same oxygen concentration as air (20.7% of oxygen). The other face was flushed with 100% concentration oxygen that was released from a standard oxygen cylinder at the rate of 150 standard cubic centimeters per minute (SCCM) [5.30E-3 ft³/min]. This required threaded inlet and outlet openings in the bottom plate that were fabricated as shown in Figure 3-1. These connections were made leak-proof by using liquid threaded seal Teflon in conjunction with a Swagelok male connector.

Two oxygen sensors were used to monitor the oxygen concentration at the top and bottom of the diffusion cell. The connections to both sensors were also made leak-proof using specially fabricated threaded openings and liquid threaded seal Teflon.

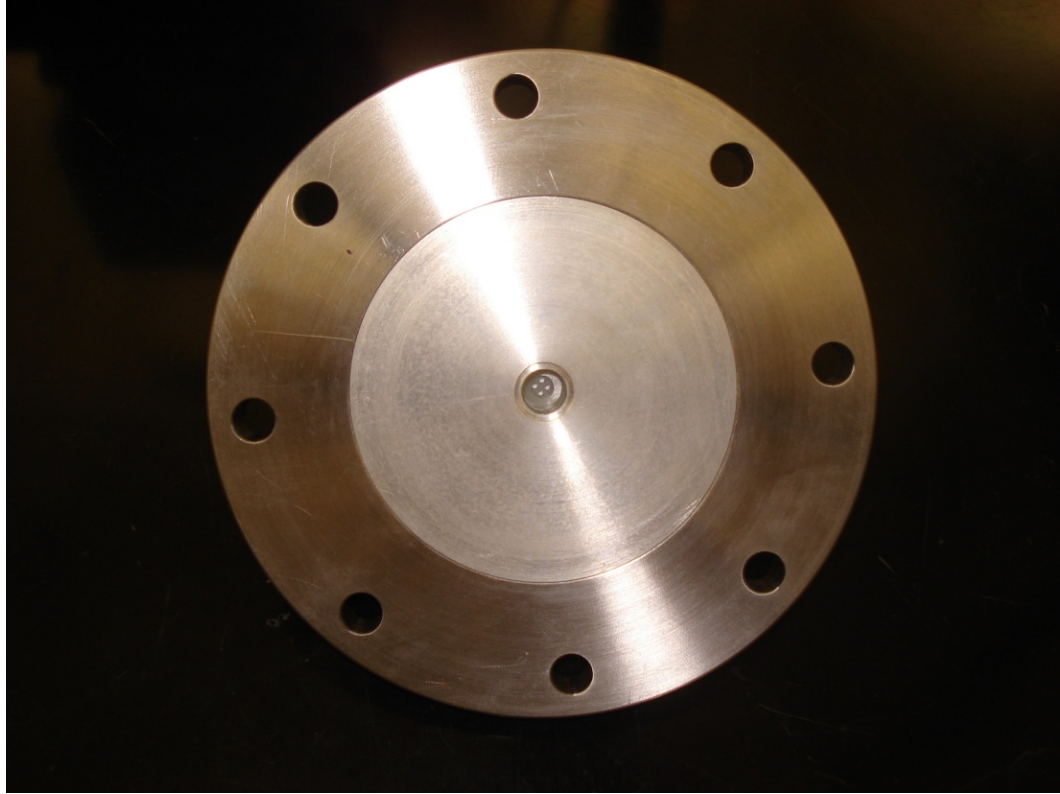


Figure 3-2 Aluminum Insert to Reduce Chamber Volume

3.8 Oxygen Sensor

The galvanic cell type oxygen sensors used by CSIRO, rather than the coulometric sensor used in the ASTM standards, were selected for the study because of their lower cost. These 50 mm x 23 mm diameter [1.97 in. x 0.91 in.] sensors were developed by Figaro (Model KE-25 F3). They incorporate a lead anode and a gold cathode in a weak acid electrolyte. Oxygen molecules entering the cell are reduced at the cathode; the sensor is designed so that the resulting current (mV) is proportional to the oxygen concentration.

However, the current generated is not the same in all the sensors but falls within a narrow band. For this reason, each sensor has to be individually calibrated against certified oxygen concentration levels. Figure 3-3 shows typical calibration curves that were obtained for four different sensors. The calibration plots show the relationship between sensor readings in millivolts and the partial pressure of oxygen.

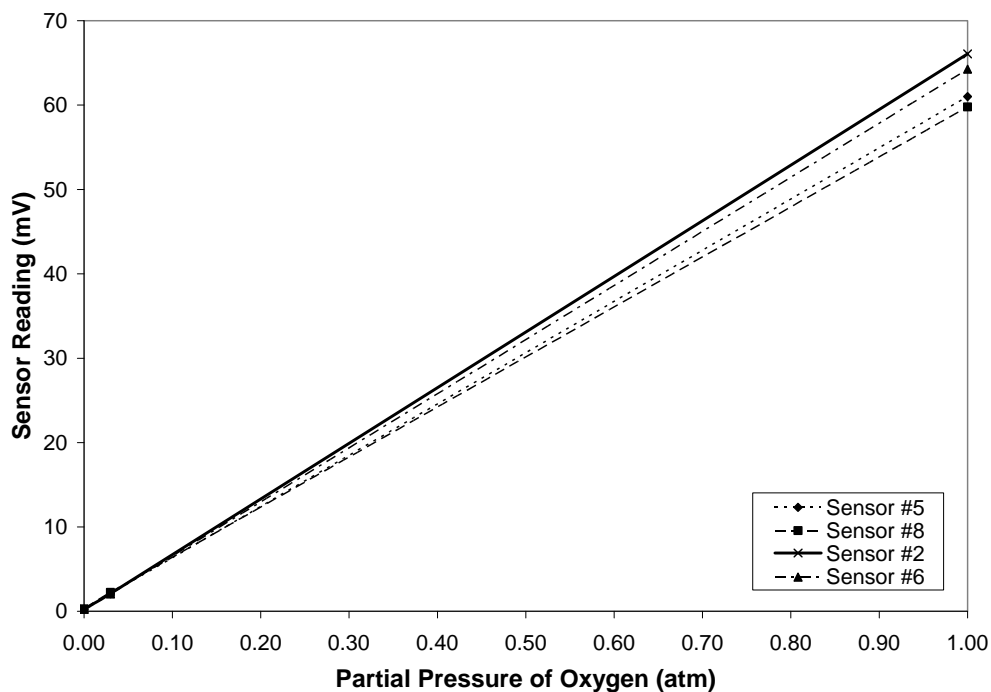


Figure 3-3 Calibration Curves of Sensors

The sensors were connected to an Agilent 34970A data acquisition system to allow data to be recorded at a desired scan rate and stored. This data set could be retrieved later for subsequent analysis. A data acquisition switch unit with two multiplexers attached to 16 channels and 20 channels was used. Temperature data were also recorded at the same time.

3.9 Sensor Oxygen Consumption

As the readings generated by the sensor are the result of electro-chemical reactions with oxygen molecules, some oxygen is consumed during testing.

Figaro's technical literature (Figaro 2004) provides generic information but this may not fully apply for test conditions. For this reason, tests were conducted to determine the actual consumption rates in individual sensors used in this study.

Four series of tests were conducted to measure the variation in the oxygen consumption rate with the concentration varying from 19-89%. In each case, an airtight cell, that is a diffusion cell with a stainless steel test specimen was assembled inside a glove box with a known oxygen concentration level. Subsequently, the cell was removed from the glove box and the sensor measurements recorded continuously for 24 hours - the typical duration for a test.

The variation in sensor readings with time for different initial oxygen concentrations inside airtight cells are shown in Figure 3-4. If no oxygen had been consumed, the readings would have remained constant. Instead, readings may be seen to continuously decrease with time.

Inspection of Figure 3-4 shows that though the change in sensor reading due to consumption varies linearly, the lines are not parallel. This implies that the consumption rate (CR_{O_2}) is a function of concentration / partial pressure of

oxygen (p_{O_2}). Consumption tends to be greater at higher oxygen concentration / partial pressure levels (shown in mV in Figure 3-4).

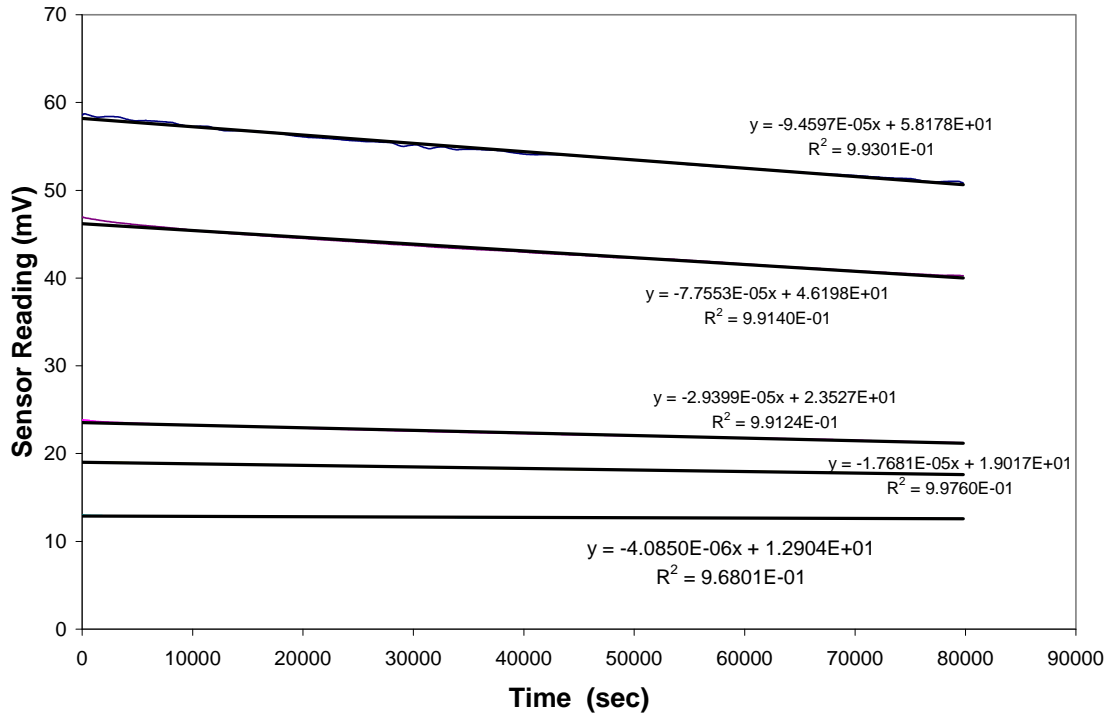


Figure 3-4 Consumption Rate Effect for the Sensors in Different O₂ Concentrations

As consumption varies linearly with time, the consumption rates of sensors at different oxygen partial pressures may easily be extracted from the slopes of sensor reading *vs.* time curves (Figure 3-4). The plot of consumption rate (mV/sec) *vs.* partial pressure (atm.) of oxygen is shown in Figure 3-5. A polynomial function, Equation 3-1, was fitted to this curve to obtain an interpolation of expression for the rate of change in the sensor reading due to consumption.

$$CR_{O_2} = -3.25 \times 10^{-4} p_{O_2}^4 + 7.60 \times 10^{-4} p_{O_2}^3 - 5.58 \times 10^{-4} p_{O_2}^2 + 5.10 \times 10^{-6} p_{O_2} + 1.08 \times 10^{-5} \quad (3-1)$$

At any time t , the corrected sensor reading (S_{cor_n} , mV) was obtained by subtracting the total change in sensor reading due to consumption until time t (sec) from the raw sensor reading (S_{raw_n} , mV) as given by Equation 3-2.

$$S_{cor_n} = S_{raw_n} - \int_0^t CR_{O_2} dt = S_{raw_n} - \int_0^t f(p_{O_2}) dt \quad (3-2)$$

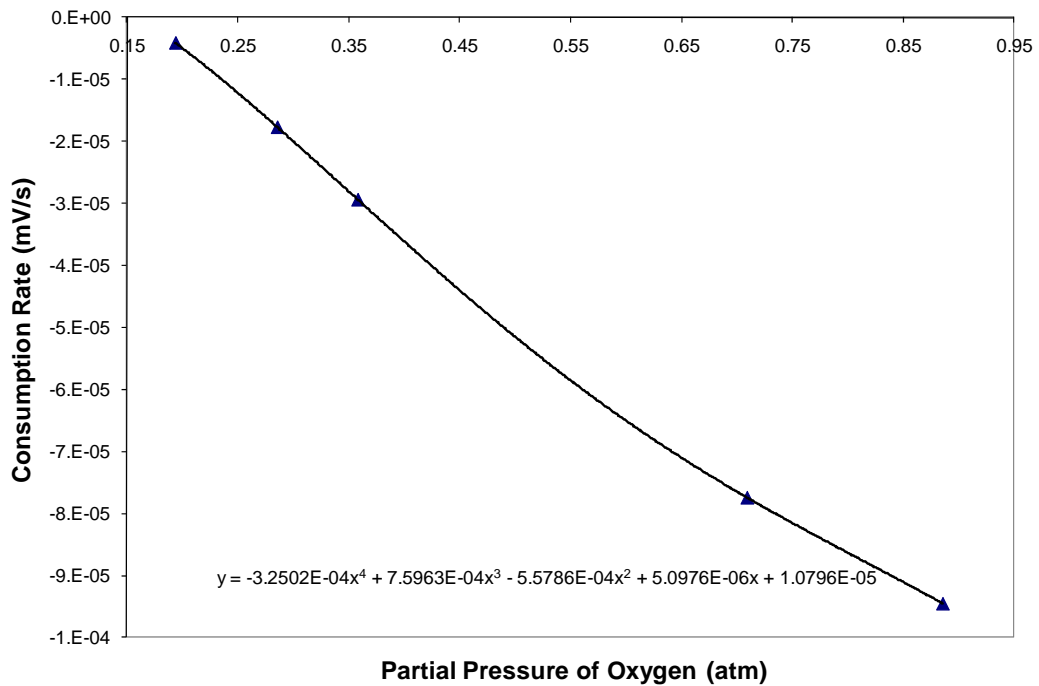


Figure 3-5 Consumption Rate vs. Oxygen Concentration

The consumption rate, CR_{O_2} , (mV/s) is a function of the oxygen partial pressure inside the diffusion cell, according to Equation 3-1. In contrast, the integral in Equation 3-2 is over time. Therefore, to evaluate this integral, at any time t , the raw sensor reading for a particular sensor (S_{raw}) was first converted to a partial pressure using the linear calibration curve in Figure 3-3. This partial

pressure was then utilized to calculate the instantaneous consumption rate using Equation 3-1. Subsequently, the integral in Equation 3-2 was evaluated numerically using the trapezoidal rule, from the generated $f(p_{O_2})$ vs. time data.

The corrected oxygen partial pressure (p_{cor}) inside the diffusion cell is obtained from the corrected sensor reading (S_{cor}) according to the calibration curve for the appropriate sensor as shown in Figure 3-3.

3.10 Sample Preparation

All test specimens were approximately 98 mm [3.86 in.] in diameter to allow sufficient bearing length on either side of the 83 mm [3.27 in.] annular opening in the diffusion cell.

3.11 Calibration Specimens

The polymer materials tested for calibrating the experimental technique were relatively thin. These were Polyethylene Terephthalate (PET) Mylar (0.076 mm [0.003 in.] thick) and Teflon (0.025 mm [0.0001 in.] thick). They were selected because information on their oxygen permeability is available in the literature (Vasquez-Borucki et al. 1978, Koros et al. 1981).

Preparation for these specimens was relatively simple. It merely comprised of cutting them to size by placing the material on a 98 mm [3.86 in.] diameter circular stainless steel template and scoring around it with a sharp knife. Four samples were prepared for each test.

3.12 Epoxy Specimens

Five different commercially available epoxies were tested. These are identified as A, B, C, D and E. Properties of the epoxies as specified by their producers (Fyfe Co 2003, Sika 2003, Air Products 2008, and West System 2008) are summarized in Table 3-1. In all cases, the epoxies were prepared strictly in accordance with the directions specified by the producers. Four sets of specimens for each epoxy type were tested.

Table 3-1 Epoxy Specimens Properties (Fyfe Co 2003, Sika 2003, Air Products 2008, West System 2008)

Description	Value				
	A	B	C	D	E
Tensile Strength, MPa (ksi)	72.4 (10.5)	25 (3.63)	55 (7.98)	44.13 (6.4)	N/A
Tensile Modulus, GPa (ksi)	3.18 (461)	N/A	1.724 (250)	1.25 (181)	N/A
Elongation at Break (in %)	4.8%	10.0%	3.0%	5.9%	N/A
Flexural Strength, MPa (ksi)	123.4 (17.8)	50 (7.25)	79 (11.45)	87.6 (12.70)	N/A
Flexural Modulus, GPa (ksi)	3.12 (452)	3 to 4 (435-580)	3.45 (500)	2.7 (391)	N/A
Density in g/cc (lbs/ in. ³)	1.1567 (0.042)	1.3500 (0.0488)	1.80 (0.065)	0.9466 (0.0342)	N/A
Specific Gravity	1.1597	N/A	0.94 to 1.17	0.95	1.15
Glass Transition Temperature (T _g), C (°F)	86.7 (188)	N/A	N/A	51.7 (125)	N/A
Curing Time (hours)	72	216	336	168	24 to 96
Viscosity (in cps)	600 to 700	N/A	500	300	1000

Special measures were needed for preparing the epoxy specimens. Release agents could not be used since they could compromise the diffusion characteristics of the epoxy. For this reason the specimens were cast on a 0.15

mm [0.006 in.] thick polyethylene sheet that could be easily peeled off after the resin had cured. Particular attention was paid to ensure that all air bubbles had been removed by placing the resin inside a laboratory vacuum oven for 15 to 30 minutes and using a hard roller that was applied repeatedly during fabrication.

Twenty four hours after the epoxy had been cast it was still pliable enough to be cut to a circular 98 mm [3.86 in.] diameter without damage to the 83 mm [3.27 in.] diameter test region (Figure 3-1). All specimens were tested after the resin had cured for at least seven days.



Figure 3-6 Test Specimens Set Up – 1 Control and 3 Test Cells

3.13 Test Details

All tests were conducted at ambient temperatures inside an air-conditioned laboratory. Three specimens were tested at a time. To account for oxygen consumption, an impermeable control (with a stainless steel specimen) was tested alongside. This set up is shown in Figure 3-6.

Aside from providing information on the oxygen consumed by the sensor, the control facilitated the detection of leaks and the identification of the effect of environmental variations, such as temperature fluctuations.

3.14 Corrected Data

Data obtained from testing were corrected for oxygen consumption as discussed earlier. Since the oxygen consumed by the sensor would otherwise have been present, it must be added to the raw data. This is shown in Figure 3-7 in which the broken line represents the raw data and the solid line the corrected data. The magnitude of the correction increases with concentration (see Figure 3-5).

3.15 Extraction of Permeation Constants

An analytical model using quasi-steady-state approximations, and based on standard diffusion theory (Crank 1968 and 1975, Bird et al. 2002) was developed to extract the permeation constants from the experimental data. In this model, time is divided into arbitrarily small intervals and the diffusion

process is considered to be at steady-state for each of these time intervals. Steady-state differential material balance and Fick's law with a constant permeation constant were then utilized with boundary conditions of ambient oxygen on the outside and concentration of the accumulated oxygen inside the cell, obtained from the previous time interval.

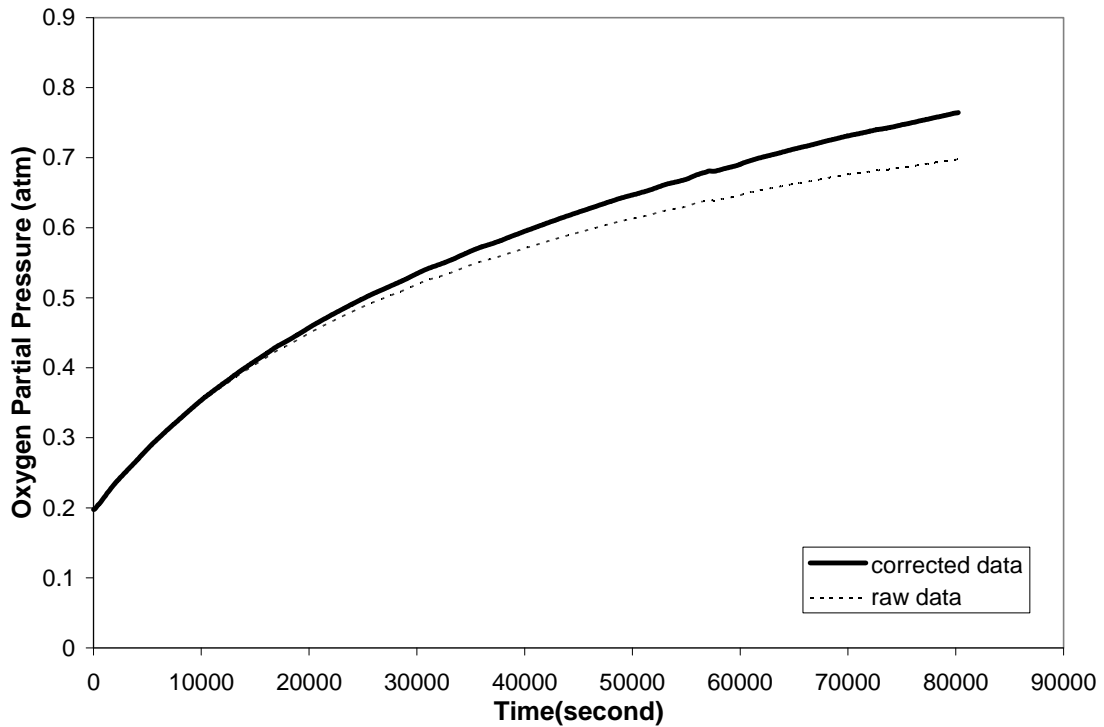


Figure 3-7 Raw and Corrected Data for Teflon Specimen

The partial pressure for oxygen, p , is calculated from its concentration, C , using the ideal gas law as

$$p = CRT \tag{3-3}$$

, where R is universal gas constant and T is temperature in Kelvin.

For each time interval, the steady-state differential material balance results in

$$\frac{dF}{dx} = 0 \quad (3-4)$$

Thus, the oxygen flux F is constant, *that is*

$$F = \text{Constant} \quad (3-5)$$

From Fick's law for constant permeation constant P ,

$$F = -P \frac{dp}{dx} \quad (3-6)$$

For each time interval Δt_i , the surface $x = 0$ is maintained at the constant, ambient partial pressure $p_{0,t}$ corresponding to the mole percentage of oxygen. At $x = h$, the thickness of the specimen, the partial pressure $p_{h,i-1}$ is assumed to be that of the accumulated oxygen in the diffusion cell at the end of the previous time interval, $i-1$. Solving the above model for the flux, the amount of oxygen accumulated (M_i moles) into the diffusion cell at time t_i , is given by

$$M_i = M_{i-1} + F_i \cdot A \cdot \Delta t_i = M_{i-1} + P \cdot \frac{p_{0,t} - p_{h,i-1}}{h} \cdot A \cdot (t_i - t_{i-1}) \quad (3-7)$$

where F is a molar flux, A is a surface area of membrane exposed to gas, p_0 and p_h are partial pressure of oxygen inside and outside of diffusion cell, respectively, and V is diffusion cell volume. Partial pressure p of oxygen in the cell at i^{th} interval is given by

$$p_{h,i} = \frac{M_i}{V} RT \quad (3-8)$$

where V is the diffusion cell volume. In this model, A is the surface area over which diffusion takes place.

The above model is fitted to the corrected data (p_{corr} raw experimental data corrected for oxygen consumption of sensor) of concentration vs. time to regress a value of P for each of the specimens. These values are summarized in Tables 3-2 and 3-3. It may be seen from Figures 3-8 to 3-14 that this quasi-steady-state model in MATLAB software program (Appendix I) fits the experimental data quite nicely.

Table 3-2 Teflon and PET Mylar Results

Specimens	Thickness in mm (in.)	Permeation from Quasi Steady State Model (mol m ² /m ³ atm. sec [mol ft ² /ft ³ atm. sec])		Published Data
Teflon	0.025 (0.0001)	7.12E-11 (2.17E-11)	8.83E-11 (2.69E-11) ± 2.17E-11 (6.61E-12)	16.2E-11 [4.93E-11] (Koros and Felder 1981)
	0.025 (0.0001)	7.48E-11 (2.28E-11)		
	0.025 (0.0001)	8.83E-11 (2.69E-11)		
	0.025 (0.0001)	1.19E-10 (3.6E-11)		
PET Mylar	0.076 (0.003)	4.13E-13 (1.26E-13)	3.7E-13 (1.13E-13) ± 4.7E-14 (1.43E-14)	4E-13 to 6.7E-13 [1.22E-13 to 2.04E-13] (Vasquez-Borucki et al. 2000)
	0.076 (0.003)	3.61E-13 (1.1E-13)		
	0.076 (0.003)	3.07E-13 (9.35E-14)		
	0.076 (0.003)	3.97E-13 (1.21E-13)		

3.16 Results

Table 3-2 compares the results for thin films of Teflon and PET Mylar obtained from this study with those available in the published literature. Each

test was carried out four times and as mentioned earlier, the set-up always included a control with a steel insert to provide a check on possible leaks.

It may be seen that even when samples of the same thickness are tested identically, the results obtained are not identical but fall within a range, e.g. for the four PET Mylar specimens with a thickness of 0.076 mm [0.003 in.], the permeation constants range from 3.07×10^{-13} to 4.13×10^{-13} mol m²/m³ atm. sec [9.35×10^{-14} to 1.26×10^{-13} mol ft²/ft³ atm. sec]. The difference in the results is due to unavoidable minor variations in the experimental conditions, e.g. air flow rate, temperature. The results compare favorably with the 4×10^{-13} to 6.7×10^{-13} (mol m²/m³ atm. sec [1.22×10^{-13} to 2.04×10^{-13} mol ft²/ft³ atm. sec] reported in the literature (Vasquez-Borucki et al. 2000). The results for Teflon $8.83 \times 10^{-11} \pm 2.17 \times 10^{-11}$ mol m²/m³ atm. sec [$2.69 \times 10^{-11} \pm 6.61 \times 10^{-12}$ mol ft²/ft³ atm. sec] are also of the same order of magnitude reported in the literature (Koros and Felder 1981) 16.2×10^{-11} mol m²/m³ atm. sec [4.93×10^{-11} mol ft²/ft³ atm. sec]. This agreement validates the test method developed in this research project.

3.16.1 Epoxy Results

The five different commercially available epoxies tested (Table 3-1) are used either with fiber reinforced polymers (A, Fyfe Co 2003 ; C, Sika 2003), waterproofing (B, Sika 2003), concrete repair (D, Air Products 2008) or boat repair (E, West System 2008).

Table 3-3 summarizes the oxygen permeation results for these epoxies. In each case, four separate samples of each type were tested. As with all tests on polymers, values fall within a range. For example, for epoxy B used for water proofing, the values range from 2.98×10^{-12} to 4.96×10^{-12} mol m²/m³ atm. sec [9.08×10^{-13} to 1.51×10^{-12} sec mol ft²/ft³ atm. sec] with an average value of $3.48 \times 10^{-12} \pm 1.278 \times 10^{-12}$ mol m²/m³ atm. sec [$1.06 \times 10^{-12} \pm 3.89 \times 10^{-13}$ mol ft²/ft³ atm. sec]. Most of the epoxies tested have permeation rates that are of the same order of magnitude.

Table 3-3 Permeation Results for Epoxy Polymers Tested

Specimens	Thickness in mm (in.)	Permeation from Quasi Steady State Model(mol m ² /m ³ atm. sec [mol ft ² /ft ³ atm. sec])		Application
A	0.285 (0.0112)	3.97E-12 (1.21E-12)	3.57E-12 (1.09E-12) ± 4.902E-13 (1.49E-13)	FRP
	0.233 (0.0093)	2.98E-12 (9.08E-11)		
	0.256 (0.010)	3.97E-12 (1.20E-12)		
	0.238 (0.0094)	3.34E-12 (1.02E-12)		
B	0.286 (0.0113)	2.98E-12 (9.08E-13)	3.48E-12 (1.06E-12) ± 1.278E-12 (3.89E-13)	Waterproofing
	0.326 (0.0128)	1.99E-12 (6.06E-13)		
	0.305 (0.0120)	3.97E-12 (1.21E-12)		
	0.349 (0.0137)	4.96E-12 (1.51E-12)		
C	0.253 (0.00994)	1.54E-12 (4.69E-13)	2.56E-12 (7.8 E-13) ± 1.272E-12 (3.87E-13)	FRP
	0.244 (0.0096)	3.66E-12 (1.11E-12)		
	0.266 (0.0105)	3.66E-12 (1.11E-12)		
	0.191 (0.00753)	1.39E-12 (4.22E-13)		
D	0.285 (0.0112)	8.92E-12 (2.72E-12)	7.68E-12 (2.34E-12) ± 9.479E-13 (2.89E-13)	Concrete Repair
	0.249 (0.0098)	6.94E-12 (2.11E-12)		
	0.345 (0.0136)	6.94E-12 (2.11E-12)		
	0.219 (0.0086)	7.93E-12 (2.42E-12)		
E	0.211 (0.00832)	3.52E-12 (1.07E-12)	2.87E-12 (8.74E-13) ± 1.224E-12 (3.72E-13)	Boat Repair
	0.239 (0.0094)	2.80E-12 (8.53E-13)		
	0.211 (0.00832)	1.18E-12 (3.59E-13)		
	0.229 (0.009)	3.97E-12 (1.21E-12)		

One of the materials, epoxy E was included in this study because in tests conducted by Wootton et al. 2003, its performance in corrosion repair was found to be poorer in comparison to epoxy B. The test results however, show their oxygen permeation rates to be comparable. This suggests that other factors (Baiyasi and Harichandran 2001) may have been responsible for their result.

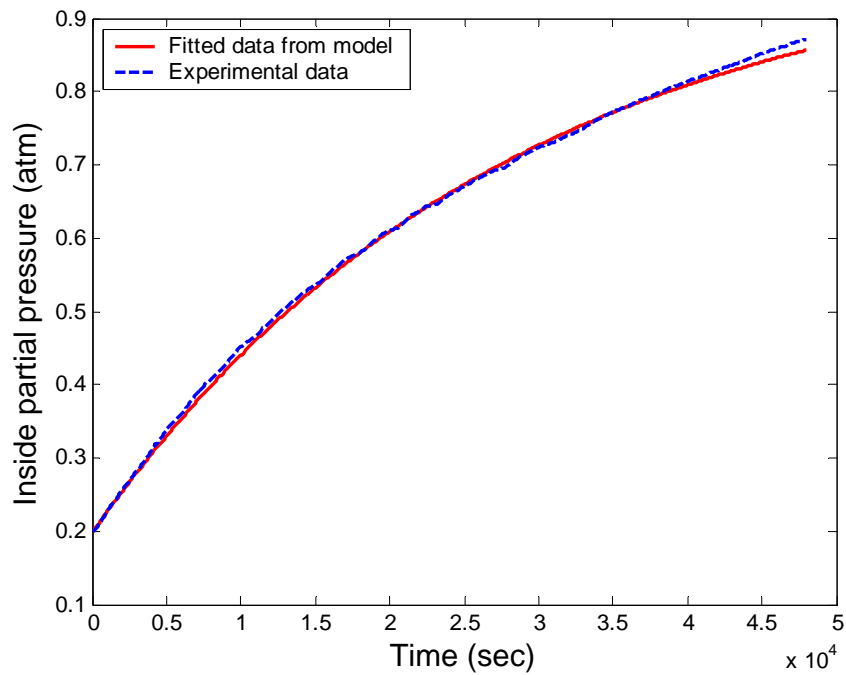


Figure 3-8 Experimental and Fitted Data for Teflon Specimen

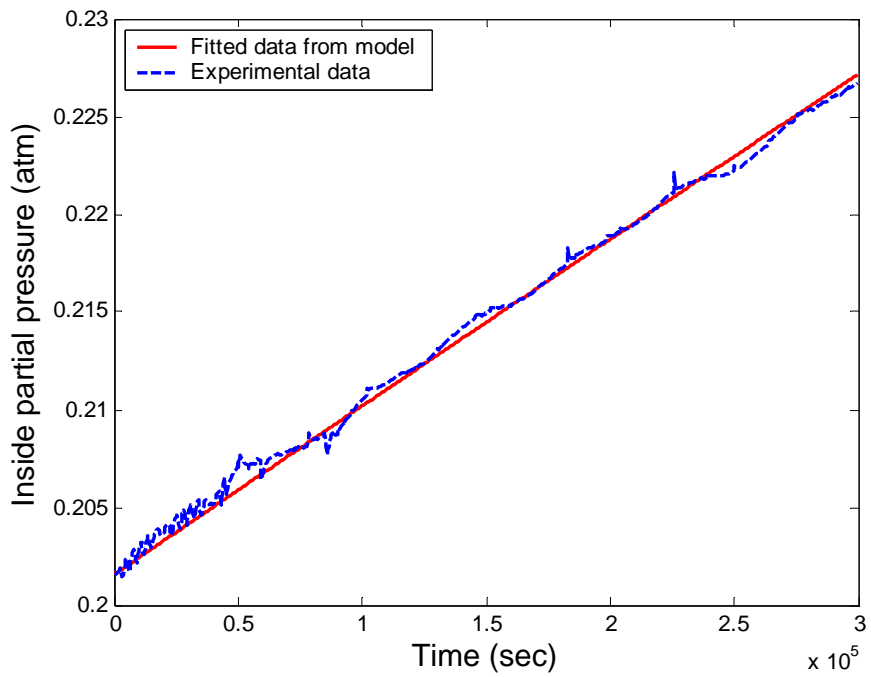


Figure 3-9 Experimental and Fitted Data for PET Mylar Specimen

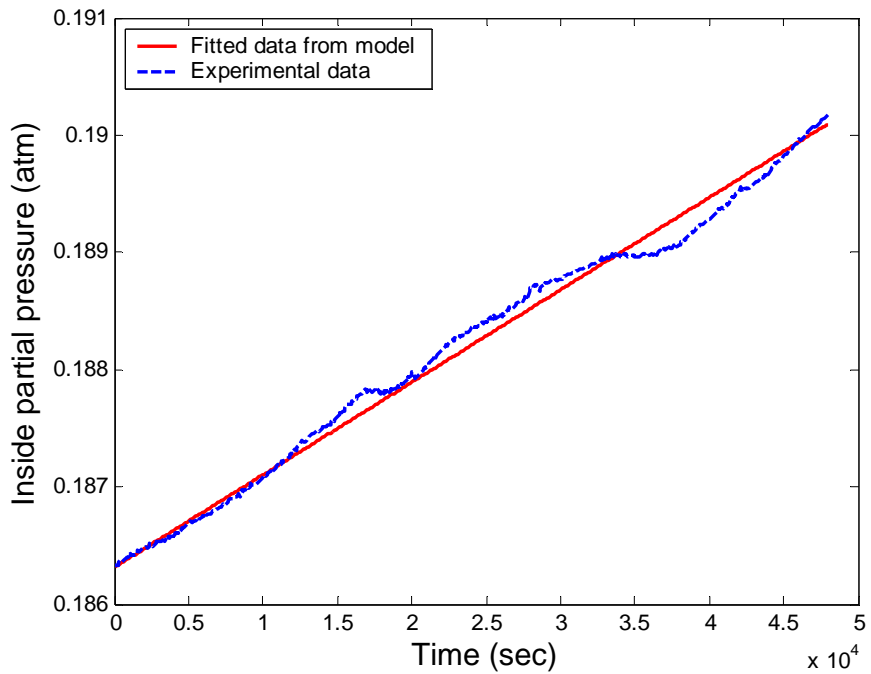


Figure 3-10 Experimental and Fitted Data for Epoxy A

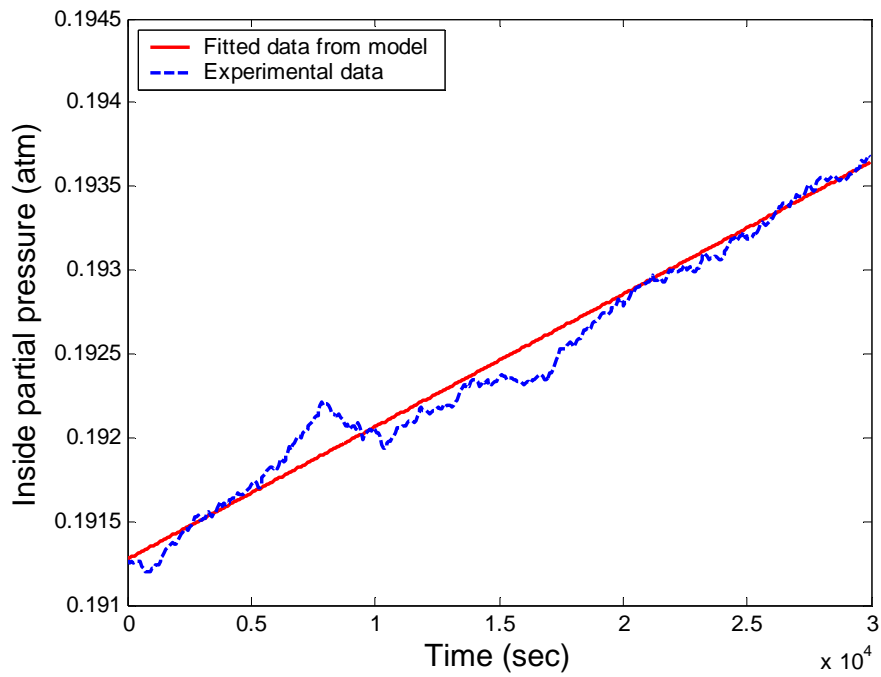


Figure 3-11 Experimental and Fitted Data for Epoxy B

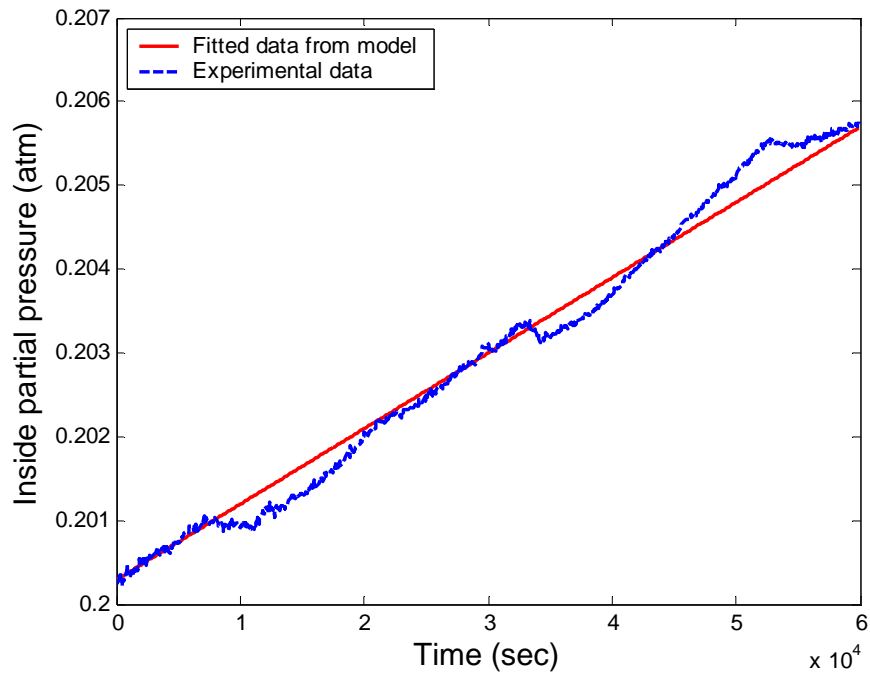


Figure 3-12 Experimental and Fitted Data for Epoxy C

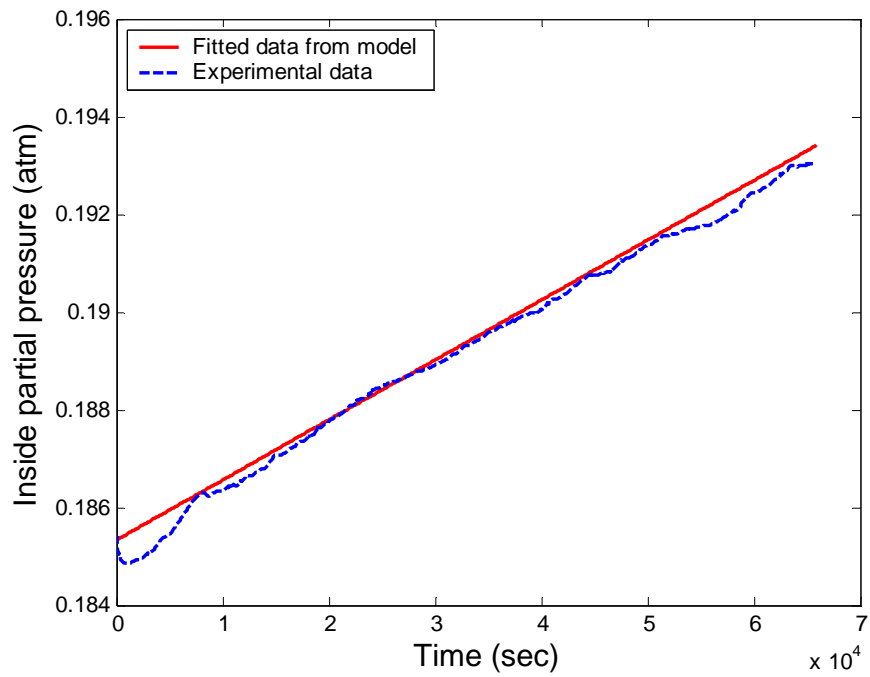


Figure 3-13 Experimental and Fitted Data for Epoxy D

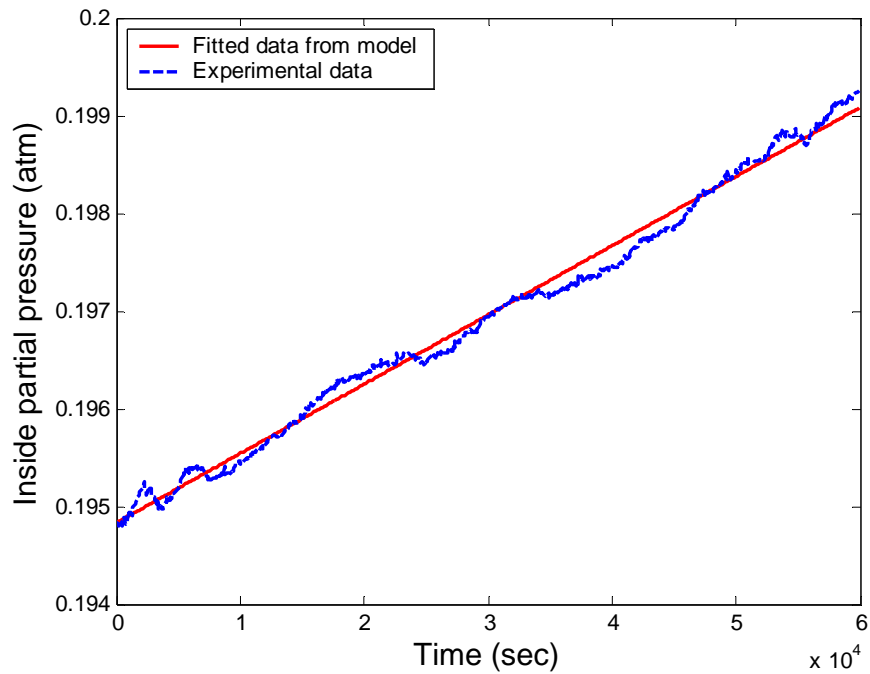


Figure 3-14 Experimental and Fitted Data for Epoxy E

3.17 Discussion

Available techniques for measuring oxygen diffusion constants developed for the food packaging or for the mining industry are not completely suitable for infrastructure applications where polymer elements used may be 5-10 times thicker requiring much longer testing time. The new diffusion cell (Figure 3-1) developed is versatile and can be used to test polymer samples having a wide range of thicknesses. This is made possible by the incorporation of several new features such as (1) the adjustable bolt length (2) the option for inserts (Figure 3-2) to reduce the diffusion chamber volume thereby reducing the time required to obtain results for thick, highly impermeable materials and (3) the use of two sensors (top and bottom, in Figure 3-1) to monitor the oxygen gradient.

Several improvements were made to the test procedure; these include the development of correction factors (Equation 3-2) to account for oxygen consumption by individual sensors and a test protocol in which four specimens were tested at a time with an impermeable stainless steel specimen control included in each test (Figure 3-6).

An analytical model developed allowed the extraction of the oxygen permeation constants. Tests on specimens for which results are available in the published literature showed very good agreement (Table 3-2). This provides confirmation on the validity of the proposed technique.

3.18 Application to Concrete

As noted earlier, epoxy coatings are applied to concrete surfaces as barrier elements to prevent deleterious materials from reaching the steel reinforcement and thereby control corrosion. The permeability constants obtained from this study may be used to *estimate* the reduction in corrosion rate by making appropriate simplifying assumptions (*an "exact" solution requires information on the corrosion reaction rate and the diffusion of oxygen through both the concrete cover and any iron oxide (rust) formed on the steel surface*).

In the simplified analysis presented, the corrosion process is assumed to be diffusion step limited. And both concrete and iron oxide are assumed to offer no resistance to oxygen diffusion because of their porous structure.

The analysis permits the determination of the corrosion rate of steel in chloride contaminated concrete whose exposed surface is protected by an epoxy coating. In essence, results from the study allow calculation of the number of moles of oxygen that reach the steel surface. The metal loss corresponds to the number of moles of iron that react with this oxygen (Broomfield 1997) as explained later.

3.19 Simplified Analysis

In practice, the thickness of the epoxy coating applied to a concrete surface varies from 1.5 to 2 mm [0.06 to 0.08 inch] (Liu and Vipulanandan 2005). This is much thicker than the epoxy specimens tested that ranged in

thickness from 0.19 to 0.35 mm [0.0075 to 0.0138 inch] (see Table 3-3). Nonetheless, the results are still applicable because permeability is a property of the polymer that is *independent* of thickness.

The *permeation rate*, N , (mol/m².sec [mol/ft².sec]), however, depends on the thickness of the coating. By definition, N (mol/m².sec) is given by

$$N = P \times (p_o - p_i) / x \quad (3-9)$$

In Equation 3-9, P is the permeability constant, x the thickness of the (epoxy) barrier, and p_o and p_i the partial pressures on its outer and inner surfaces. If the epoxy coated surface is exposed outdoors, p_o is 1 atm. The partial pressure on the inner surface, p_i , is taken as zero since it is assumed that whatever oxygen permeates through the barrier is immediately consumed. This implies that there is good bond between the epoxy and the concrete surface.

The total amount of oxygen (M in moles) that can reach the steel surface through the epoxy coated concrete (area A in m² [ft²]) over time t (in seconds) is obtained from the permeation rate, N by multiplication. Substituting $p_i = 0$, in Equation 3-9, M is given by Equation 3-10 as:

$$M = N \times A \times t = \frac{P \times p_o \times A \times t}{x} \quad (3-10)$$

Equation 3-10 may be used to calculate the number of moles of oxygen that reach the steel surface.

3.20 Numerical Example

A 2 mm [0.08 inch] thick epoxy A coating ($P = 3.57 \times 10^{-12}$ mol.m²/m³.atm.sec) is applied to a concrete slab reinforced by #16 [#5] bars uniformly spaced in the longitudinal and transverse directions. There are exactly three bars in each direction per m length as shown in Figure 3-15. The concrete surrounding the steel is chloride contaminated and its passive layer destroyed. Estimate the corrosion rate of the steel /year.

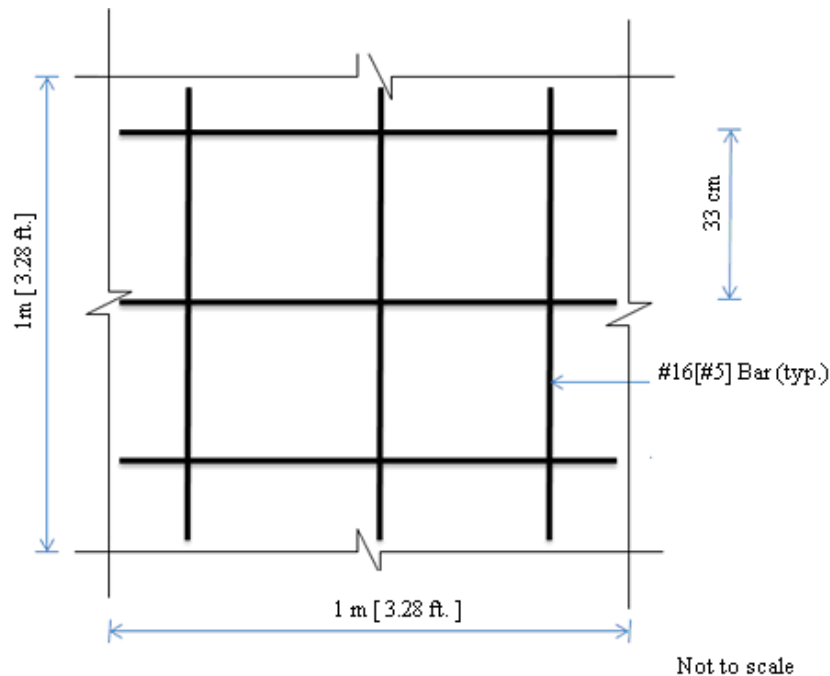


Figure 3-15 Steel Layout in Numerical Example

3.21 Solution

From basic electro-chemical corrosion theory (Broomfield 1997), 1 mole of oxygen reacts with 2 moles of iron to form rust. Therefore, if the number of

moles of oxygen reaching the steel surface is known (from Equation 3-10), the number of moles of iron converted to rust is twice this quantity. Using the relationship between molecular weight and moles, the metal loss can be determined. Knowledge of the metal loss allows calculation of the corrosion rate.

Calculate M using Equation 3-11,

$$M = \frac{P \times p_o \times A \times t}{x} = \frac{3.57 \times 10^{-12} \times 1 \times 3.15 \times 10^7}{0.002} = 5.63 \times 10^{-2} \text{ moles.} \quad (3-11)$$

This reacts with $2 \times 5.63 \times 10^{-2} = 0.1126$ moles of iron, equivalent to 6.29 g/m². This is the metal loss over one year over each square meter.

3.22 Calculation of Corrosion Rate

If corrosion is assumed to be uniform, its rate can be calculated. The 6.29 g [0.0139 lb] metal loss corresponds to a volume of 0.799cc [0.0488 in³] in six bars or $0.799/6 = 0.133$ cc [0.00813 in³] per bar over their 1 m [39.37 in.] length or 0.00133cc [2.065×10^{-4} in²] in its cross-section. The initial radius, r_o , of the #16 [#5] bar is 0.7958 cm [0.3125 in.] and its final radius, r_f can be calculated from the change in cross-section. That is,

$$\pi r_o^2 - \pi r_f^2 = 0.00133 \quad \text{or} \quad r_c = 0.7935 \text{ cm}$$

Thus, the corrosion depth is $0.7958 - 0.7935 = 3 \times 10^{-4}$ cm/yr [0.12 mils per year].

Using Faraday's law, the corrosion current density can be calculated as $0.2 \mu\text{A}/\text{cm}^2$ (for metal loss of 1.0488 g/bar) which is a very low corrosion rate.

This rate would be doubled if the thickness of the epoxy layer were halved since the metal loss is inversely proportional to the thickness of the epoxy coating (Equation 3-10).

More accurate predictions are possible if data on the permeability of the epoxy coated concrete members were available. In the interim, the permeability data provides a simple means for assessing its effectiveness as a protective barrier against electro-chemical corrosion of steel in reinforced concrete.

3.23 Summary and Conclusions

This chapter describes a new test method for measuring the oxygen diffusion characteristics of thicker polymer elements typically used in infrastructure applications. A quasi-steady-state model for the diffusion process was constructed, which allowed for the calculation of permeation constants from the experimental data. Permeation constants were obtained by fitting this model. Results obtained from the study show good agreement with those reported in the literature (Vasquez-Borucki et al. 2000, Koros et al. 1981).

The results presented show that all the epoxies tested had oxygen permeabilities that were of the same order of magnitude. This indicates that a range of available products are suitable for corrosion repair. Thus, it may be possible to optimize repair costs by selecting the most cost-effective epoxy system. A numerical example illustrates the application of the results.

Chapter 4 – Oxygen Permeability of Fiber Reinforced Laminates

4.1 Introduction

The poor performance of conventional repairs has led to renewed interest in the application of fiber reinforced polymer (FRP) for rehabilitating corroded concrete structures. Despite higher material costs, FRP may be more economical if it results in fewer re-repairs. Indeed, several highway agencies have used FRP for corrosion repair for precisely this reason. For example, in 1993, the Florida Department of Transportation selected FRP to repair a corrosion-damaged bridge over SR 24 in Melbourne, Florida. In 1994, the Vermont Transportation Agency chose FRP for repairing corrosion-damaged columns over conventional repairs as it led to 35% savings, Tarricone 1995. Later, New York State DOT opted for FRP for repairing corrosion damaged columns because it cost less, Alampalli 2001. More details on the use of FRP by various highway agencies may be found in a state-of-the-art paper Sen 2003.

Several investigators have presented data confirming that the rate of corrosion is reduced when FRP is used, e.g. Sheikh et al. 1997, Berver et al. 2001. The mechanism for such a reduction is not known; however, it is speculated that the FRP serves as a barrier element that slows down corrosion

by preventing the ingress of deleterious materials. Experimental results reported were sometimes anomalous and counter intuitive. For example, researchers reported that the performance was poorer when a greater number of FRP layers were used, e.g. Wootton et al. 2003, Suh et al. 2007.

Chloride-induced corrosion is by far the most pervasive corrosion in reinforced or prestressed concrete elements. Diffusion of chloride ions to the level of the steel reinforcement results in the destruction of the passive layer that normally protects steel from corroding. Following its destruction, the presence of oxygen and moisture allows the electro-chemical reactions to continue unabated resulting in corrosion of steel.

Hence, it is evident, that the effectiveness of FRP corrosion repairs is contingent on its ability to keep out both moisture and oxygen. As the size of the oxygen molecule is smaller than that of water or chloride molecules, its diffusion rate through FRP is the more critical. This is because the larger the molecular diameter and the stronger the interactions, the smaller the diffusion constant. Thus, oxygen with its smaller molecular diameter has a larger diffusion constant and will therefore diffuse faster than both chlorides and water.

Several experimental and theoretical studies have been conducted by the aerospace industry to investigate thermo-oxidation effects of CFRP laminates, e.g. Colin et al. 2005, Pochiraju and Tandon 2009. The focus of these studies was chemical degradation caused by extended exposure to high temperature, e.g. Pochiraju and Tandon 2009 reported that tests were carried out at a

temperature of 288° C. Since reaction rates are exponentially dependent on temperature, such degradation is likely to be negligible for FRP used in infrastructure applications where they are exposed to ambient outdoor environments.

This chapter focuses on the determination of the oxygen diffusion characteristics of FRP used in infrastructure applications. In the study, a new test method and a new analytical method were developed. Results obtained using this method showed excellent agreement with published data, Khoe et al. 2010. The application of this method to determine the oxygen permeation rates for the two most commonly used FRP materials; carbon and glass are presented in this chapter. A brief summary of relevant information on diffusion testing is first presented followed by details of the test program, results and their discussion.

4.2 Objectives

The goal of the study was to determine oxygen permeation rates of fiber reinforced laminates used in infrastructure applications that were fabricated using wet lay-up techniques. Commercially available carbon and glass material were evaluated. The laminates tested were single or dual layer, unidirectional or bidirectional. In addition, laminates with randomly oriented fibers were tested to determine the effect of fiber architecture on oxygen permeation rates.

4.3 Diffusion Basics

Barrier elements are widely used by industries as diverse as food packaging, mining, paint and petroleum refining. Its role is to preserve contents or prevent corrosion; effectiveness is gauged by the ability to prevent transmission of deleterious material. This is typically characterized by the diffusion constant, D , derived from Fick's law and expressed in units of m^2/sec . Effective barriers have small diffusion constants.

The transport of gases by diffusion is driven by concentration gradients; therefore, experimental determination of the diffusion constant requires a diffusion cell that allows the two exposed surfaces of the test material (FRP in our case) to be kept at different gas concentrations. In the analysis, partial pressures rather than concentrations were used but this yields a permeability constant P rather than a diffusion constant. The permeability constant is defined as the rate per unit area at which a gas passes through a material of unit thickness under one unit pressure difference expressed in units of $\text{mol.m}^2/\text{m}^3.\text{atm.}\text{sec}$. In practical applications, the permeability constant is more useful than the diffusion constant; for example, in diffusion-step limited corrosion processes, the permeation constant can be directly used to calculate metal loss due to corrosion, as illustrated in Khoe et al. 2010.

An analytical model was developed using quasi-steady-state approximations to extract the permeation constants from the experimental data. This is based on standard diffusion theory, Crank 1975; Bird et al. 2002. In the

model, time is divided into arbitrarily small intervals, e.g. 60 seconds, and the diffusion process is assumed to be steady-state for each time interval. Steady-state differential material balance and Fick's law for a constant permeation constant are then utilized to satisfy the boundary conditions used in the testing. These were ambient oxygen on one FRP surface exposed to air and the measured accumulated oxygen inside the diffusion chamber for the previous time interval for the other surface. More details on the analysis may be found elsewhere, Khoe et al. 2010.

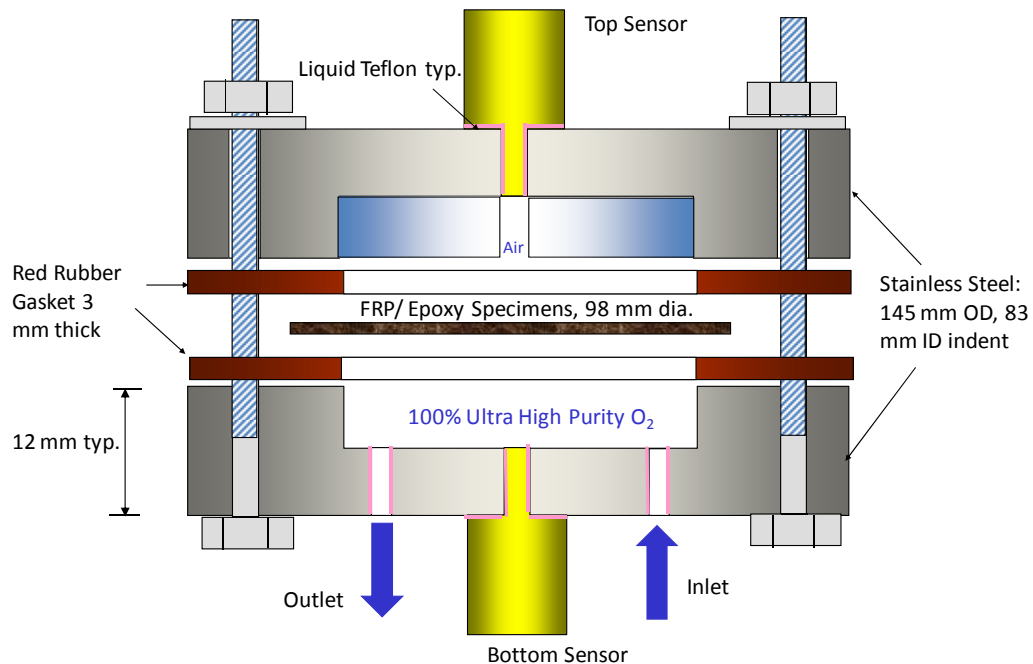


Figure 4-1 Schematic Diagram of Diffusion Cell

4.4 Measuring Permeability Constants

Concentration gradients can be experimentally set up using vacuum or non-vacuum based systems. Since non-vacuum based systems are less complex,

a new non-vacuum based diffusion cell was developed in this study. The new system is based on existing systems described in ASTM standards and in the published literature, ASTM D3985-05 2005; ASTM F1307-02 2002; Trefry 2001, but refined so that it can be used for infrastructure applications involving FRP and concrete. Brief details are presented here; more complete information may be found elsewhere, Khoe et al. 2009.

4.5 Diffusion Cell

The diffusion cell developed for the study is shown in Figure 4-1. It consists of two 12 mm thick circular stainless steel plates 145 mm outside diameter. The central part of these plates was machined to create a diffusion chamber for the test specimen with a volume of $1.7617E-5 \text{ m}^3$. However, this volume can be reduced by using appropriate aluminum inserts.

The FRP test specimen is positioned between the two 145 mm diameter plates and 3 mm thick red rubber gaskets that were used to provide an airtight seal, Paul 1965. The two parts of the diffusion cell are assembled together using eight stainless steel bolts, nuts and washers. A special, calibrated digital torque wrench was used to ensure uniformity in the tightening force. As the lengths of the bolts can be varied, it provides a simple method for testing samples of different thickness.

The cell is assembled in air and therefore one surface of the specimen has the same oxygen concentration as air (20.7% of oxygen). The other surface is

flushed with 100% concentration oxygen that is released from a standard oxygen cylinder at the rate of 100 Standard Cubic Centimeters per Minute (SCCM). This required threaded inlet and outlet openings in the bottom plate that were fabricated as shown in Figure 4-1. These connections were made leak proof by using liquid threaded seal Teflon in conjunction with a Swagelok male connector.

4.6 Oxygen Sensor

Two galvanic cell type oxygen sensors 50 mm x 23 mm diameter were used to monitor the oxygen concentration at the top and bottom of the diffusion cell. The connections to both sensors were also made leak proof using specially fabricated threaded openings and liquid threaded seal Teflon. Each sensor has to be individually calibrated against certified oxygen concentration levels.

The sensors were connected to an Agilent 34970A data acquisition system to allow data to be recorded and stored at a desired scan rate. This data set could be retrieved later for subsequent analysis. A data acquisition switch unit with two multiplexers attached to 16 channels and 20 channels was used. Temperature data was recorded simultaneously.

4.7 Sensor Oxygen Consumption

The oxygen concentrations measured by the sensors rely on electro-chemical reactions with oxygen molecules. As a result, some oxygen is consumed during the testing. Information on this consumption provided by the

manufacturers Figaro 2004 is generic and may not fully apply for all test conditions. For this reason, extensive tests were conducted to determine the actual consumption rates in individual sensors used in this study.

Five series of tests were conducted to measure the variation in the oxygen consumption rate with the concentration varying from 19-89%. This data was used to develop appropriate consumption rates at different oxygen concentrations to correct the experimental data. More details may be found in Khoe et al. 2010.

Table 4-1 Epoxy Materials Property

Property	A	B	C	D
Density, pcf [kg/m ³]	99.9 [1,600]	61.3 [983]	67.6 [1,082]	72.3[1,160]
Tensile Strength, psi [MPa]	N/A	8,000 [55.2]	7,150 [49.3]	8,000 [55]
Elastic Modulus, ksi [MPa]	N/A	440 [3,034]	289.3 [1,995]	250 [1,724]
Flexural Strength, psi [MPa]	8,000 [55.2]	20,000 [138]	11,140 [76.8]	11,500 [55]
Flexural Elastic Modulus, ksi [MPa]	N/A	540 [3,724]	252.4 [1,740]	500 [3,450]
Viscosity at room temperature (25°C), cps	14,000-18,000	1600	1500-1600	500
Mixing time, min.	5	3	3	5
Mixer speed, rpm	400-600	600	400-600	400-600
Color	gray	Blue	pigmented syrup, amber	clear, amber
Approx. Cure Time, days	7	7	3	14

Note: N/A is not available

4.8 Experimental Program

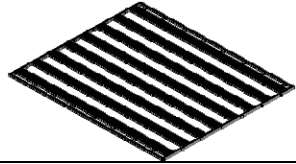
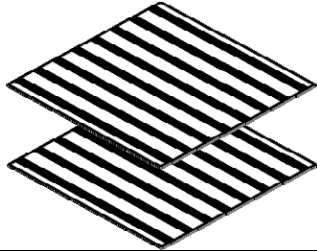
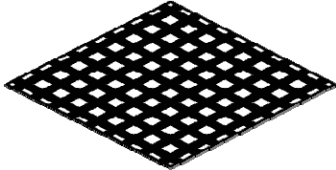
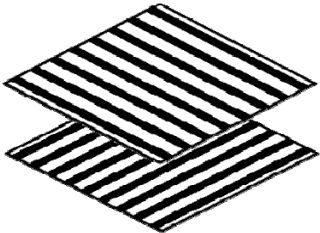

To meet the goals of this research, four commercially available FRP systems were evaluated. These are identified as systems A-D in this chapter. In each system, both carbon and fiberglass were tested and four alternative configurations shown in Figure 4-2 evaluated. These were unidirectional /

bidirectional that are most commonly used in repairs (Figure 4-3). In addition, a random orientation was explored in which fibers were cut into small pieces and saturated with resin to prepare the specimen. This simulated repair applications in which FRP is installed using shotcreting, Banthia and Boyd 2000.

Material properties of the resin and the four fiber systems are summarized in Tables 4-1 and 4-2. Table 4-1 provides information on the physical and mechanical properties of the resin including viscosity, mixing and cure time. Table 4-2 summarizes mechanical and physical properties of the fibers for the four systems. Excepting for System B that only had unidirectional fibers, the remaining three systems had at least one material with both unidirectional and bidirectional fibers.

Table 4-2 FRP Fabric Material Property

System	Fiber Type	Fiber Orientation	Fiber Density, lb/in ³ [g/cm ³]	Areal Weight, lb/ft ² [g/m ²]	Fabric Width, inch [mm]	Nominal Thickness, t _r in/ply [mm/ply]	Tensile Strength, ksi [MPa]	Tensile Modulus, ksi [GPa]	Elongation, %
A	Carbon	0°	0.063 [1.74]	0.1331 [644]	24 [610]	0.04 [1.0]	550 [3,790]	33,400 [230]	1.00%
	Glass	0°	0.092 [2.55]	0.1891 [915]	54 [1,373]	0.014 [0.36]	470 [3.240]	10,500 [72.4]	4.50%
	Glass	0°/90°	0.092 [2.55]	0.0611 [295]	50 [1,270]	0.01 [0.25]	470 [3.240]	10,500 [72.4]	4.50%
B	Carbon	0°	0.0614 [1.7]	0.062 [300]	20 [500]	0.0065 [0.165]	720 [4,950]	33,000 [227]	1.67%
	Glass	0°	0.0936 [2.6]	0.186 [900]	24 [610]	0.0147 [0.373]	220 [1,517]	10,500 [72.4]	2.10%
C	Carbon	0°	0.065 [1.8]	0.128 [627]	25 [635]	0.0399 [1.01]	550 [3,800]	33,500 [231]	1.10%
	Carbon	0°/90°	0.065 [1.8]	0.139 [677]	50 [1,270]	0.05 [1.27]	550 [3,800]	33,500 [231]	1.00%
	Glass	0°	0.0556 [1.54]	0.139 [677]	50 [1,270]	0.037 [0.94]	63.7 [439]	2,940 [20.27]	2.20%
	Glass	0°/90°	0.556 [1.54]	0.1667 [812]	50 [1,270]	0.04 [1.0]	45.6 [314]	2,130 [14.685]	1.90%
D	Carbon	0°	0.065 [1.8]	0.1269 [618]	25 [635]	0.04 [1.0]	550 [3,793]	34,000 [234.5]	1.50%
	Carbon	0°/90°	0.065 [1.8]	0.04 [196]	50 [1,270]	0.010 [0.025]	66 [456]	6,000 [41.4]	1.50%
	Glass	0°	0.092 [2.54]	0.187 [913]	50 [1,270]	0.014 [0.359]	330 [2,276]	10,500 [72.413]	4%

Type	Fiber Architecture		Remarks
1	Unidirectional one layer		N/A
2	Unidirectional two layers		N/A
3	Bidirectional		Bidirectional one layer
			Bidirectional using 0°/90° unidirectional fibers (two layers)
4	Random		Chopped fibers (25-75 mm) placed randomly in matrix

Note: N/A is not available

Figure 4-2 Fiber Orientation in Laminates Tested

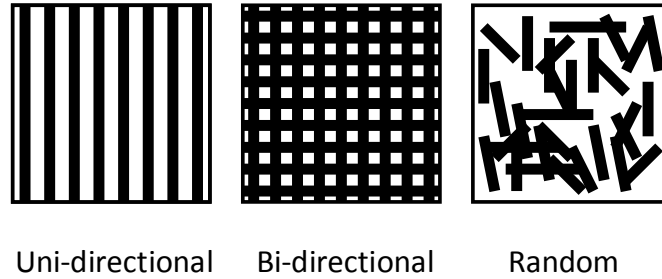


Figure 4-3 Fiber FRP Orientation

4.9 Sample Preparation

The diffusion cell was designed to be circular to facilitate the application of uniform pressure along the perimeter of the test specimen using the eight symmetrically placed bolts. This was an important consideration since pressure prevented leakage. This meant that the test specimens also had to be circular. The approximate diameter of the test specimen was 98 mm to provide adequate bearing length on either side of the 83 mm annular opening in the diffusion cell (Figure 4-1).

To prepare circular specimens, the FRP fabric has to be cut into the required circular shape. However, if this approach is used, there is a tendency for the fibers to spread along the perimeter that can introduce voids in the 83 mm of diameter test window. This would result in artificially higher permeation values that would not be representative of actual practice. Several attempts were made to solve this problem. For example, after the fabric had been cut to a circular shape, the fibers along the edges were stitched. But, this approach resulted in resin overrun along the boundaries that could crack. Moreover, stitching along

the perimeter of small diameter specimens was very time consuming and did not yield reproducible results.

In view of this, an alternative fabrication method was devised. In this method, 30 cm x 30 cm fiber strips were saturated with resin and placed on a 0.1524 mm thick polyethylene sheet that rested on a flat surface. A second polythene sheet was placed over the resin soaked fibers and a steel roller was used to remove air bubbles. Circular specimens were obtained after 8-10 hours of curing by carefully cutting around a circular template. At that time, the resin was rubbery and did not crack. This method allowed four specimens to be made at a time. The approach was faster and yielded specimens that were more representative of wet lay-up used in field applications. The thickness of the test specimens ranged from 0.3 mm to 3.25 mm; and the volume fiber fraction average for test specimens systems A-D ranged from 22% to 42% (Kaw 2005, Appendix II).

4.10 Test Details

All tests were conducted after the laminate had cured for the time recommended by the manufacturer (Table 4-1). In the testing, the FRP laminate was carefully centered over the opening in the lower plate and placed on a rubber gasket. The upper rubber gasket was then placed over it. The two parts of the cell were now assembled using bolts, nuts and washers that were symmetrically tightened to a specified torque of 10.2 N-m using a digital torque

wrench. This operation is crucially important for preventing leaks from developing.

Oxygen concentrations on both faces of the test specimen were monitored throughout. One face was subjected to ultra high purity (100%) oxygen while the other face was exposed to air. To ensure steady state conditions, oxygen was circulated constantly for 24 hours using a flow rate of 100 SCCM.

To verify that there were no leaks, two diffusion cells were tested at a time - one containing the FRP test specimen and the other a control containing an impermeable steel insert. The top sensor reading in Figure 4-1 corresponding to the surface of the stainless steel specimen exposed to air showed a decrease over time since no oxygen permeated through the steel. This decrease was due to oxygen consumed by the sensor in that chamber. In contrast, the same sensor showed increases over time for the FRP specimen. This increase offset the oxygen consumed by the sensor and was due to diffusion of oxygen through the FRP. Any departures from this response would indicate leaks in the system.

The transport of gases is very sensitive to temperature. Minor fluctuations in temperature caused by opening of doors, movement of personnel, changes in air-conditioning can lead to poor results. Therefore, particular attention was paid to minimize such effects by enclosing the diffusion cells inside an insulated box. Readings were recorded every minute and a typical test ran for 24 hours.

4.11 Corrected Data

Data was corrected for oxygen consumption as discussed earlier. Since the oxygen consumed by the sensor would otherwise have been present, it must be added to the raw data. The correction is greater at higher concentrations, Khoe et al. 2010.

Table 4-3 Oxygen Permeation Constant Values for Epoxy and FRP Laminates

Type	Specimens Permeation in mol m ² /m ³ atm sec							
	A		B		C		D	
	Permeation	Average	Permeation	Average	Permeation	Average	Permeation	Average
Epoxy only	4.060E-12	3.670E-12	1.288E-11	8.920E-12	1.540E-12	2.956E-12	3.466E-12	3.764E-12
	4.150E-12	±	4.960E-12	±	3.664E-12	±	3.970E-12	±
	2.800E-12	7.548E-13	8.920E-12	3.960E-12	3.664E-12	1.226E-12	3.856E-12	2.643E-13
CFRP unidirectional one layer	1.900E-12	5.260E-12	2.710E-12	2.380E-12	3.160E-12	2.620E-12	3.970E-12	4.116E-12
	3.970E-12	±	1.630E-12	±	2.180E-12	±	4.521E-12	±
	9.910E-12	4.158E-12	2.800E-12	6.511E-13	2.520E-12	4.976E-13	3.857E-12	3.553E-13
CFRP unidirectional two layers	9.910E-12	1.294E-11	6.535E-11	6.998E-11	4.654E-11	3.588E-11	2.872E-11	4.677E-11
	9.910E-12	±	4.550E-11	±	3.541E-11	±	4.586E-11	±
	1.900E-11	5.248E-12	9.910E-11	2.710E-11	2.568E-11	1.044E-11	6.574E-11	1.853E-11
GFRP unidirectional one layer	9.820E-12	6.700E-12	7.822E-12	4.924E-12	4.960E-12	5.862E-12	7.930E-12	5.592E-12
	6.400E-12	±	2.980E-12	±	6.940E-12	±	2.980E-12	±
	3.880E-12	2.981E-12	3.970E-12	2.558E-12	5.687E-12	1.002E-12	5.867E-12	2.486E-12
GFRP unidirectional two layers	2.620E-11	2.203E-11	1.720E-11	1.336E-11	1.387E-11	1.335E-11	5.950E-12	1.316E-11
	2.530E-11	±	1.099E-11	±	1.288E-11	±	1.585E-11	±
	1.460E-11	6.453E-12	1.189E-11	3.356E-12	1.330E-11	4.969E-13	1.768E-11	6.311E-12
CFRP bidirectional one layer	8.920E-12	5.740E-12	7.802E-12	8.844E-12	1.981E-11	2.535E-11	1.090E-11	3.317E-11
	4.330E-12	±	9.900E-12	±	2.125E-11	±	2.986E-11	±
	3.970E-12	2.760E-12	8.830E-12	1.049E-12	3.498E-11	8.374E-12	5.876E-11	2.410E-11
GFRP bidirectional one layer	5.545E-11	4.660E-11	3.706E-12	4.602E-12	3.548E-11	2.634E-11	4.877E-12	4.100E-12
	6.535E-11	±	4.555E-12	±	2.476E-11	±	5.877E-12	±
	1.900E-11	2.441E-11	5.545E-12	9.203E-13	1.877E-11	8.466E-12	1.547E-12	2.267E-12

Note: ± in the average value is based on standard deviation

4.12 Results

The results from the study are summarized in Tables 4-3 and 4-4. Table 4-3 contains results for the unidirectional and bidirectional systems for the three fiber orientations, Types 1-3, shown in Figure 4-2. In addition, the results for the epoxy used to make the laminate are also included. The results for randomly oriented fibers, Type 4 in Figure 4-2, are presented separately in Table 4-4. Each table provides results for the four different systems A-D (Table 4-2) that were tested. Overall, twenty seven tests were carried out for each system and for the four systems, a total of one hundred and eight tests were conducted.

Table 4-4 Oxygen Permeation Constant Values for Randomly Oriented FRP Laminates

Type	Specimens Permeation in mol m ² /m ³ atm sec							
	A		B		C		D	
	Permeation	Average	Permeation	Average	Permeation	Average	Permeation	Average
Random CFRP	2.530E-12	4.630E-12	3.961E-09	1.409E-09	5.877E-10	6.767E-10	1.387E-11	3.588E-11
	8.920E-12	±	2.530E-10	±	5.950E-10	±	2.588E-11	±
	2.440E-12	3.716E-12	1.180E-11	2.214E-09	8.475E-10	1.479E-10	6.789E-11	2.836E-11
Random GFRP	1.189E-11	1.453E-11	1.099E-09	7.300E-10	1.099E-10	4.676E-10	2.080E-10	3.758E-10
	2.575E-11	±	2.980E-10	±	6.940E-10	±	1.048E-10	±
	5.950E-12	1.016E-11	7.930E-10	4.042E-10	5.988E-10	3.134E-10	8.145E-10	3.834E-10

Note: ± in the average value is based on standard deviation

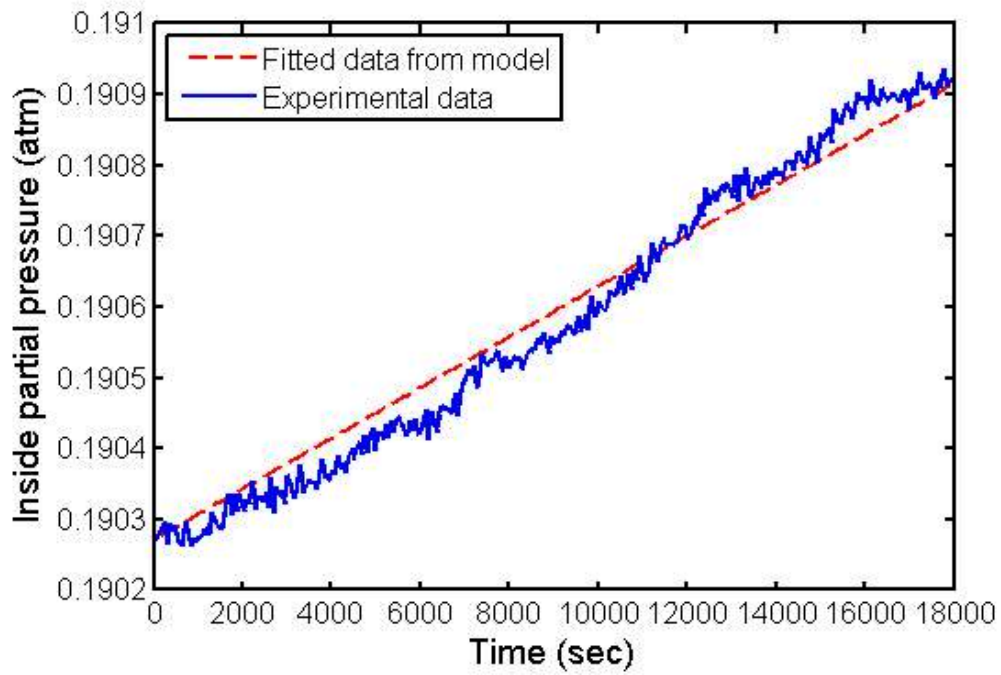


Figure 4-4 Experiment and Fitted Data for Glass FRP One Layer of Fiber

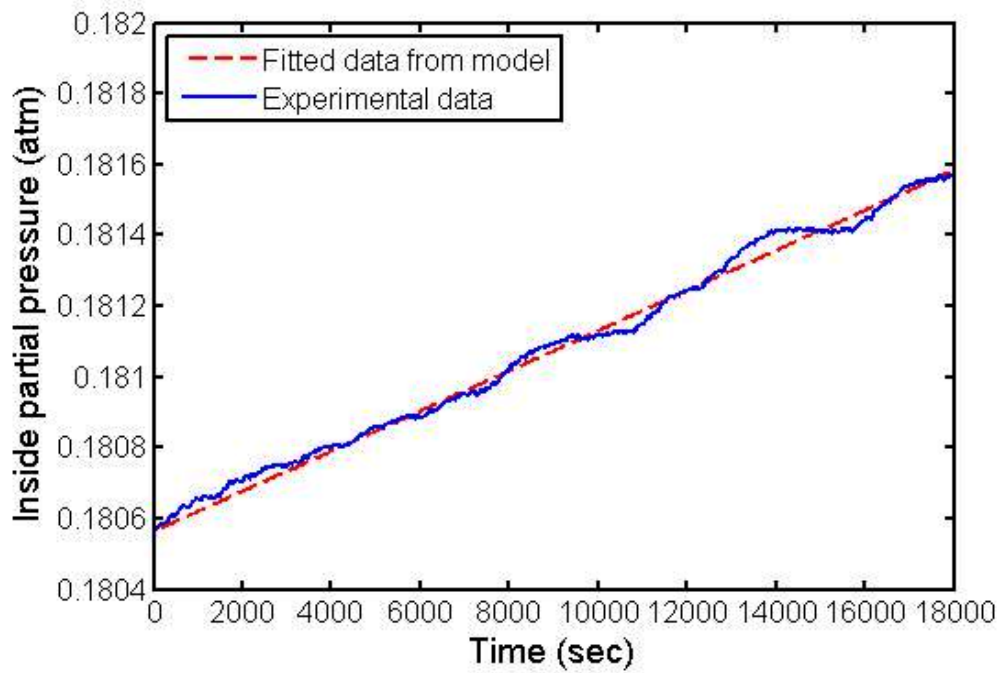


Figure 4-5 Experiment and Fitted Data for Glass FRP Two Layers of Fiber

As noted earlier, the permeation constants reported in Tables 4-3 and 4-4 were obtained from a quasi-steady state model. Typical plots showing the variation in partial pressure (atm.) inside the chamber with time (seconds) are shown in Figures 4-4 to 4-5 for one layer and two layer laminates. Though data was recorded continuously for 24 hours only 5-6 hours of data was necessary to obtain the permeation constant as shown in these figures. The dotted line corresponds to the fitted data obtained from the model used to extract the permeation constant. Despite some noise in the data, there is good agreement between the experimental and the fitted data from the model.

Results reported in Tables 4-3 and 4-4 show some variation in the values of the permeation constant that is characteristic of such measurements and accounts for unavoidable variations in the laboratory environment while the test was in progress. However, in this case, they also incorporate the random effects of workmanship since not all the 108 specimens tested were made at the same time.

Table 4-3 shows that in general, permeation constants for epoxies are lower than that for the FRP laminates. Very limited data is available on the diffusion constant of FRPs; however, the values for unidirectional CFRP laminates obtained from this study are comparable to that reported by Collins et al. 2005. In their study, optical microscopy was used and the diffusion constant reported as $2.1 \times 10^{-10} \text{ m}^2/\text{s}$. This converts to $3.7 \times 10^{-11} \text{ mol.m}^2/\text{m}^3.\text{atm.}\text{sec}$, Bird 2002.

It may be seen from Table 4-3 that permeability constants tend to be smaller for one layer systems regardless of whether they are carbon or glass ($\sim 10^{-12}$). Typically, there is an order of magnitude difference between single and two layer laminates ($\sim 10^{-11}$). This difference is best illustrated in Figure 4-6 in which normalized results are plotted in bar diagram form. The normalization is relative to the respective average epoxy value. Inspection of Figure 4-6 shows that though there are instances where FRP has a lower permeability constant than the epoxy, e.g. System B one layer unidirectional CFRP, in most cases, permeability is considerably higher. In some instances there is an order of magnitude difference in the results, e.g. systems C, D for 2-layer unidirectional CFRP.

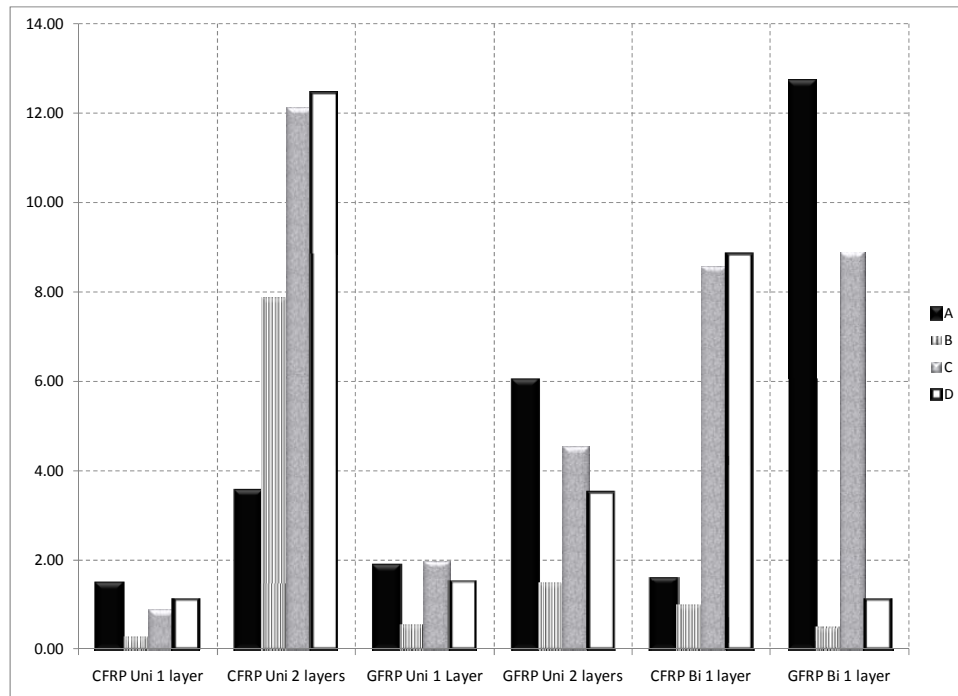


Figure 4-6 Comparison of Normalized Permeation Constant

Figure 4-7 plots the corresponding normalized results for the specimens with randomly oriented chopped fibers. Again, the normalization is with respect to the average oxygen permeation value for epoxy. It may be seen that system A gave good results for both CFRP and GFRP and system D gave good results for CFRP. The results for the remaining systems were significantly poorer.

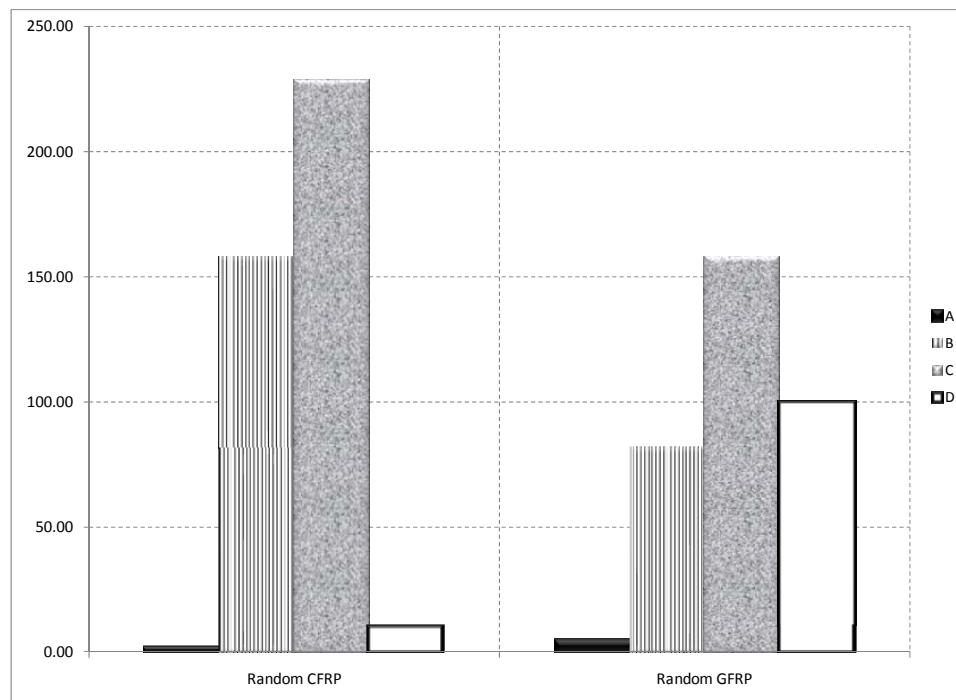


Figure 4-7 Comparison of Normalized Permeation Constant for Random Laminates

4.13 Discussion

The results clearly indicate that oxygen permeability is a function of fiber architecture. Results for laminates with randomly oriented chopped fibers were

much poorer than those for unidirectional or bidirectional lay-up as expected. However, the finding that single layer laminates were less permeable than two layer laminates was puzzling. Interestingly, this finding supports experimental results presented earlier by researchers, e.g. Debaiky et al. 2002, Wootton et al. 2003, and Suh et al. 2007.

Table 4-5 Void Ratios in CFRP Laminates

Layers	T_d^1 in % (gr/cm ³)	M_d^2 in % (gr/cm ³)	Void Ratio	Average
1 Layer	1.1446	1.1336	0.97%	1.22%
	1.086	1.0723	1.26%	
	1.0917	1.076	1.44%	
2 Layers	1.0746	1.06	1.36%	1.94%
	1.1643	1.1391	2.16%	
	1.1338	1.108	2.28%	

¹Theoretical composite density, ²Measured composite density

To understand these results, the void content of selected 1-layer and 2-layer specimens was determined. Available facilities to determine void content in accordance with ASTM D2584/D2734 limited testing to CFRP specimens. The results of tests on six representative 1-layer and 2-layer CFRP specimens are summarized in Table 4-5. This table contains values of the measured (M_d) and the theoretical composite (T_d) densities that are used in the calculation of the void ratio in accordance to ASTM D2734. Inspection of Table 4-5 shows that the average void content in the 1-layer specimen was 1.22% versus 1.94% for the two layer specimens. The higher void content in the 2-layer specimen explains why its oxygen permeation constant value was higher.

It should be noted, however, that the experimentally obtained void content is very small. In field applications, the void content will be much higher and vary between 3-5% because of the unevenness of the bonding surface that make it more difficult to expel air bubbles using rollers. In such cases, only mechanical methods, e.g. vacuum can remove the air bubbles.

The main difference between 1-layer and 2-layer systems is the interface between the two layers. Whereas, the surface of a single layer permits air bubbles to directly dissipate in the air, this is less possible where two layers are present. In this case, air bubbles can be trapped at the interface.

To test this hypothesis, the micro-structure of selected specimens was examined using a Focus Ion Beam (FIB) in Scanning Electron Micrograph (SEM) mode. The samples for examination were prepared by cutting the test specimens using a diamond saw in directions perpendicular to the fiber. For specimens with randomly oriented fibers, no special attention was paid to the direction of the cut. The test specimens were then mounted in the FIB SEM machine and images at various magnifications viewed. A selected number of these images were saved.

Figures 4-8 to 4-11 show typical micrographs obtained for the glass fiber laminates (similar micrographs were also obtained for the carbon & laminates are shown in Appendix III & IV). These were taken at relatively low magnifications so that layers and voids could be clearly seen. It should be emphasized that the

micrographs focus on a very small localized region and it took considerable amount of time and effort to detect the voids.

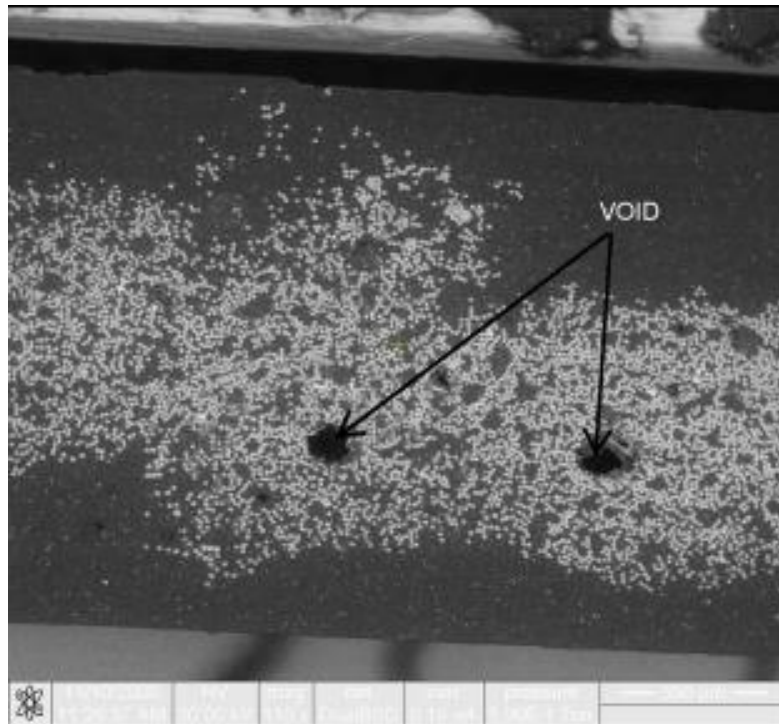


Figure 4-8 SEM Micrograph One Layer GFRP Specimen

Figure 4-8 is the micrograph for a single layer unidirectional laminate while Figure 4-9 is for a two layer unidirectional laminate for the same system. Comparison of the two micrographs shows that in the two layer laminate, there is an elongated void separating the two layers. Similar large voids are present between the two layers in the 0/90 bidirectional configuration shown in Figure 4-10. Large voids are also present in the micrograph for the specimen with randomly oriented fibers in Figure 4-11.

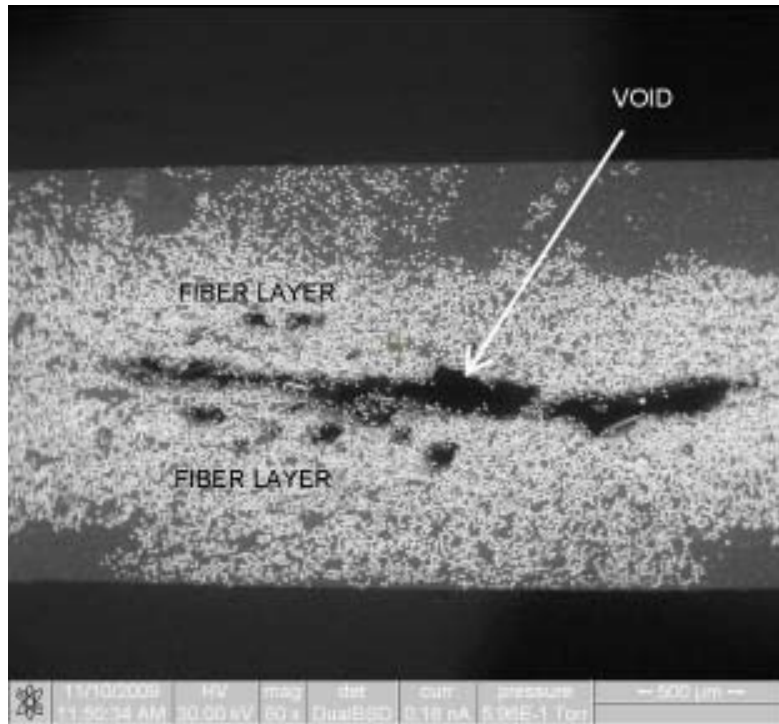


Figure 4-9 SEM Micrograph Two Layers GFRP Specimen

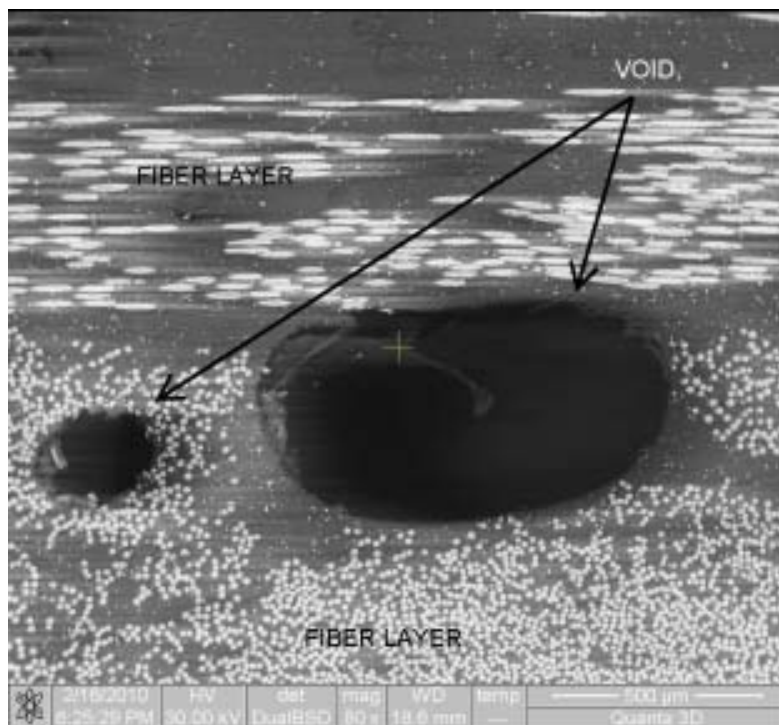


Figure 4-10 SEM Micrograph Bidirectional GFRP Specimen

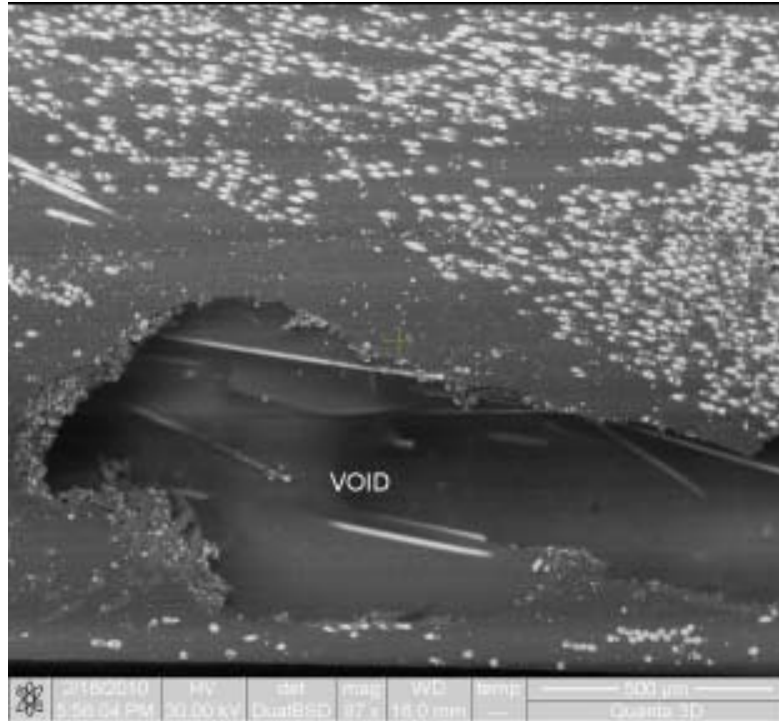


Figure 4-11 SEM Micrograph Random GFRP Specimen

These micrographs are consistent with the void content summarized in Table 4-4 to 4-5 and corroborate the findings from the experimental study. Poorer performance of the two-layer laminates can be attributed to the presence of inter-layer voids that are inevitable in specimen prepared using manual wet lay-up. Their magnitude will depend on factors such as the weave of the fabric; if the interface is smooth, fewer voids can be expected. Alternatively, if techniques such as pressure or vacuum bagging are used in fabrication, Aguilar et al. 2009 fewer voids can be expected.

4.14 Summary and Conclusions

This chapter describes the application of a new test method that was used to determine the oxygen permeation constants of FRP materials. In the study, four different commercially available FRP systems were investigated and four different fiber configurations investigated. Both carbon and glass were evaluated and standard wet lay-up procedures used to make the test samples. The permeation constants were extracted from the experimental data using a quasi-steady state model, Khoe et al. 2010 that had previously been calibrated against published data.

This chapter describes the application of a new test method that was used to determine the oxygen permeation constants of FRP materials. In the study, four different commercially available FRP systems were investigated and four different fiber configurations investigated. Both carbon and glass were evaluated and standard wet lay-up procedures used to make the test samples. The permeation constants were extracted from the experimental data using a quasi-steady state model, Khoe et al. 2010 that had previously been calibrated against published data.

The following conclusions can be drawn:

1. The oxygen permeation constants of four different commercially available carbon and glass fiber laminates (Figure 4-2) were comparable but were generally somewhat poorer than the epoxy used in their fabrication (Table 4-3).

2. The oxygen permeation constant of the FRP laminates was found to be dependent on fiber architecture. Single layer laminates were less permeable than two layer systems (Table 4-3, Figure 4-6). Laminates fabricated using randomly oriented chopped fibers (Figure 4-3) were the most permeable (Table 4-4).
3. Scanning electron micrographs indicate that poorer results in two-layer unidirectional and one layer bidirectional laminates were a consequence of inter-layer voids (Figures 4-8 to 4-11). This result clarifies experimental results reported by researchers, e.g. Debaiky et al. 2002, Wootton et al. 2003.
4. The oxygen permeation constants have positive, non-zero values. For this reason, FRP can slow down but cannot stop corrosion of steel in concrete. This confirms findings from numerous laboratory tests.

Chapter 5 – Oxygen Permeability of FRP-Concrete Repair Systems

5.1 Introduction

Conventional chip and patch repair of corrosion-damaged reinforced concrete elements has a very poor track record. For example, the Florida Department of Transportation reported that only 2% of “good” repairs on 47 bridge piers lasted more than three years (Kessler et al. 2006). This dismal performance has made highway authorities more open to considering alternative repair materials and systems such as fiber reinforced polymers (FRP).

FRP serves as a barrier to the ingress of deleterious materials such as chlorides, moisture and oxygen responsible for electro-chemical corrosion of steel in concrete. Therefore, its performance in corrosion repair depends on the extent to which it stops the passage of these materials. Since oxygen molecules are smaller and can diffuse faster, its role in controlling the rate of corrosion of steel in concrete is the most critical.

Oxygen diffusion through concrete has been studied, e.g. Lawrence 1984, Gjørv et al. 1986, Kobayashi and Shuttoh 1991, Tittarelli 2009. However, similar information for FRP-concrete systems is unavailable. The authors recently reported results on the oxygen permeation of epoxies, Khoe et al. 2010 and FRP

laminates, Khoe et al. 2011a. This chapter presents experimental results for oxygen permeation of concrete and FRP-concrete systems. Although the test setup used earlier was retained, some important changes were necessary in both specimen preparation and the testing protocol. Additionally, to allow the results to be applied, a theoretical model was developed to determine an “equivalent thickness” of FRP-concrete systems for use in design, Chapter 6. These developments are described in this chapter.

5.2 Scope

The overall goal of the study was to obtain experimental data that could be used to optimize the design of FRP-concrete systems used for corrosion repair. This required separate measurement of oxygen permeation of concrete and FRP-concrete systems. Three different water-cementitious ratios were evaluated and FRP-concrete specimens prepared using CFRP and GFRP in single and two-layer configuration. Additionally, the performance of the epoxies used in these FRP-concrete systems was also determined for comparison. A theoretical model was developed to determine the equivalent thickness of FRP-concrete systems.

5.3 Background

Fick’s law served as the basis of the experimental set up. According to this law, if the oxygen concentrations on two parallel faces separated by a thickness

h are C_1 and C_2 , the steady state flux F passing through the material (cc/s or in³/min) is related to the diffusion constant D (units cm²/sec. or in²/ sec.) by Equation 5-1 as :

$$F = -D \frac{dC}{dx} = D \frac{(C_1 - C_2)}{h} \quad (5-1)$$

If the thickness, h , the concentrations C_1 and C_2 and F were known, the diffusion constant D can be directly determined from Equation 5-1. However, for our study it is easier to measure partial pressures p_1 and p_2 than concentrations. Equation 5-2 gives the relationship between the partial pressures, flux and the permeability constant, P as:

$$F = P \frac{(p_1 - p_2)}{h} \quad (5-2)$$

Unlike the diffusion constant D , there is some variation in the units and even the definition of P , Crank 1968. In this chapter, P is defined in units of mol.m²/m³.atm.sec. (mol.ft²/ft³.atm.sec.).

The surface concentration of a gas, C , and its vapor pressure p are related through the solubility constant S by Henry's law as:

$$C = Sp \quad (5-3)$$

From Equations 5-1 to 5-3, it is seen that the diffusion constant and the solubility constant are related by Equation 5-4 as:

$$P=DS \quad (5-4)$$

5.4 Measuring Permeability

The measurement of oxygen permeation relies on the development of appropriate concentration gradients on the two faces of a test specimen. A number of ASTM based methods, ASTM D3985 2005, ASTM F1307 2002 are available but these are primarily directed towards measuring oxygen permeability of thin materials used by the food packaging industry. In the study, available systems, Paul 1965, Trefry 2001 were refined and adapted for materials used in infrastructure. More details may be found elsewhere, Khoe et al. 2010.

5.5 Diffusion Cell

The diffusion cell developed needed to accommodate specimens of different thickness. Since a large numbers of specimens had to be tested, it had to be easy to assemble and disassemble yet simple to leak proof.

A pair of round, stainless steel plates 12 mm (0.472 in.) thick and 145 mm (5.709 in.) outside diameter were used. Eight bolt holes were drilled symmetrically along the perimeter in each of these plates. The central part of the plates was machined to create an 83 mm (3.27 in.) diameter and 4.5 mm (0.18 in.) deep recess that constituted the diffusion chamber. The volume of this chamber could be reduced by placing appropriately sized metal inserts in the opening.

The test specimen is positioned between the two 145 mm (5.709 in.) diameter stainless plates. Originally, grooves were cut so that O-rings could be

used to make it airtight as had been used previously, Trefry 2001. But this was found to be unreliable. The problem was solved by replacing the O-rings by 3 mm (0.12 in.) thick red rubber gaskets, a solution recommended over 40 years ago, Paul 1965.

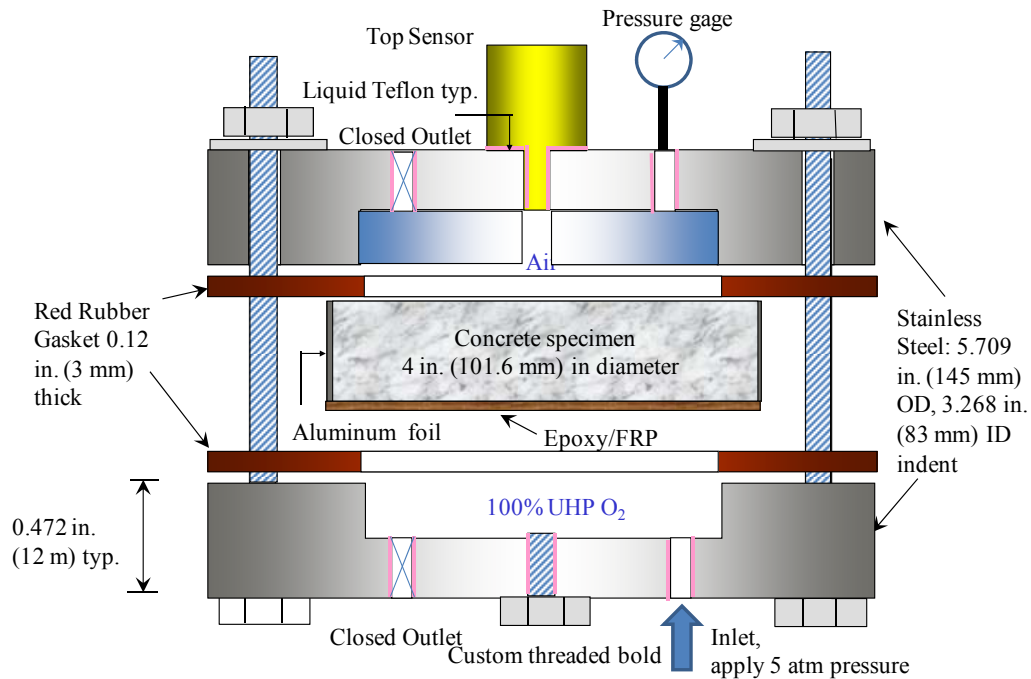


Figure 5-1 Diffusion Cell for Testing FRP-Concrete Systems

The diffusion cell is assembled by bolting the two stainless steel plates together using eight stainless steel bolts, nuts and washers. A special, calibrated digital torque wrench was used to ensure uniformity in the applied force. As the length of the bolts can be varied, it provides a simple yet effective means for testing samples of different thicknesses.

The cell is assembled in air one surface of the specimen has the same oxygen concentration as air (20.7% of oxygen). The other surface was exposed to 100% concentration oxygen at the rate of 100 standard cubic centimeters per

minute (SCCM). This required threaded inlet and outlet openings in the bottom plate that were fabricated as shown in Figure 5-1. These connections were made leak proof by using liquid threaded seal Teflon in conjunction with a Swagelok male connector.

Two galvanic cell type oxygen sensors, Figaro 2004 50 mm x 23 mm dia. (2 in. x 0.9 in.) were used to monitor the oxygen concentration at the top and bottom of the diffusion cell. The connections to both sensors were also made leak proof using specially fabricated threaded openings and liquid threaded seal Teflon. Each sensor was individually calibrated against certified oxygen concentration levels. The sensors were connected to an Agilent 34970A data acquisition system for the data to be recorded and stored at a desired scan rate. This was retrieved later for subsequent analysis. A data acquisition switch unit with two multiplexers attached to 16 channels and 20 channels was used. Temperature data was recorded simultaneously.

The oxygen concentrations measured by the sensors rely on electro-chemical reactions with oxygen molecules. As a result, some oxygen is consumed during the testing. Data had to be corrected to account for this consumption as described in Khoe et al. 2010.

Unlike the epoxy and FRP laminates tested earlier, FRP-concrete systems are significantly more rigid. Therefore, advantage was taken of this rigidity to increase the concentration gradient by applying an initial pressure of 5 atm. The

increased gradient led to a reduction in the time required for specimens to attain steady state conditions.

Table 5-1 Concrete Mix Design (FDOT 2010)

Property	Concrete		
	I	II	III
Concrete type	I	II	III
w/c ratio	0.4	0.45	0.5
Unit weight (kg/m ³)	2,287	2,268	2,268
PC volume (%)	11%	10%	10%
Aggregate volume (%)	55%	55%	49%
Cementitious content (kg/m ³)	430	406	380
Strength 28 days (MPa)	54.8	49.2	35.7
Slump (cm)	15	15	15

5.6 Experimental Program

To meet the goals of this research project, it was necessary to test concrete and FRP-concrete specimens made using the same concrete. Three representative concrete mixes having water-cementitious ratios of 0.4, 0.45 and 0.50 were evaluated, FDOT 2010. These water-cementitious ratios also permitted experimental results to be compared against published data, Lawrence 1984, Tittarelli 2009. The cementitious content varied from 380 to 430 kg/m³ and the measured compressive strength from 35.7 to 54.8 MPa. Details are summarized in Table 5-1. Scanning Electron Micrograph (SEM) for these concrete mixes is shown in Appendix V.

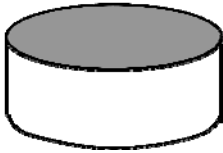
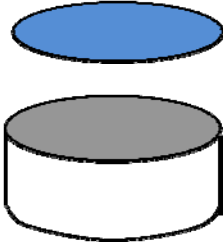
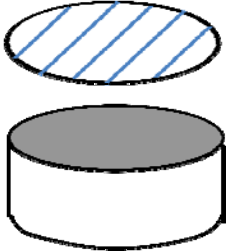
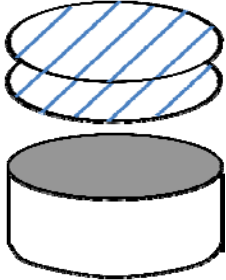
Type	FRP-Concrete Layout		Remarks
1	Concrete only		Circular plain concrete
2	Epoxy-concrete		Circular plain concrete with epoxy at the top
3	FRP-concrete one layer unidirectional		Circular plain concrete with one layer unidirectional FRP at the top
4	FRP-concrete two layer unidirectional		Circular plain concrete with two layer unidirectional FRP at the top

Figure 5-2 Concrete, Epoxy-Concrete and FRP-Concrete Specimen

Two commercially available FRP systems identified in this chapter as systems A and B were used. For each system, both carbon and fiberglass were tested using two alternative configurations, identified as Types 3-4 in Figure 5-2.

Additionally, epoxy-concrete specimens were tested in which the same epoxy used for fabricating the FRP laminates was used (Type 2).

Table 5-2 Epoxy Details (Fyfe Co 2003, BASF 2007)

Property	A	B
Density (kg/m ³)	1,600	983
Flexural strength (MPa)	55.2	138
Viscosity, cps	14,000-18,000	1600
Mixing time, min.	5	3
Mixer speed, rpm	400-600	600
Color	Gray	Blue
Full cure time, days	7	7

Table 5-3 FRP Fabric Properties (Fyfe Co 2003, BASF 2007)

Property	A		B	
	Carbon	Glass	Carbon	Glass
Fiber orientation	0°	0°	0°	0°
Fiber density (g/cm ³)	1.74	2.55	1.7	2.6
Areal weight (g/m ²)	644	915	300	900
Fabric width (mm)	610	1,373	500	610
Nominal thickness (mm/ply)	1	0.36	0.165	0.373
Tensile strength (MPa)	3,790	3.24	4,950	1,517
Tensile modulus (GPa)	230	72.4	227	72.4
Elongation (%)	1.00%	4.50%	1.67%	2.10%

Material, physical and mechanical properties of the two FRP systems as provided by the manufacturers are summarized in Tables 5-2 to 5-3. Table 5-2

provides information on the epoxy resin including viscosity, mixing/ cure time. Table 5-3 summarizes the properties of the fibers for the two FRP systems.

5.6.1 Concrete Specimen – Type 1

Concrete was cast in 10 cm x 30 cm (4 inch diameter x 12 in.) high PVC molds. Following curing, the cylinders were cut into discs approximately 25 mm (1 in.) thick using a diamond blade (Figure 5-3). All tests were conducted using the 25 mm (1 in.) thick specimens since previous research had shown that concrete's diffusion constant was relatively insensitive to thickness (Gjorv et al. 1986).

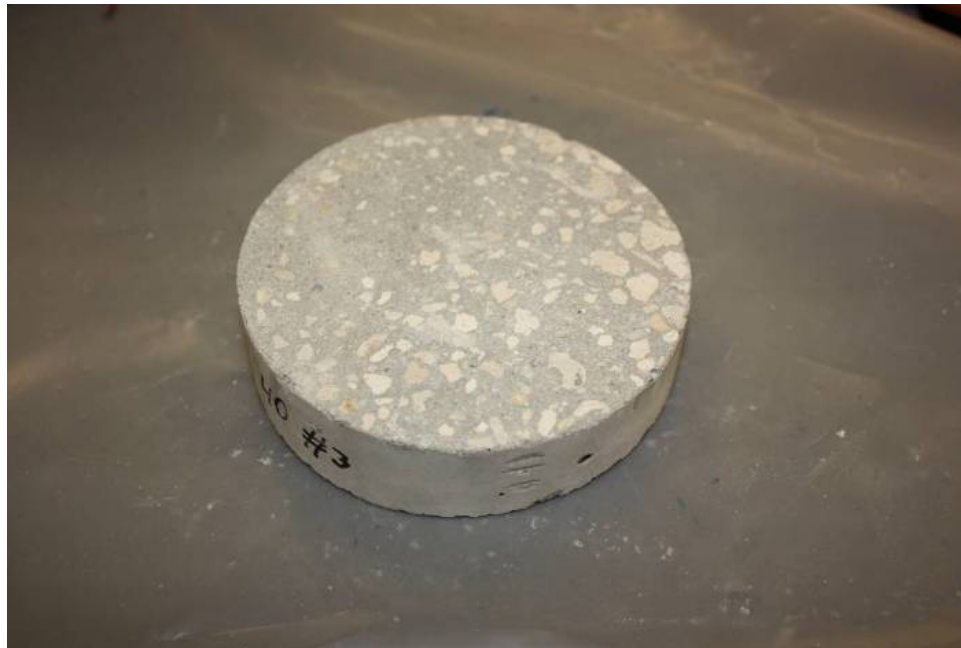


Figure 5-3 Concrete Specimen

The concrete specimens were placed in a vacuum chamber for 24 hour conditioning following ASTM F710 2008. Subsequently, their thickness was

measured and the specimen numbered along the circumference. The top and bottom surfaces were cleaned with acetone prior to testing.

5.6.2 Epoxy-Concrete – Type 2

Epoxy resin was first prepared in accordance with the manufacturer's recommendations and placed in a vacuum chamber for 30 minutes to remove air bubbles. Pristine polythene sheets approximately 45 cm x 45 cm (18" x 18") were placed on a flat surface and sufficient epoxy deposited to make nine 10 cm (4 in.) diameter specimens. The concrete specimens were then carefully laid on the epoxy to ensure that the circular contact surface was completely covered by epoxy. The test specimens were obtained after 8-10 hours of curing by carefully trimming any protruding epoxy resin around the circular edges. The specimens were numbered and their thickness measured. The average thickness of the epoxy layer was determined by subtracting the known thickness of the concrete specimen from the total thickness.

5.6.3 FRP-Concrete – Types 3-4

The procedure used for making FRP-concrete specimens was similar to that for the epoxy-concrete specimen. As before, a pristine polythene sheet was placed on a flat surface. However, in this case rectangular 10 cm x 30 cm fiber strips (1 or 2 layer) were first saturated with epoxy and a steel roller used to remove excess resin and air bubbles. The concrete specimens were then

carefully placed on top of the resin saturated FRP (Figure 5-4). Circular specimens were obtained after 8-10 hours of curing by carefully trimming around the circular concrete edge. At that time, the resin was rubbery and did not crack (Figure 5-5). This method allowed three specimens to be made at a time. The approach was faster and yielded specimens that were more representative of wet layup used in field applications.



Figure 5-4 FRP-Concrete Specimen Preparation



Figure 5-5 FRP-Concrete Specimen

5.7 Test Details

All tests were conducted after the concrete had fully cured. Where epoxy or FRP material was bonded to the concrete surface (Types 2-4 in Figure 5-2) tests were only conducted after the resin had cured for the time recommended by the manufacturer (Table 5-2).

In the testing, the specimen was carefully centered over the opening in the bottom plate of the diffusion cell and placed on a rubber gasket (Figure 5-1). The upper rubber gasket was then placed over it. The two parts of the cell were now assembled using bolts, nuts and washers that were symmetrically tightened

to a specified torque of 10.2 N-m using a digital torque wrench. This operation is crucially important for preventing leaks from developing.

Oxygen concentrations on both faces of the test specimen were monitored throughout. One face was subjected to ultra high purity (100%) oxygen under 5 atm pressures while the other face was exposed to air (1 atm pressure). To ensure steady state conditions, oxygen was pressurized constantly for 24 hours using a flow rate of 100 SCCM.

To verify that there were no leaks two diffusion cells were tested at a time - one containing the FRP-concrete or epoxy-concrete test specimen (Type 2-4 in Figure 5-2) and the other a control containing an impermeable concrete-steel insert. Three layers of aluminum foil tape were used to cover the exposed circumference of the test specimen to prevent diffusion through the sides as shown in Figure 5-1.

The top sensor reading in Figure 5-6 corresponding to the surface of the stainless steel specimen exposed to air showed a decrease over time since no oxygen permeated through the steel. This decrease was due to oxygen consumed by the sensor in that chamber. In contrast, the same sensor showed increases over time for the FRP-concrete specimen. This increase offset the oxygen consumed by the sensor and was due to diffusion of oxygen through the FRP. Any departures from this response would indicate leaks in the system.

The transport of gases is very sensitive to temperature. Minor fluctuations in temperature caused by opening of doors, movement of personnel, changes in

air-conditioning can lead to poor results. Therefore, particular attention was paid to minimize such effects by enclosing the diffusion cells inside an insulated box. Readings were recorded every minute and a typical test ran for 24 hours.

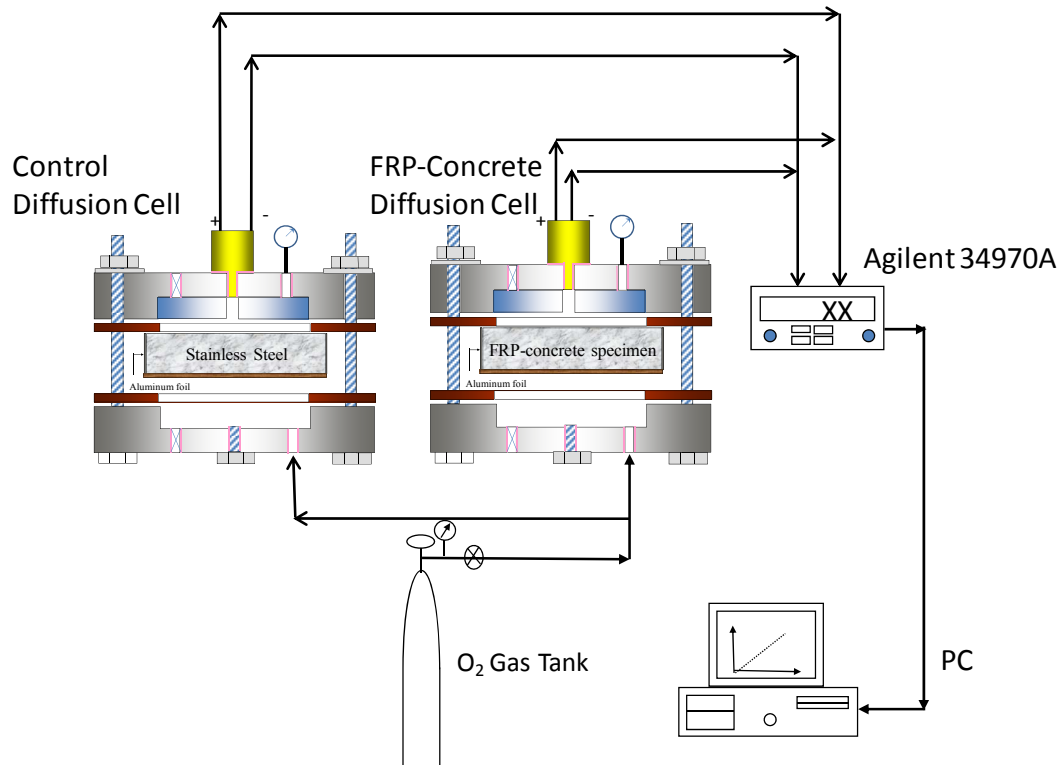


Figure 5-6 Diffusion Test Set Up for FRP-Concrete Systems

5.8 Corrected Data

Data was corrected for oxygen consumption as discussed earlier. Since the oxygen consumed by the sensor would otherwise have been present, it must be added to the raw data. The correction is greater at higher oxygen concentrations, Khoe et al. 2010.

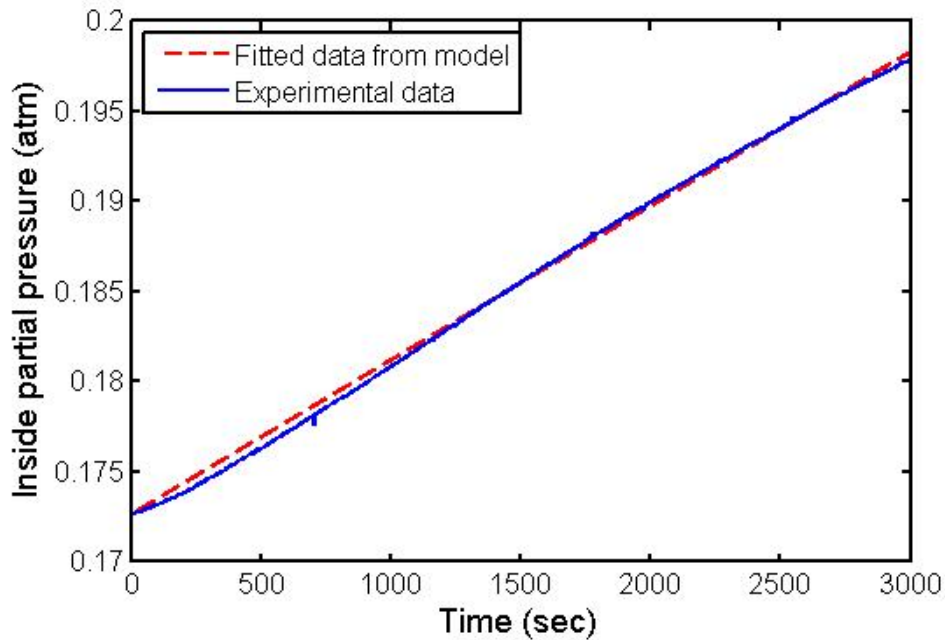


Figure 5-7 Experiment and Fitted Data for Concrete with w/c 0.40

5.9 Results

The results from the tests are summarized in Tables 5-4 to 5-6. Each result corresponds to tests on three different specimens. A total of 99 specimens were tested overall.

Table 5-4 contains results for concrete specimens (Type 1) with three different water-cementitious ratios of 0.4, 0.45 and 0.5. Table 5-5 summarizes results for the corresponding epoxy-concrete specimens (Type 2) for epoxies A and B. The epoxies A and B correspond to the those used for making the FRP-concrete systems.

Table 5-6 summarizes results for the FRP-concrete systems (Type 3-4) for carbon and glass. Uni-directional, one layer and two layer configurations were

tested (Figure 5-2). Results show characteristic variation associated with unavoidable changes in the laboratory environment while the test was in progress. They also reflect the random effects of workmanship since not all the test specimen were made at the same time.

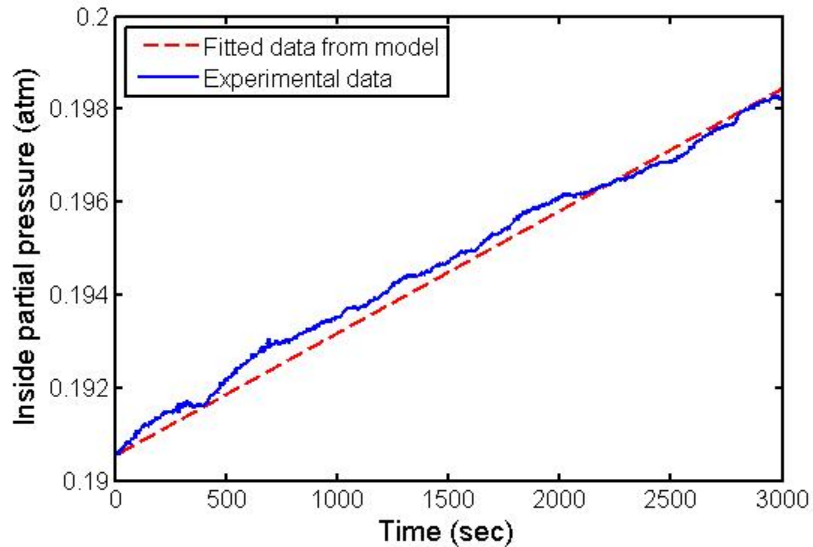


Figure 5-8 Experiment and Fitted Data for Epoxy-Concrete System B

The permeation constant reported in Tables 5-4 to 5-6 was obtained from a quasi-steady state model, Khoe et al. 2010. The initial partial pressure was taken as 5 atm pressure to reflect the pressure used in the testing. Typical plots showing the variation in partial pressure (atm.) inside the chamber with time (seconds) are shown in Figures 5-7 to 5-10 for concrete only, epoxy-concrete, and FRP-concrete one layer and two layer configuration respectively.

Though data was recorded continuously for 24 hours only 5-6 hours of data was necessary to obtain the permeation constant as shown in these figures. In the plots the dotted line corresponds to the fitted data obtained from the

model used to extract the permeation constant. Despite some noise in the data, there is generally good agreement between the experimental and the fitted data from the model.

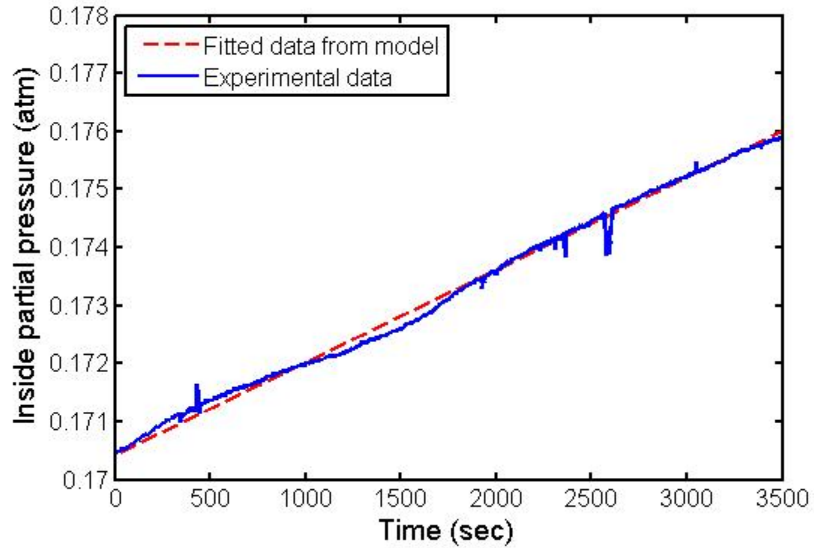


Figure 5-9 Experiment and Fitted Data for CFRP-Concrete One Layer System B

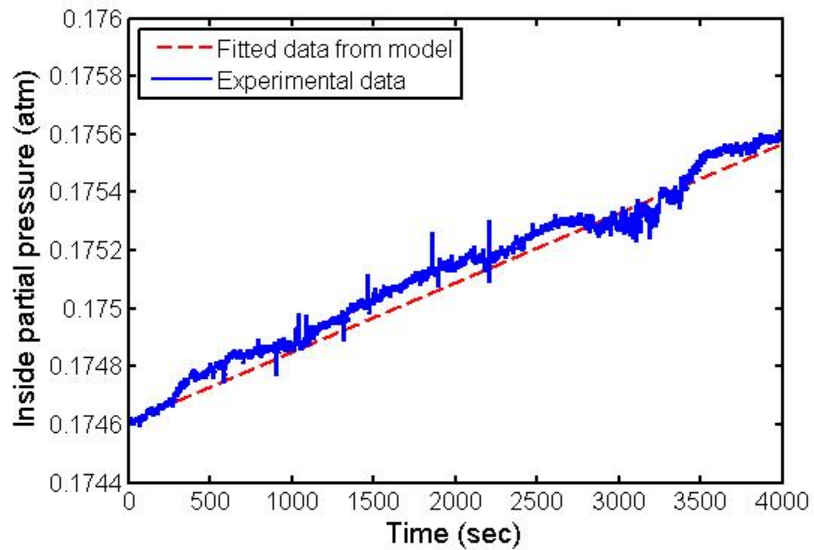


Figure 5-10 Experiment and Fitted Data for CFRP-Concrete Two Layer System B

5.9.1 Concrete

Table 5-4 presents the permeation constants for three different water-cementitious ratios of 0.4, 0.45 and 0.5. Inspection of this table shows that the permeation constant varies directly with the water-cementitious ratio. The values increase by approximately one order of magnitude (10^{-1}) as the water-cement ratio increases by 0.05. Thus, the permeation constant for concrete with a water-cementitious ratio of 0.5 (average 4.11×10^{-7}) is one orders of magnitude larger than that of the concrete with a water-cementitious ratio of 0.45 (average 4.48×10^{-8}). Similar trends were also reported by Gjorv et al. 1986 and Khan 2003 though their tests evaluated diffusion rates for dissolved oxygen corresponding to submerged applications.

Table 5-4 Oxygen Permeation Constant for Concrete with Different w/c Ratios

Type of Specimens	P in mol.m ² /m ³ .atm.sec					
	0.40 w/c		0.45 w/c		0.50 w/c	
	Result	Average	Result	Average	Result	Average
Concrete	4.65E-09	4.79E-09	5.95E-08	4.48E-08	2.51E-07	4.11E-07
	4.56E-09	±	4.52E-08	±	3.98E-07	±
	5.15E-09	3.18E-10	2.97E-08	1.49E-08	5.84E-07	1.67E-07

5.9.2 Comparison with Published Values

The average oxygen permeability constant values in Table 5-4 are in broad agreement with the limited information available in the literature. Lawrence 1984 reported that the oxygen diffusion constant for concrete with a w/c ratio of 0.45 as $62 \text{ mm}^3/\text{s}$. The corresponding permeability constant is determined from Equation 5-4 using the solubility constant, Crank 1975. From

the calculated value of the solubility constant the corresponding permeation constant is $1.1 \times 10^{-8} \text{ mol.m}^2/\text{m}^3.\text{atm}.\text{sec}$. compared to $4.48 \times 10^{-8} \text{ mol.m}^2/\text{m}^3.\text{atm}.\text{sec}$. obtained in this study. More recently, Tittarelli 2009 obtained the oxygen diffusion constant using a completely different electro-chemical potentiostatic technique. He reported a diffusion constant for concrete with a w/c ratio of 0.45 as $7.7 \times 10^{-6} \text{ cm}^2/\text{s}$ that corresponds to a permeation constant of $1.1 \times 10^{-9} \text{ mol.m}^2/\text{m}^3.\text{atm}.\text{sec}$. This is smaller than the 4.48×10^{-8} value obtained from this study. Experimental results cannot agree exactly because of differences in material composition, specimen preparation, moisture content, and environmental conditions, e.g. temperature, humidity.

Table 5-5 Oxygen Permeation Constant for Epoxy-Concrete Systems A & B in $\text{mol.m}^2/\text{m}^3.\text{atm}.\text{sec}$

Type of Specimens	Concrete					
	0.4 w/c		0.45 w/c		0.50 w/c	
	Result	Average	Result	Average	Result	Average
Epoxy-Concrete System A	1.23E-11	1.03E-11	1.50E-11	1.79E-11	1.08E-11	1.82E-11
	9.84E-12	±	1.99E-11	±	1.29E-11	±
	8.90E-12	1.76E-12	1.88E-11	2.57E-12	3.10E-11	1.11E-11
Epoxy-Concrete Epoxy system B	1.10E-11	4.23E-11	2.10E-11	3.19E-11	1.11E-11	1.57E-11
	4.25E-11	±	5.92E-11	±	1.50E-11	±
	7.33E-11	3.11E-11	1.55E-11	2.38E-11	2.10E-11	4.99E-12

Table 5-6 Oxygen Permeation Constant for FRP-Concrete Systems A & B in mol.m²/m³.atm.sec

Type of Specimens	Concrete											
	0.40 w/c				0.45 w/c				0.50 w/c			
	FRP type A		FRP type B		FRP type A		FRP type B		FRP type A		FRP type B	
	Result	Average	Result	Average	Result	Average	Result	Average	Result	Average	Result	Average
CFRP-Concrete Uni 1 Layer	2.86E-11	2.85E-11	2.97E-11	2.71E-11	7.30E-11	6.85E-11	4.06E-11	4.79E-11	9.91E-12	1.54E-11	9.19E-12	2.30E-11
	3.87E-11	±	1.49E-11	±	6.45E-11	±	3.37E-11	±	2.54E-11	±	3.97E-11	±
	1.81E-11	1.03E-11	3.66E-11	1.11E-11	6.80E-11	4.27E-12	6.93E-11	1.89E-11	1.08E-11	8.69E-12	2.01E-11	1.55E-11
CFRP-Concrete Uni 2 Layers	5.58E-11	4.57E-11	6.94E-11	6.51E-11	9.09E-10	6.10E-10	8.88E-11	1.11E-10	3.39E-11	4.92E-11	9.01E-11	5.28E-11
	4.55E-11	±	6.49E-11	±	7.93E-10	±	9.54E-11	±	5.17E-11	±	1.29E-11	±
	3.59E-11	9.95E-12	6.09E-11	4.25E-12	1.29E-10	4.21E-10	1.50E-10	3.36E-11	6.19E-11	1.42E-11	5.55E-11	3.87E-11
GFRP-Concrete Uni 1 Layer	1.88E-11	2.23E-11	3.50E-11	3.47E-11	4.56E-11	5.19E-11	3.86E-11	3.53E-11	2.08E-11	2.58E-11	3.14E-11	3.72E-11
	2.81E-11	±	4.10E-11	±	5.97E-11	±	3.17E-11	±	1.80E-11	±	3.16E-11	±
	1.99E-11	5.08E-12	2.80E-11	6.51E-12	5.03E-11	7.18E-12	3.55E-11	3.47E-12	3.87E-11	1.12E-11	4.87E-11	9.93E-12
GFRP-Concrete Uni 2 Layers	6.72E-11	7.01E-11	7.50E-11	6.73E-11	1.01E-10	1.46E-10	1.50E-10	1.53E-10	2.77E-11	2.86E-11	5.58E-11	6.57E-11
	7.87E-11	±	5.81E-11	±	1.50E-10	±	2.10E-10	±	1.93E-11	±	7.68E-11	±
	6.44E-11	7.59E-12	6.87E-11	8.54E-12	1.88E-10	4.36E-11	9.85E-11	5.57E-11	3.87E-11	9.73E-12	6.45E-11	1.06E-11

5.9.3 Epoxy-Concrete

The oxygen permeation constants for the 18 epoxy-concrete specimens are summarized in Table 5-5. Inspection of this table shows that the values for the two different epoxies are comparable. The permeability constant is of the order of 10^{-11} mol.m²/m³.atm.sec. These values are higher than that for neat epoxies, Khoe et al. 2010 and reflects the difficulty of eliminating air voids when epoxy is applied to a concrete surface.

5.9.4 FRP-Concrete

The oxygen permeation constants for 72 FRP-concrete specimens tested are summarized in Table 5-6. This contain contains results for unidirectional fiber orientations for one/two layer carbon and glass (Types 3 and 4 in Figure 5-2) systems. Inspection of Table 5-6 shows that the results for carbon and glass are comparable. The permeation constants are somewhat larger for two layer systems in some instances (w/c ratio = 0.45). This may be because air voids in two layer systems tend to be bigger as found from scanning electron micrographs, Khoe et al. 2011a. Moreover, since the time taken for oxygen to diffuse is greater for thicker specimen, environmental disturbance may affect the data, e.g. data fluctuations in Figure 5-10.

5.10 Discussion

The oxygen permeation constants obtained from this study can be used to predict corrosion rates of repaired FRP-concrete specimens. Where the concrete is significantly more permeable than the FRP, the thickness of the concrete can be disregarded in the calculations, Khoe et al. 2010. However, the test results show that there can be cases where the permeation values for concrete and FRP are closer, e.g. Table 5-4 w/c = 0.45 (4.48×10^{-8} average concrete value) and Table 5-6 for GFRP 2-layer (1.46×10^{-10} average value). In this context it is helpful to determine an "equivalent thickness" of multi-layer systems that can be used for designing appropriate FRP repair.

5.10.1 Equivalent Thickness for FRP-Concrete Systems

FRP-concrete systems can be idealized as different materials having known permeation properties bonded at an interface whose permeation characteristics are unknown. Tests have shown that the permeation characteristics of FRP laminates (Khoe et al. 2011a) and those for FRP-concrete systems (reported in Table 5-6) are comparable. This suggests that the interfacial resistance is negligible, and the FRP-concrete system can be idealized as a two-layer system, as shown in Figure 5-11.

A simplified quasi-steady state, one dimensional diffusion model of the FRP-concrete system is developed to determine an equivalent thickness for

multi-layer systems. This can be used to assess alternate FRP-concrete systems and optimize the repair.

A schematic of the idealized FRP-concrete system is shown in Figure 5-11. In this figure, a FRP laminate of thickness ΔX_A with an oxygen permeation constant P_A is bonded to a concrete specimen of thickness ΔX_B with a permeation constant P_B . The partial pressures at the two external faces are p_1 and p_3 as shown. The oxygen permeabilities P_A , P_B , the thicknesses ΔX_A and ΔX_B and the partial pressures p_1 and p_3 are known from experimental results.

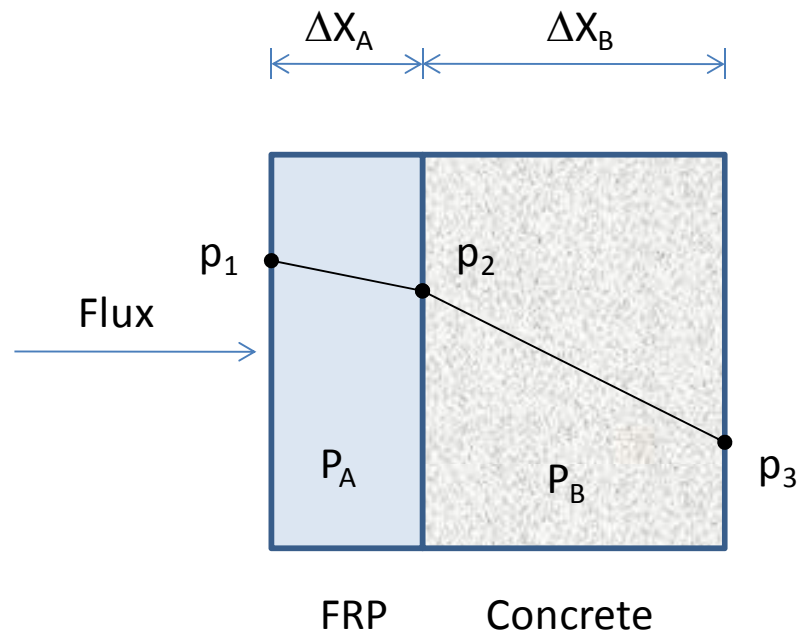


Figure 5-11 Diffusion Model for FRP-Concrete Specimen

Under steady state conditions, the flux, F , is constant and has to be the same in each layer. Fick's equation for each layer can be approximated as:

$$F = \frac{P_A}{\Delta X_A \cdot RT} (p_1 - p_2) = \frac{P_B}{\Delta X_B \cdot RT} (p_2 - p_3) \quad (5-5)$$

where R is universal gas constant and T the temperature in degrees Kelvin.

The change in the partial pressures in the two materials is obtained from Equation 5-5 and is given by Equation 5-6 as:

$$p_1 - p_2 = F \frac{\Delta X_A \cdot RT}{P_A} \quad p_2 - p_3 = F \frac{\Delta X_B \cdot RT}{P_B} \quad (5-6)$$

By adding the equations for p_1-p_2 and p_2-p_3 in Equation 5-6, the unknown interval partial pressure p_2 can be eliminated and the final equation arranged as

$$p_1 - p_3 = F \left(\frac{\Delta X_A \cdot RT}{P_A} + \frac{\Delta X_B \cdot RT}{P_B} \right) = F(R_A + R_B) \quad (5-7)$$

where the first two terms are replaced by resistances $R_A = \frac{\Delta X_A \cdot RT}{P_A}$ and $R_B = \frac{\Delta X_B \cdot RT}{P_B}$.

Equation 5-7 can be written in terms of an equivalent thickness ΔX_{eqv} in Equation 5-8 as:

$$p_1 - p_3 = F \frac{\Delta X_{eqv} \cdot RT}{P} \quad (5-8)$$

In this equation, P is permeation constant for the multilayer specimen that is obtained from experimental results.

By combining Equation 5-7 and 5-8, the equivalent thickness equation is given by Equation 5-9 as:

$$\frac{\Delta X_{eqv}}{P} = \frac{\Delta X_A}{P_A} + \frac{\Delta X_B}{P_B} \quad (5-9)$$

Equation 5-9 allows the oxygen permeation characteristics of FRP-concrete systems to be represented by a homogeneous system. If the permeability of the two materials were identical, the equivalent thickness is the sum of the thicknesses of the two materials. This applies to repairs where

multiple FRP layers are used. On the other hand, if the permeability differs significantly (typical for concrete), the thickness of the more permeable material can be disregarded, Khoe et al. 2011b. For values that are in-between, Equation 5-9 allows the determination of an equivalent thickness that can be used to predict the corrosion rate of steel in FRP-repaired concrete specimens as illustrated in Chapter 3, Chapter 6 and Appendix VI.

5.11 Summary and Conclusions

This chapter describes the application of a new test method to determine the oxygen permeation constant for concrete, epoxy-concrete and FRP-concrete specimens. The concrete tested comprised three different water-cementitious ratios of 0.4, 0.45 and 0.50. Two commercially available FRP systems and their respective epoxies were tested. Both carbon and glass, unidirectional one and two layer, were evaluated and standard wet lay-up procedures used to make the test samples. The permeation constants were extracted from the experimental data using a quasi-steady state model, Khoe et al. 2010 that had previously been calibrated against published data.

The following conclusions can be drawn:

1. Concrete only specimens were the most permeable (Table 5-4). The oxygen permeation constant was directly related to the water-cementitious ratio. It increased by one order of magnitude for each 0.05 increase in the water-cementitious ratio.

2. The oxygen permeation constants of epoxy-concrete and FRP-concrete specimens were similar (Table 5-5 and 5-6).
3. The oxygen permeation constants of FRP-concrete systems for two different commercially available CFRP and GFRP materials are comparable (Table 5-6).
4. The greatest reduction in oxygen permeation rate was obtained when FRP was bonded to concrete with the highest water-cementitious ratio (Table 5-4 and 5-6).
5. A simplified model has been developed that can be used to determine the equivalent thickness of FRP-concrete systems (Equation 5-9). This can be used to investigate the effectiveness of alternate FRP repairs.

Chapter 6 – Design of Optimal FRP Corrosion Repair

6.1 Introduction

This chapter provides an overview of the results reported in Chapters 3-5 to illustrate how the findings can be used to optimize FRP repairs. Results are shown qualitatively to provide a better appreciation of the relative orders of magnitude of the various components that are part of a repair system.

For simplicity, average oxygen permeation constants for epoxy, concrete, FRP and FRP-concrete systems are summarized and a parametric study conducted to identify the most favorable FRP/concrete combinations. A typical calculation relating to the parametric study is included in Appendix VI for completeness.

6.2 Results

Average values from tests reported in Chapters 3-5 are shown in a graphical form in Figure 6-1 (concrete) and Figure 6-2 (for epoxy, FRP, and FRP-concrete systems). The numbers in parentheses in these figures indicate the number of results used to obtain the average value.

It may be seen from these figures that the order of magnitude for oxygen permeability (in mol. m²/m³.atm.sec.) ranges from 10⁻⁷ to 10⁻⁹ for concrete to 10⁻¹² for epoxies. The results for FRP and FRP-concrete systems show more scatter.

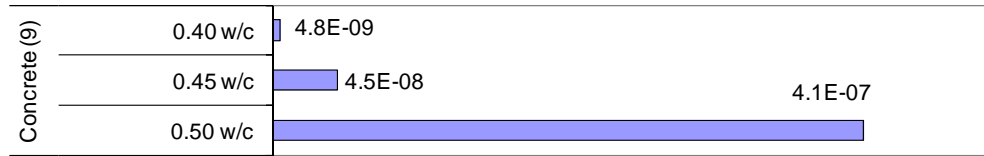


Figure 6-1 Average Oxygen Permeation Constant for Concrete Specimens in mol. m²/m³.atm.sec. (Note: 1 mol. m²/m³.atm.sec. = 3.28 mol. ft²/ft³.atm.sec.)

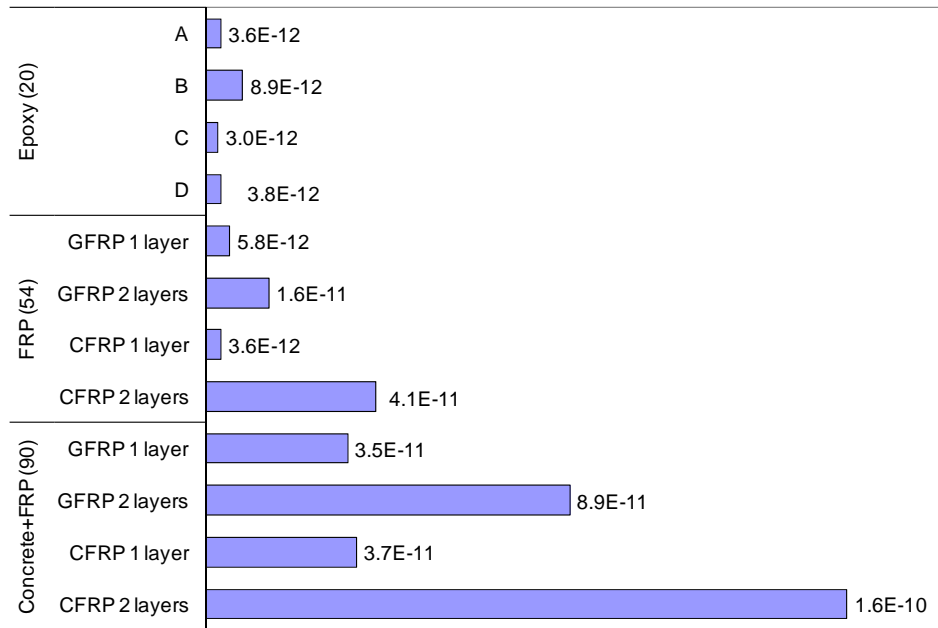


Figure 6-2 Average Oxygen Permeation Constant for Epoxy, FRP, and FRP-Concrete Specimens in mol. m²/m³.atm.sec. (Note: 1 mol. m²/m³.atm.sec. = 3.28 mol. ft²/ft³.atm.sec.)

6.2.1 Comments on Results

It may be seen from Figure 6-2 that the results for two FRP layers are inferior to those for single layer systems. SEM studies (Figures 4-8 to 4-11, Chapter 4) indicated that more voids were present between the layers in two-layer specimens. This phenomenon helps to explain anomalous results reported in the literature (Paul 1965, Suh et al. 2007) in which the performance of multiple FRP layers were sometimes inferior to that compared with fewer layers.

In general, the permeability constants for FRP-concrete systems are higher than those for FRP. This may be due to fabrication issues though no SEM studies were conducted. Nonetheless, the oxygen permeability for FRP-concrete systems is notably better compared to concrete.

6.3 Discussion

Information on the oxygen permeability constant for concrete, epoxy, FRP, and FRP-concrete systems makes it possible to determine relative corrosion rates of steel in repairs conducted using different systems.

In chloride-induced corrosion, oxidation occurs at the anode (steel) producing two electrons and a ferrous ion; simultaneous reduction occurs at the cathode producing hydroxyl ions (Bertolini et al. 2004). As a result, one mole of oxygen reacts with two moles of iron to form rust. Therefore, if the number of moles of oxygen, M , reaching the steel surface is known, the number of moles of iron converted to rust is twice this quantity. Using the relationship between

molecular weight and moles, the metal loss can then be determined. Knowledge of the metal loss allows calculation of the corrosion rate using Faraday's law.

6.3.1 Equivalent FRP Thickness

The thickness of the different materials needs to be accounted for in calculations for predicting the post repair corrosion state. The calculations are simplified if use is made of an equivalent FRP thickness. As derived in Chapter 5, the equivalent FRP thickness for a two layer system, ΔX_{eqv} , is given by Equation 6-1 as:

$$\frac{\Delta X_{eqv}}{P} = \frac{\Delta X_A}{P_A} + \frac{\Delta X_B}{P_B} \quad (6-1)$$

Equation 6-1 can be used to calculate the equivalent FRP thickness if the permeation constants of the constituent materials are known. It also requires information on the thicknesses, $\cdot X_A$ and $\cdot X_B$, of the layers.

6.3.2 Numerical Example

Table 6-1 summarizes results used to determine the equivalent FRP thickness using Equation 6-1 for FRP-concrete systems that were tested. In the tests, the thickness of the FRP was typically 2 mm while that for the concrete was 25 mm. In the calculations, the average permeation constant values for FRP and concrete were taken from Figures 6-1 and 6-2 respectively and are listed in Table 6-1. Substituting these values the equivalent FRP thickness can be seen to vary from 2.0025 mm for w/c ratio of 0.5 to 2.25 mm for w/c ratio of 0.4. Thus,

where the permeability of concrete differs from that of FRP by more than one order of magnitude, the calculation of an equivalent FRP thickness is not warranted.

Table 6-1 Equivalent FRP Thickness

w/c ratio	P_A	P_B	ΔX_A (mm)	ΔX_B (mm)	ΔX_{eqv} (mm)
0.4	1E-11	1.E-09	2	25	2.25
0.45	1E-11	1.E-08	2	25	2.025
0.5	1E-11	1.E-07	2	25	2.0025

6.4 Parametric Study

The results presented indicate that the order of magnitude for oxygen permeability (in mol.m²/m³.atm.sec) varies from 10⁻⁷ to 10⁻⁹ for concrete and is in the 10⁻¹¹ range for FRP-concrete systems. In order to draw general conclusions, a parametric study was conducted in which the variation in corrosion depth/yr in reinforcing steel was calculated. In the study, a concrete slab reinforced orthogonally by #13 (#4) bars spaced at 30 cm (12 in.) on centers was evaluated.

To determine the effect of different concrete/FRP combinations, the oxygen permeability constant for concrete was varied from 1 x 10⁻⁸ to 1 x 10⁻⁹ corresponding to water cement ratios of 0.45 and 0.4 respectively. Also, since test data showed that the oxygen permeability was influenced by fabrication, three different oxygen permeabilities reflecting fair (1 x 10⁻¹⁰), good (1 x 10⁻¹¹) and outstanding (1 x 10⁻¹²) workmanship were evaluated.

Table 6-2 Variation in Corrosion Depth in Steel Reinforcement in Concrete Slab

Materials	Description	Permeation Constant (mol.m ² /m ³ .atm.sec)	Corrosion Depth (cm/yr)
Concrete	0.45 w/c	1.00E-08	1.08E-01
Concrete	0.4 w/c	1.00E-09	9.93E-03
FRP-Concrete	Fair	1.00E-10	9.43E-03
FRP-Concrete	Good	1.00E-11	9.37E-04
FRP-Concrete	Outstanding	1.00E-12	9.36E-05

Note: 1 mol. m²/m³.atm.sec. = 3.28 mol. ft²/ft³.atm.sec., 1 cm/yr = 0.393 in./yr

The results of the study are summarized in Table 6-2. For completeness, a sample calculation is included in Appendix VI. Table 6-3 shows the corrosion depth in a FRP repaired slab is a small fraction of that in the concrete slab alone. For example, the corrosion depth in the reinforcing steel is 0.108 cm (0.0425 in.) in a concrete slab with a water cement ratio of 0.45. The corresponding depth in a FRP repaired slab varied from 9.43 x 10⁻³ cm to 9.36 x 10⁻⁵ cm (3.71 x 10⁻³ in. to 3.68 x 10⁻⁵ in.) depending on whether the FRP repair was classified as fair, good or outstanding.

Table 6-3 Comparative Effect of Corrosion Repair

Materials	FRP Repair		
	Fair	Good	Outstanding
Concrete 0.45 w/c	11	115	1,150
Concrete 0.4 w/c	1	11	106

The information in Table 6-2 is re-calculated as ratios of the corrosion depth in the plain concrete slab vs. that in the corresponding FRP repaired slab. This is summarized in Table 6-3. For example, for a combination of "good repair"

and a water cement ratio of 0.45, the ratio is $1.08E-01/9.37E-4 = 115$. Other values are obtained in a similar manner.

Table 6-3 shows that the benefits of FRP repair are greater when the concrete is more porous and vice versa. Improvement is limited unless the oxygen permeability of the FRP is two orders of magnitude smaller than the concrete.

This simplified analysis is intended to illustrate the use of information relating to the oxygen permeation constant for designing durable FRP repairs. It assumes that the protective passive layer that forms on steel was destroyed for the entire steel area and that there was no cracking. Corrosion is also assumed to take place at a constant rate over the entire year. This is an idealized condition and disregards the effect of factors such as temperature and humidity that significantly modify the corrosion rate. Nonetheless, it provides an approach for selecting suitable FRP/concrete combinations and making the FRP repairs more durable.

Chapter 7 – Contributions and Recommendations

7.1 Introduction

This is the first study to measure the oxygen permeation characteristics of FRP used in infrastructure repair. The results presented in Chapters 2-6 are new and provide many insights on seemingly anomalous findings reported by researchers. The intent of this chapter is not to reproduce the conclusions listed earlier but rather to highlight notable contributions from this study. These are listed in Section 7.2. The techniques developed in this research can be applied to solve other problems. Suggestions on follow-up research are presented in Section 7.3.

7.2 Contributions

1. The most significant contribution is the development of a robust, versatile method to characterize oxygen permeation of a wide variety of materials ranging from 0.5 mm polymer films to FRP-concrete systems. The volume of the chamber can be reduced using appropriate inserts and thereby expedite testing. Development covered techniques for making specimens, theoretical modeling and sensor calibration.

2. Concept of equivalent thickness for multi-layer FRP-concrete repairs. The development of a theoretical model to determine equivalent thickness for multi-layer specimens allows designers to optimize FRP-concrete repairs.
3. The results for epoxy, epoxy-concrete, FRP-concrete and wet and dry concrete (Appendix VII) are new to the published literature.
4. Explanation of anomalous results. Several researchers reported that the performance of multi-layer FRP laminates was poorer than laminates with fewer layers. Scanning electron micrographs demonstrated how wet lay-up processing led to air being trapped at the interface between layers thereby making multi-layer laminates more pervious.
5. Contributions to design. The application of oxygen permeation constants for designing appropriate FRP corrosion repairs is illustrated in the study. The results from FRP-concrete systems show that the critical parameter is the water-cementitious ratio; the larger this ratio, the more effective the FRP repair.

7.3 Recommendations for Future Work

The following are logical extensions of the study.

1. Refining the test method. Environmental effects, leakage, sensor consumption and specimen thickness made experimentation difficult. Improvements can be made to reduce duplication used, e.g. testing a control in every test. Similarly, using coulometric sensors that do not

consume oxygen simplifies data analysis. Consideration should be given to using clamped rather than bolted connections to expedite assembly and disassembly of the diffusion cell.

2. Multi-layer systems. The tests can be extended to determine the oxygen permeation characteristics of multi-layer systems. In the study, only two layer laminates were tested.
3. Reducing oxygen permeability. By studying the oxygen permeation characteristics of different coatings, it will be possible to develop systems that can reduce oxygen permeation. This can lead to more durable repairs. Similarly, it may be possible to assess the role of marine growth on FRP surfaces in tidal zones and determine their role in changing permeation characteristics.
4. Effect of moisture on oxygen permeation. In many applications where FRP is used its surface can have a layer of water over it, e.g. in pile repairs in the splash zone. Since the solubility of oxygen in water is much lower, this will result in lower permeation rates. The experimental procedures developed in this study can be readily extended to measure the change in the permeation constant in the presence of moisture.
5. Effect of exposure on permeability. Since the thermal expansion characteristics of FRP are different from concrete, outdoor exposure is likely to result in deterioration of the matrix. By exposing specimens to outdoor environments and then measuring the oxygen permeation

constant before and after exposure it will be possible to quantify the role of environment on FRP's performance.

6. Pressure/Vacuum bagging. FRP-concrete bond is improved when these techniques are used. The determination of the oxygen permeation constant of specimens that were prepared using these techniques will allow quantification of their benefit and encourage adoption by industry.
7. Application for studying carbon sequestration. The same set up can be used to measure diffusion of carbon-dioxide but using different sensors (Figure 7-1). This can be used to assess carbon dioxide absorptive properties of different materials.

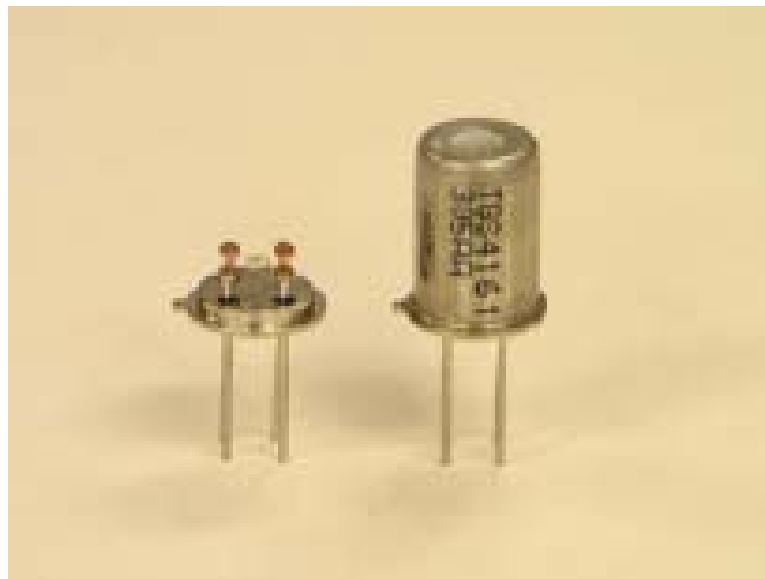


Figure 7-1 Figaro Carbon Dioxide Sensor TGS 4161

References

- Abbas, A., Carcasses, M. and Oliver, J.P. (1999). "Gas permeability of Concrete in relation to its degree of saturation." *Materials and Structures*, Vol. 32. January-February, pp. 3-8.
- Aguilar, J., Winters, D., Sen. R., Mullins, G. and Stokes, M. (2009). "Improvement in FRP-concrete bond by external pressure." *Transportation Research Record, Journal of the Transportation Research Board, No. 2131*. pp. 145-154.
- Air Products and Chemicals, Inc. (2008). Allentown, PA.
- Alampalli, S. (2001). "Reinforced polymers for rehabilitation of bridge columns." *Proceedings 5th National Workshop on Bridge Research in Progress*. 8-10 October, 39-41.
- ASTM D2584 (2008). "*Standard test methods for ignition loss of cured reinforced resins.*" ASTM International, West Conshohocken, PA.
- ASTM D2734 (2009). "*Standard test methods for void content of reinforced plastics.*" ASTM International, West Conshohocken, PA.
- ASTM D3985 (2005). "*Standard test method for oxygen gas transmission rate through plastic film and sheeting using a coulometric sensor.*" ASTM International, West Conshohocken, PA.
- ASTM F710 (2008). "*Standard practice for preparing concrete floors to receive resilient flooring.*" ASTM International. West Conshohocken, PA.
- ASTM F1307 (2002). "*Standard test method for oxygen transmission rate through dry packages using a coulometric sensor.*" ASTM International, West Conshohocken, PA.

- Badawi, M. and Soudki, K. (2005). "Control of corrosion-induced damaged in reinforced concrete beams using carbon fiber-reinforced polymer laminates." *Journal of Composites for Construction*. Vo. 9, No. 2, pp. 195-201.
- Baiyasi, M. and Harichandran, R. (2001). "Corrosion and wrap strains in concrete bridge columns repaired with FRP wraps." Paper No 01-2609, 80th Annual Meeting, *Transportation Research Board*, Washington, DC.
- Banthia, N. and Boyd, A. (2000). "Sprayed fibre-reinforced polymer for repairs." *Canadian Journal of Civil Engineering*. Vol. 27, pp. 907-915.
- BASF The Chemical Company (2007). Shakopee, MN.
- Berver, E., Jirsa, J., Fowler, D., Wheat, H. and Moon, T. (2001). "Effects of wrapping chloride contaminated concrete with fiber reinforced plastics." *FHWA/TX-03/1774-2, University of Texas, Austin*. October.
- Bertolini, L., Elsener, B., Pedferri, P. and Polder, R. (2004). *Corrosion of Steel in Concrete*. Wile-VCH, Weinheim, Germany
- Bird, B.R., Steward, W.E., and Lightfoot E.N. (2002). *Transport Phenomena*. Second Edition, University of Wisconsin-Madison: John Wiley & Sons, Inc.
- Broomfield, J. (1997). *Corrosion of steel in concrete understanding, investigation and repair*. E & FN Spon, New York.
- Buenfeld, N. R. and Okundi, E. (1998). "Effect of cement on transport in concrete." *Magazine of Concrete Research*, Vol. 50, No. 4, December, pp. 339-351.
- Castellote, M., Alonso, C. Andrade, C., Chadbourn, Page, C.L." (2001). "Oxygen and chloride diffusion in cement pastes as a validation of chloride diffusion coefficients obtained by steady-state migration tests." *Cement and Concrete Research*, Vol. 31, pp. 621-625.
- Chowdhury, S. (2010). "Application of Luminescence Sensors in Oxygen Diffusion Measurement and Study of Luminescence Enhancement/Quenching by Metallic Nanoparticles." Ph.D dissertation. University of South Florida, Tampa.
- Christopher L. S. and Albert F. Y. (2000). "A discussion of the molecular mechanisms of moisture transport in epoxy resins." *Journal of Polymer Science: Part B: Polymer Physics*, Vol. 38, No. 5, pp. 792-802.

- Colin, X. Mavel, A., Marais, C. and Verdu, J. (2005). "Interaction between cracking and oxidation in organic matrix composites." *Journal of Composite Materials*, Vol. 39, No. 15, pp. 1371-1389.
- Crank, J (1968). *Diffusion in Polymers*. New York: Academic Press.
- Crank, J. (1975). *The Mathematics of Diffusion*. Second Edition, Brunel University Uxbridge: Oxford University Press.
- Debaiky, A., Green, M., and Hope, B. (2002). "Carbon fiber-reinforced polymer wraps for corrosion control and rehabilitation of reinforced concrete columns." *ACI Materials Journal*. Vol. 99, No.2, pp. 129-137.
- Emmons, P. H. (1993). *Concrete Repair and Maintenance Illustrated*. RSMears, Kingston, MA. 295 pages.
- Florida Department of Transportation, FDOT (2010). "*Standard specifications for road and bridge construction*," Tallahassee, FL
- Figaro (2004). *Technical information for KE-Series*. Glenview, IL.
- Fyfe Co. LLC (2003). San Diego, CA.
- Gjorv, O.E., Vennesland, O., and El-Busaidy, A.H.S. (1986). "Diffusion of dissolved oxygen through concrete." *Materials Performance*, Vol. 25, No. 12, pp. 39-44.
- Hansson, C. M. (1986). "Oxygen diffusion through Portland cement mortars." *Corrosion Science*. Vol. 35. No. 5-8, pp. 1551-1556.
- Hussain, R. R., and Ishida, T. (2010)." Influence of connectivity of concrete pores and associated diffusion of oxygen on corrosion of steel under high humidity." *Construction and Building Materials*, Vol. 24, pp. 1014-1019.
- Kaw, Autar K. (2005). *Mechanics of Composite Materials*. CRC Press LLC. Boca Raton, FL.
- Kessler, R., Powers, R. and Lasa, I. (2006). "Case studies of impressed current cathodic protection systems for marine reinforced concrete structures in Florida." Paper No 06330, *Corrosion NACE* .
- Khan, M.I. (2003). "Permeation of high performance concrete." *Journal of Materials in Civil Engineering*, Vol. 15, No. 1, pp. 84-92.

- Khoe, C., Bhethanabotla, V., and Sen, R. (2009). "A new diffusion cell for characterizing oxygen permeation of fiber reinforced polymers." *Proc., COMPOSITES & POLYCON 2009, American Composites Manufacturers Association*. Tampa, FL, Jan. 15-17.
- Khoe, C., Chowdhury, S., Bhethanabotla, V., and Sen, R. (2010). "Measurement of oxygen permeability of epoxy polymers." *ACI Materials Journal*, Vol. 107, No. 2, Mar.-Apr. pp. 138-146.
- Khoe, C., Sen, R. and Bhethanabotla, V. (2011a). "Oxygen permeability of fiber reinforced polymers." *ASCE, Journal of Composites for Construction*. DOI:10.1061/(ASCE)CC.1943-5614.0000187.
- Khoe, C., Sen, R. and Bhethanabotla, V. (2011b). "Characterization of FRP as an oxygen barrier." *ACI SP-275-18*, ACI, First printing March, Farmington Hills, MI.
- Khoe, C., Sen, R. and Bhethanabotla, V. (2011c). "Oxygen permeability of FRP-concrete repair systems." *ASCE, Journal of Composites for Construction* (submitted). April.
- Kobayashi, K. and Shuttoh, K. (1991). "Oxygen diffusivity of various cementitious materials." *Cement and Concrete Research*, Vol. 21 No. 2-3, pp. 273-284.
- Koros, WJ, Wang, J, and Felder, RM (1981). "Oxygen Permeation through FEP Teflon and Kapton Polimide." *Journal of Applied Polymer Science*, Vol. 26, pp 2805-2809.
- Lawrence, C. D. (1984). "Transport of oxygen through concrete." *British Ceramic Society Proceedings*, No. 35, pp. 277-293.
- Liu, J. and Vipulanandan, C. (2005). "Tensile bonding strength of epoxy coatings to concrete substrate." *Cement and Concrete Research*, Vol. 35, pp. 1412-1419.
- Lu, X. (1997). "Application of the Nernst-Einstein equation to concrete." *Cement and Concrete Research*. Vol. 27, No. 2, pp. 293-302.
- Newman, A. (2001). *Structural Renovation of Buildings*, McGraw-Hill, New York, NY.
- Ngala, V.T., Page, C. L., Parrot, L. J., and Yu, S. W. (1995). "Diffusion in cementitious materials: II. Further investigations of chloride and oxygen diffusion in well-cured OPC and OPC/30 % PFA pastes." *Cement and Concrete Research*, Vol. 25, No. 4, pp. 819-826.

- Omaha, Y., Demura, K., Kobayashi, K., Satoh, Y. and Morikawa, M. (1991). "Pore size distribution and oxygen diffusion resistance of polymer-modified mortars." *Cement and Concrete Research*, Vol. 21, pp.309-315.
- Paul, D.R. (1965). "*The properties of amorphous high polymers.*" Ph.D dissertation. University of Wisconsin-Madison: Madison, Wisconsin.
- Pantazopoulou, S. J., Bonacci, J. F., Sheikh, S., Tomas, M.D.A, and Hearn, N. (2001). "Repair of corrosion-damage columns with FRP wraps." *Journal of Composites for Construction*, Vol. (5), No. 1, pp. 3-11.
- Pochiraju, K. and Tandon, G. (2009). "Interaction of oxidation and damage in high temperature polymeric composites." *Composites A*, Vol. 40, pp. 1931-1940.
- Restrepol, J.I. and DeVino, B. (1996), "Enhancement of the axial load carrying capacity of reinforced concrete columns by means of fiberglass-epoxy jackets." *Proceedings of the First International Conference on Composites in Infrastructure*, Montreal, pp. 547-553.
- Samaan, M., Mirmiran, A., and Shahawy, M. (1998). "Model of concrete confined by fiber composites," *Journal of Structural Engineering, ASCE*, Vol. 124, No. 9, pp. 1025-1031.
- Sen, R. (2003). "Advances in the application of FRP for repairing corrosion damage." *Progress in Structural Engineering and Materials*. Vol. 5, No. 2, pp. 99-113.
- Sen, R, Mullins, G, and Snyder, D. (1999). "Ultimate capacity of corrosion damaged piles." *Final Report submitted to Florida Department of Transportation*, March.
- Shafiq, N. and Cabrera, J. G. (2006). "Calculation of the coefficients of oxygen permeability of mortar samples using PORECOR analysis." *Structural Concrete*. Vol. 7, No. 4, pp. 159-164.
- Sheikh, S., Pantazopoulou, S., Bonacci, J., Thomas, M., and Hearn. N. (1997). "Repair of delaminated circular pier columns with advanced composite materials." *Ontario Joint Transportation Research Report, No 31902. 1*. Ministry of Transport. Ontario, Toronto, Canada.
- Sika Corporation (2003). Product Data Sheet. Lyndhurst, NJ.

- Suh, K., Mullins, G., Sen, R., and Winters, D (2007). "Effectiveness of FRP in reducing corrosion in a marine environment." *ACI Structural Journal*. Vol. 104, No. 1, pp. 76-83.
- Suh, K.S., Sen, R., Mullins, D., and Winter, D. (2008)." Corrosion monitoring of FRP repaired piles in tidal waters." *ACI SP-252*, pp. 137-156.
- Tarricone, P. (1995). "Composite sketch." *ASCE, Civil Engineering Magazine*. May, pp. 52-55.
- Tittarelli, F. (2009). "Oxygen diffusion through hydrophobic cement-based materials." *Cement and Concrete Research*. Vol. 39. pp. 924-928.
- Trefry, M. (2001). "An experimental determination of the effective oxygen diffusion coefficient for a high density polypropylene geomembrane." *Technical Report 37/01, CSIRO*.
- Vasquez-Borucki, S., Carlos, W. J., and Achete, A. (2000). "Amorphous Hydrogenated Carbon Films as Barrier for Gas Permeation through Polymer Films." *Diamond and Related Materials*, Vol. 9, pp. 1971-1978.
- Winters, D., Mullins, G., Sen. R., and Stokes, M. (2008)." Bond enhancement for FRP pile repair in tidal waters." *ASCE, Journal of Composites for Construction*, Vol. 12, No. 334, 10 pages.
- Wang, C., and Shih, C. et al. (2004). "Rehabilitation of cracked and corroded reinforced concrete beams with fiber-reinforced plastic patches." *Journal of Composites for Construction*, Vol.8, No.3, pp. 219-228.
- West System Inc. (2008). Bay City, MI.
- Wheat, H. G., Jirsa, J. O., and Fowler, D. W. (2005). "Monitoring corrosion protection provided by fiber reinforced composites." *International Journal of Materials and Product Technology*, Vol. 23, No. 3-4, pp. 372-388.
- Williamson, S. J., and Clark, L. A. (2001)."The influence of the permeability of concrete cover on reinforcement corrosion." *Magazine of Concrete Research*. Vol. 53, No. 3, June, pp. 183-195.
- Wootton, I., Spainhour, L., and Yazdani, N. (2003). "Corrosion of steel reinforcement in CFRP wrapped concrete cylinders." *Journal of Composites for Construction*. Vol. 7, No.4, pp. 339-347.

Appendices

Appendix I Computer Software MATLAB Program

The following is a step by step description of the input to the Matlab program that was used to extract the permeation constant.

1. Clear memory and close previous data:

```
clear;
```

```
clc;
```

```
pack;
```

2. Input data on the diffusion cell for Area, Volume, and thickness (the thickness will be changed depend on the thickness of each specimen):

```
A=1/4*pi*(3.25*2.54/100)^2; % area in of cell m2
```

```
V=A*(1/8*2.54/100)+.25*pi*(.85/100)^2*(1.1/100); % volume of cell  
(approx. 1.7741E-5 m3)
```

```
h=xx; % xx thickness of specimen in m
```

3. Calibrate the data for each sensor:

```
calib8=1/(59.79251-0.28971);
```

```
calib2=1/(66.07233-0.24786);
```

```
calib6=1/(64.26306-0.239006);
```

4. Input pressure and temperature:

```
poutpercent=1.00;% percentage of oxygen outside
```

```
P = 1; % total pressure outside in atm
```

```
po=P*poutpercent;
```

```
pi=10.68432674*calib2; % inside pressure in atm
```

Appendix I (Continued)

R=8.314e-5; % universal gas constant

T=298; % temperature in kelvin

ci0=pi/(R*T); % inside initial concentration

5. Input the number of trial data (t); all corrected data is placed into excel.xls spreadsheet:

t=1000;

datad=xlsread('Excel.xls');

index=datad(1:t,1);

timeex=datad(1:t,2); % time of experiment

t1dat=datad(1:t,3); % test data

for i=1:t

pex(i)=t1dat(i)*calib2; % partial pressure of O₂ from experiment

end

c01=pex(1)/(R*T);

6. Set trial value of the permeability constant range (perme1 and perme2); define number of iteration (permesteps); check the time interval set up (tdif):

perme1=1e-12; % permeability in unit mol m²/m³ atm sec;

perme2=1e-9; % permeability in unit mol m²/m³ atm sec;

permsteps=100;

permn=(perme2-perme1)/permsteps;

Appendix I (Continued)

```
perme=[perme1:permn:perme2];
tdif=60; % time interval in second
% timesteps
for i=1:permsteps
c1(i,1)=c01;
    pm(i,1)=pex(1);
    for j=2:t
c1(i,j)=c1(i,j-1)+(perme(i)*(po-pi)/h)*tdif*A/V; % inside
concentration
    pi=c1(i,j)*(R*T);
    pm(i,j)=pi;
end
end
for i = 1:permsteps
    sumsqerror(i) = 0;
    for j = 1:t
        sumsqerror(i) = sumsqerror(i) + ((pm(i,j) - pex(j))/pex(j))^2;
        ind(i)=i;
    end
end
end
```

7. Check error and fitted data; plot the figure:

Appendix I (Continued)

```
[errmin,x] = min(sumsqerror);  
sum_square_of_error=errmin  
Fitted_experimental_permeability=perme(x)  
permex=perme(x);  
for i=1:t  
    pfit(i)=pm(x,i);  
end  
figure  
plot(timeex,pfit,'r',timeex,pex,'b');  
legend('Fitted data from model','Experimental data',2)  
xlabel('\fontsize {14}  
(sec)')  
ylabel('\fontsize {14}Inside partial pressure (atm)')
```

8. Run the program. If the fitted data and range do not match, change the permeation value range in step 7 and rerun the program again.

Appendix II Volume Fiber Fraction Calculation

Step by step calculation of fiber volume fraction (V_f) and matrix volume fraction (V_m) (Kaw 2005):

1. Data given by manufacturers:

Density of fiber, ρ_f

Density of matrix (epoxy), ρ_m

2. Measure weight of fiber, w_f and weight of composite, w_c .
3. Calculate weight of matrix (resin), $w_m = w_c - w_f$
4. Calculate fiber mass fraction, W_f and matrix (resin) mass fraction, W_m

$$W_f = \frac{w_f}{w_c} \quad (\text{I-1})$$

$$W_m = \frac{w_m}{w_c} \quad (\text{I-2})$$

5. Calculate density of composite, ρ_c

$$\frac{1}{\rho_c} = \frac{W_f}{\rho_f} + \frac{W_m}{\rho_m} \quad (\text{I-3})$$

6. Calculate fiber volume fraction, V_f , and matrix (resin) volume fraction, V_m

$$V_f = \frac{W_f \times \rho_c}{\rho_f} \quad (\text{I-4})$$

$$V_m = \frac{W_m \times \rho_c}{\rho_m} \quad (\text{I-5})$$

7. Check the result:

$$V_f + V_m = 1 \quad (\text{I-6})$$

Appendix II (Continued)

Example:

Step 1:

Density of CFRP (Sikawrap Hex 103C), $\rho_f = .065 \text{ lbs/in}^3$ (0.00179919 gr/mm³).

Density of matrix (epoxy) for Sikadur 300, $\rho_m = .092 \text{ lbs/in}^3$ (0.001098 gr/mm³).

Step 2:

Weight of fabric (w_f) = 8.6466 gr.

Weight of composite, $w_c = 22.8932$ gr.

Step 3:

$w_m = 22.8932 - 8.6466 \text{ gr} = 14.2466$ gr.

Step 4:

$$W_f = \frac{8.6466}{22.8932} = 0.377693 \text{ gr.}$$

$$W_m = \frac{14.2466}{22.8932} = 0.622307 \text{ gr.}$$

Step 5:

$$\frac{1}{\rho_c} = \frac{0.377693}{0.0017919} + \frac{0.622307}{0.001098} = 776.89, \rho_c = 0.001287 \text{ gr/mm}^3$$

Step 6:

$$V_f = \frac{0.377693 \times 0.001287}{0.00179919} = 0.2702 \text{ or } 27.02 \%$$

Appendix II (Continued)

$$V_m = \frac{0.622307 \times 0.001287}{0.001098} = 0.7298 \text{ or } 72.98\%$$

Step 7:

$$V_f + V_m = 0.2702 + 0.7298 = 1 \text{ (OK!)}$$

Using the above procedure, the average volume fiber fraction (V_f) (obtained from three samples) for the four FRP system A to D is summarized in Table II-1. These FRP specimens were used to develop the permeation constants in Chapters 4-6.

Table II-1 Volume Fiber Fraction Average for System A to D

Type	Systems			
	A	B	C	D
CFRP unidirectional one layer	35.77%	38.12%	37.68%	38.55%
CFRP unidirectional two layers	24.06%	39.79%	40.13%	22.32%
GFRP unidirectional one layer	24.95%	24.48%	33.26%	27.45%
GFRP unidirectional two layers	31.65%	32.79%	32.13%	29.57%
CFRP bidirectional one layers	32.79%	26.79%	28.12%	32.79%
GFRP bidirectional one layers	33.46%	32.46%	23.46%	33.16%
CFRP random	30.39%	35.11%	33.49%	22.41%
GFRP random	26.47%	34.57%	32.46%	31.17%

Appendix III Scanning Electron Micrograph (SEM) for CFRP Specimens

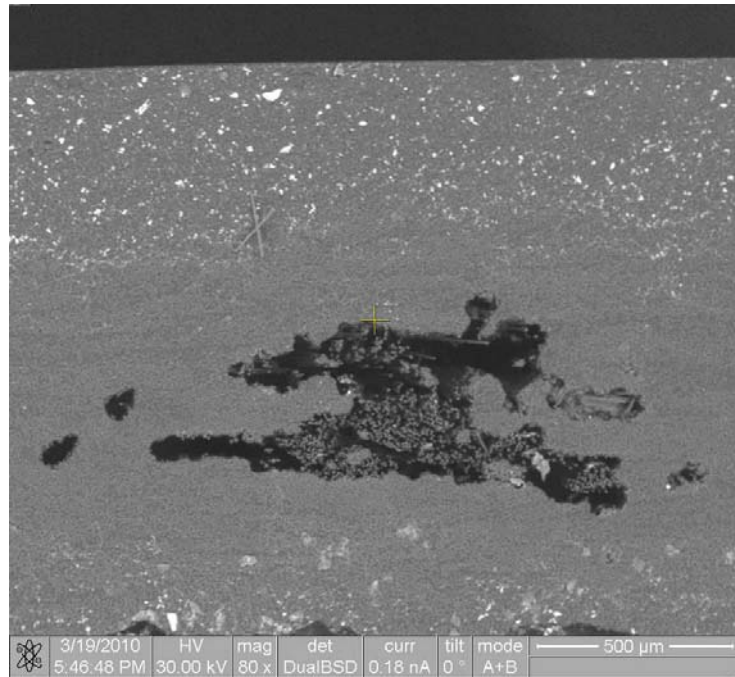


Figure III-1 SEM One Layer CFRP Unidirectional Specimen

Appendix III (Continued)

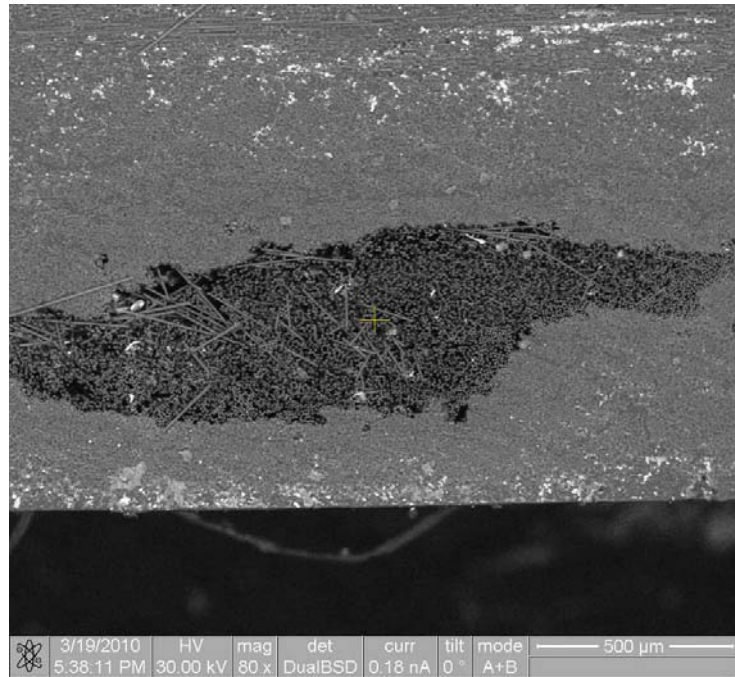


Figure III-2 SEM Two Layers CFRP Unidirectional Specimen

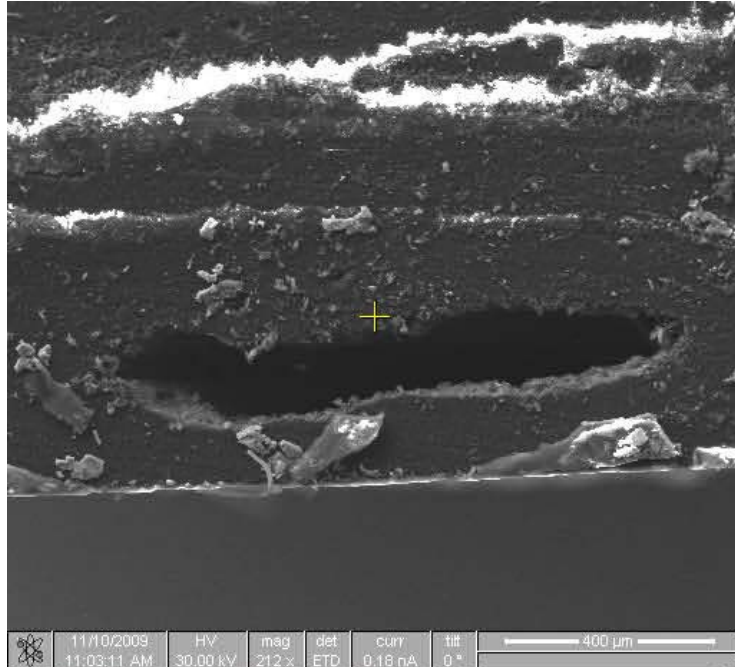


Figure III-3 SEM Random Layer CFRP Specimen

Appendix IV Scanning Electron Micrograph (SEM) for GFRP Specimens

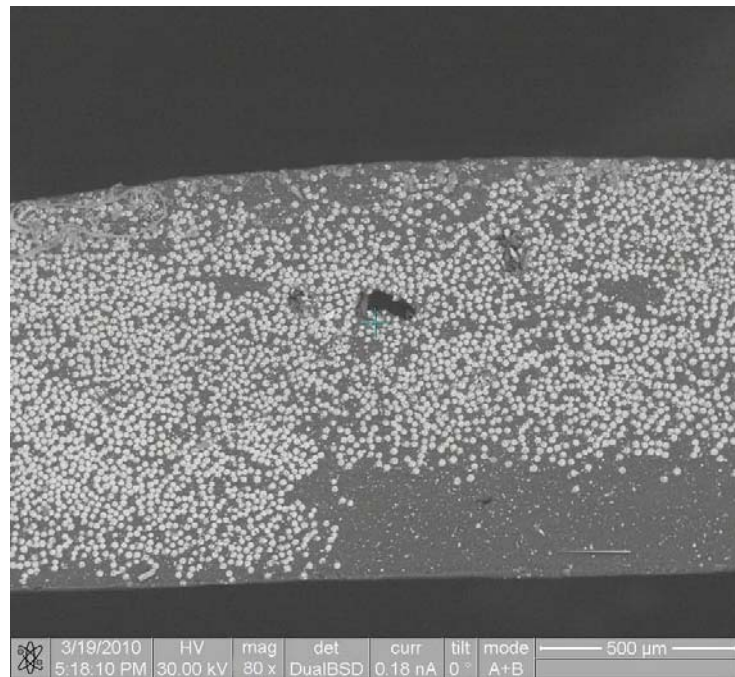


Figure IV-1 SEM One Layer GFRP Unidirectional Specimen

Appendix IV (Continued)

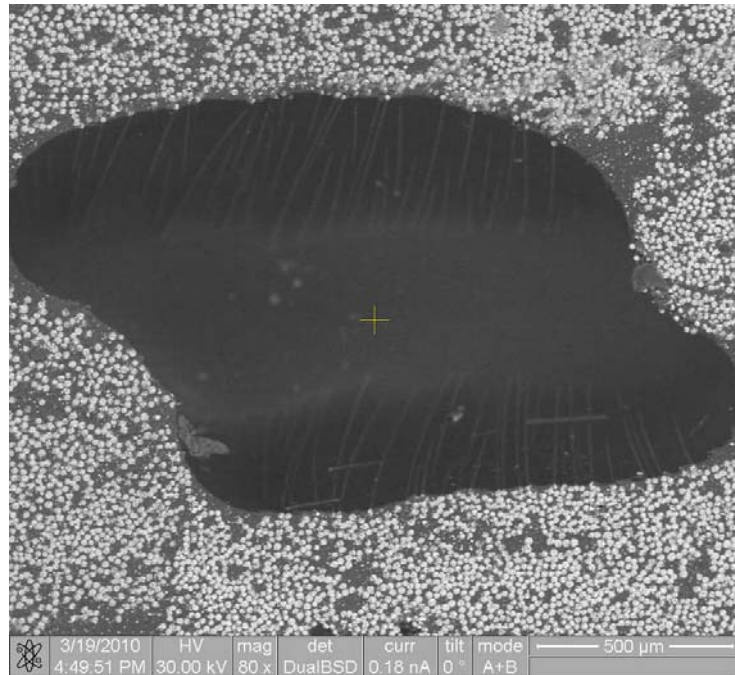


Figure IV-2 SEM Two Layers GFRP Unidirectional Specimen

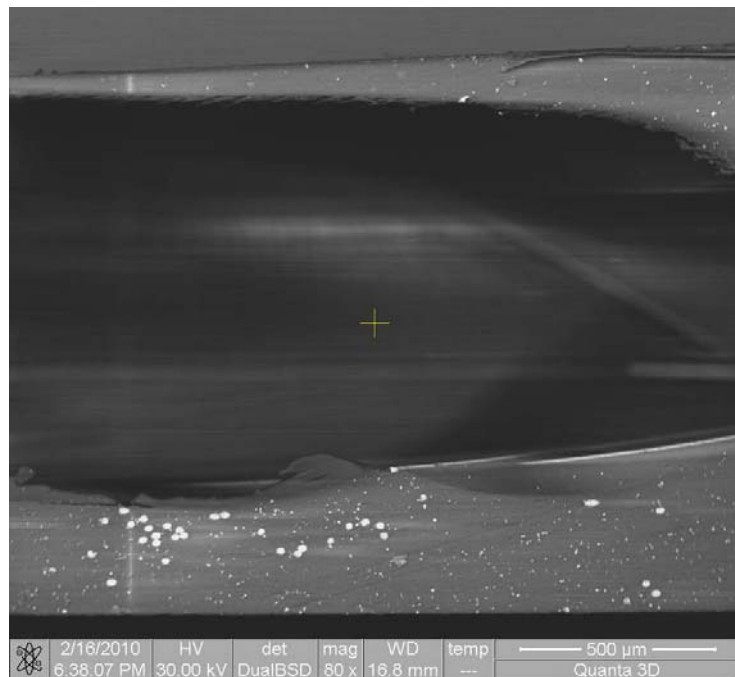


Figure IV-3 SEM Random Layer GFRP Unidirectional Specimen

Appendix V Scanning Electron Micrograph (SEM) for Concrete Specimens

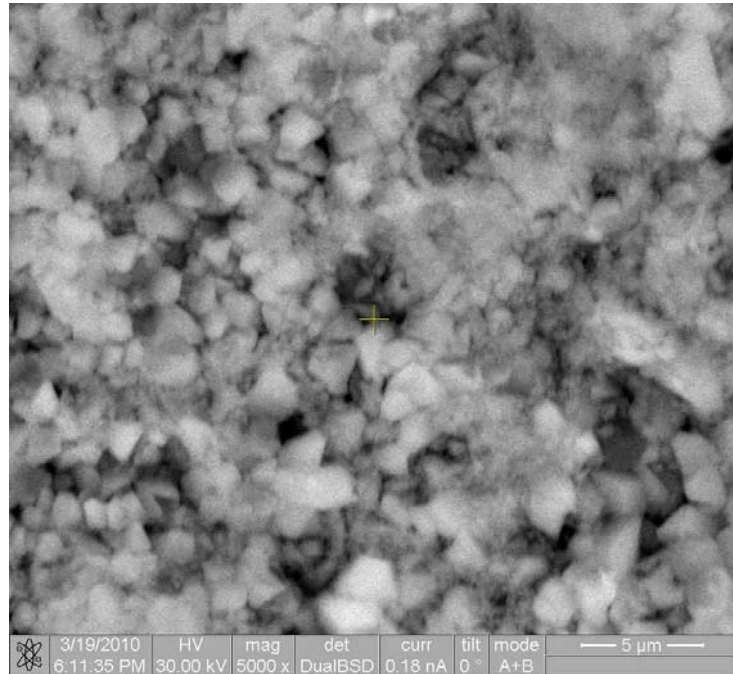


Figure V-1 SEM for Concrete with w/c Ratio 0.40

Appendix V (Continued)

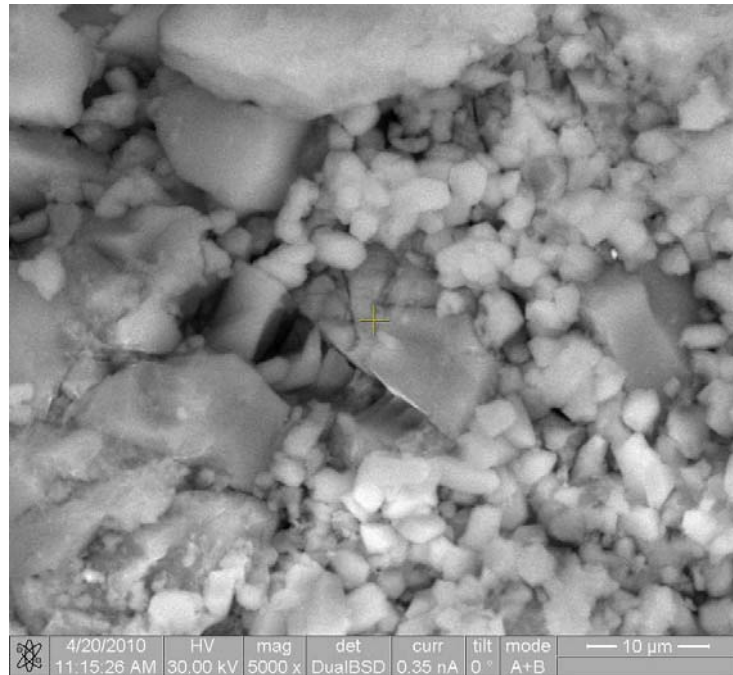


Figure V-2 SEM for Concrete with w/c Ratio 0.45

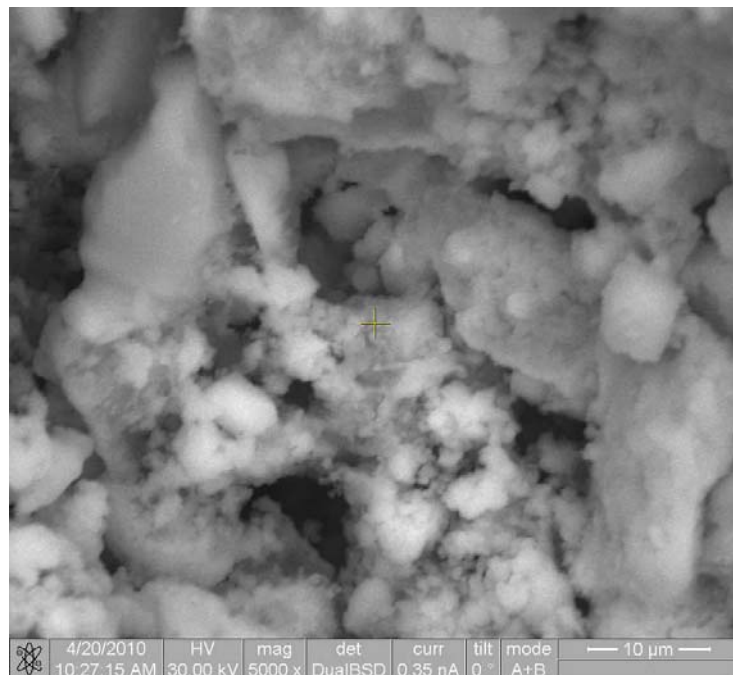


Figure V-3 SEM for Concrete with w/c Ratio 0.50

Appendix VI Sample Calculation

A concrete slab is reinforced by #13 (#4) bars spaced at 30 cm (12 in.) on centers in two orthogonal directions. The average concrete cover is 19 mm (3/4 in.). The oxygen permeation constant for concrete is 1×10^{-8} mol. $m^2/m^3 \cdot atm \cdot sec.$ (3.28×10^{-8} mol. $ft^2/ft^3 \cdot atm \cdot sec.$). After it is repaired using 2 mm (78.7 mil) thick FRP, the oxygen permeation constant for the system reduces to 1×10^{-11} mol. $m^2/m^3 \cdot atm \cdot sec.$ (3.28×10^{-11} mol. $ft^2/ft^3 \cdot atm \cdot sec.$). Compare the relative annual corrosion rates for the concrete and the FRP repair after it has stabilized.

VI.1 Solution

The permeability constant (P) is used to calculate the number of moles of oxygen (M) that reaches the steel surface to sustain the anodic reaction responsible for corrosion of steel. Each mole of oxygen consumes two moles of iron; the mass loss in steel is calculated from its atomic weight (55.85 g/mole or 0.123 lb/mole) and the volume loss from its density (7.85 g/cc or 490 lb/ ft^3). The time (t) is one year or 3.15×10^7 seconds. The radius of a #13 (#4) bar is 0.635 cm (0.25 in.).

Appendix VI (Continued)

VI.1.1 Concrete

$$M = P \times t / \text{cover thickness} = 1 \times 10^{-8} \times 1 \times 3.15 \times 10^7 / 0.019 = 16.6 \text{ moles.}$$

This reacts with two moles of iron or $2 \times 16.6 = 33.2$ moles. This is equivalent to a metal loss of $33.2 \times 55.85 = 1,854 \text{ g/m}^2$ ($3.8 \times 10^{-4} \text{ lb/ft}^2$) over one year spread over $2 \times 39.37/12 = 6.56$ bars. The loss per bar is therefore 283 g or 39 cc over a length of 1 m (3.28 ft). For uniform corrosion, this corresponds to a section loss of 0.39 cm^2 (0.06 in.^2). The initial radius r_o of a #13 (#4) bar is 0.635 cm (0.25 in) and its final radius r_f can be calculated from the change in its cross-section,

$$\pi r_o^2 - \pi r_f^2 = 0.393 \text{ or } r_f = 0.527 \text{ cm or } 0.108 \text{ cm/yr (269 mils/yr).}$$

VI.1.2 FRP Repair

$M = P \times t / \text{effective thickness} = 1 \times 10^{-11} \times 1 \times 3.15 \times 10^7 / 0.002 = 0.1577$ moles. Note that the effective thickness is used because the permeability constant used is experimentally determined for the system with a 2 mm (78.7 mil) thick FRP layer. As before, the oxygen reacts with two moles of iron or 0.3154 moles, equivalent to a metal loss of 17.6 g/m^2 ($3.61 \times 10^{-3} \text{ lb/ft}^2$) over one year spread over 6.56 bars or 2.68 g/bar (0.006 lb/bar) or 0.373 cc (0.023 in^3) over a length of 1 m (3.28 ft). This corresponds to a section loss of 0.00373 cm^2 (0.00058 in^2). If corrosion is assumed to be uniform, the final radius r_f can be calculated from the change in its cross-section,

Appendix VI (Continued)

$\pi r_o^2 - \pi r_f^2 = 0.00373$ or $r_f = 0.634$ cm (249.6 mils). Thus, the corrosion depth is 0.001 cm/yr (2.34 mils per year) [$0.635 - 0.634 = 0.001$].

VI.2 Comment

The calculations correspond to the stabilized state after the oxygen originally present in the concrete was consumed. Since the oxygen permeability of FRP is not zero, corrosion continues inside the repair as reported by independent researchers. In the example, the corrosion rate of concrete is 115 times ($269/2.34$) higher than that of the FRP wrapped steel.

Appendix VII Dry vs. Wet Concrete

A limited study was conducted to determine the difference in oxygen permeability for wet and dry concrete. In the testing 1 in. thick specimens were first vacuum dried for 2 hours and subsequently submerged for 24 hours in potable water. Following this immersion, the surface was wiped dry and the specimen weighed. It was then placed in the diffusion cell and its permeability determined.

The mix design is summarized in Table VII-1 and is the same as that in Chapter 5. Specimen details are summarized in Table VII-2. It may be seen that despite the same exposure, the percent of water absorbed varied between 1.9 to 3.4%. This could be because of the location of the concrete disc within the cylinder. Specimens near the top of the cylinder most probably had a higher water cement ratio and were more porous. Permeation constants determined are listed in Table VII-3 and the correlation between the fitted and experimental data shown in Figures VII-1 and VII-2.

Table VII-1 Properties of Concrete

Description	Data
Concrete Type	II
w/c ratio	0.45
Unit Weight (kg/m ³)	2,268.30
PC Volume (%)	10.26%
Aggregate Volume (%)	54.70%
Cementitious Content (kg/m ³)	406
Strength 28 Days (MPa)	49.2

Appendix VII (Continued)

Table VII-2 Concrete Data Measurement

Tests	Type	w/c Ratio	Weight Dry (gr)	Weight Wet (gr)	Weight of Water (gr)	% of Water	Thickness (mm)
Test 1	II	0.45	367.18	374.24	7.06	1.9%	20.52
Test 2	II	0.45	359.46	371.79	12.33	3.4%	20.30
Test 3	II	0.45	372.42	383.62	11.20	3.0%	20.61
Test 4	II	0.45	380.67	387.88	7.21	1.9%	20.96

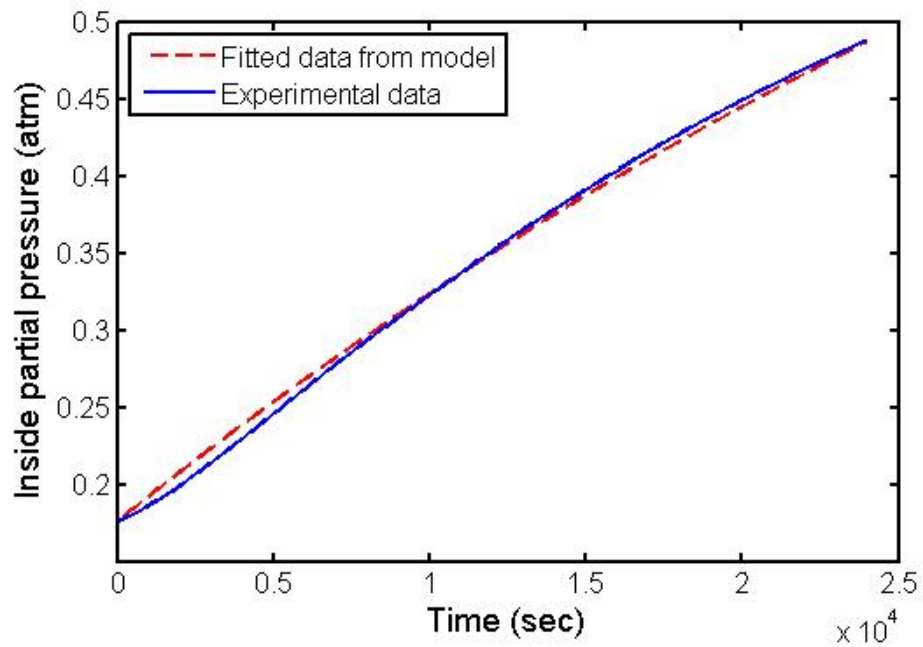


Figure VII-1 Fitted Data vs. Experimental Data for Dry Concrete Specimen

(Note: 1 atm = 0.101 MPa)

Appendix VII (Continued)

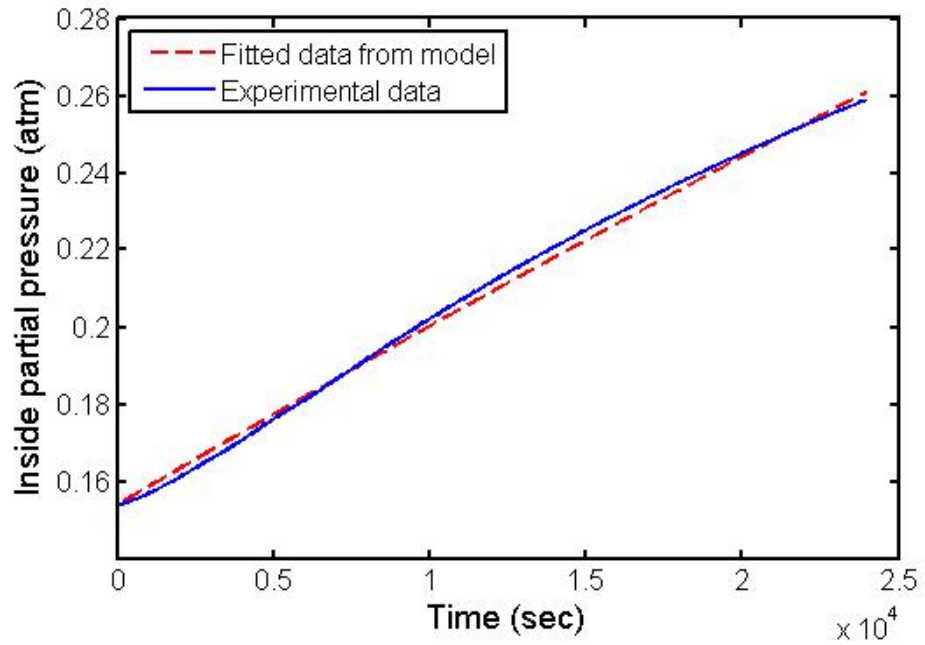


Figure VII-2 Fitted Data vs. Experimental Data for Wet Concrete Specimen

(Note: 1 atm = 0.101 MPa)

Table VII-3 Oxygen Permeation Constant for Dry and Wet Concrete (units in

mol.m²/m³.atm.sec)

Test Number	Dry Concrete		Wet Concrete	
	Result	Average	Result	Average
Concrete Test 1	4.85E-08	4.15E-08	2.51E-10	4.41E-10
Concrete Test 2	5.41E-08		6.80E-10	
Concrete Test 3	1.54E-08	1.76E-08	2.68E-10	2.15E-10
Concrete Test 4	4.80E-08		5.66E-10	

About the Author

Chandra Khoe was born in Jakarta, Indonesia. In 1995, he earned a B.S. Degree in Civil and Environmental Engineering from the Catholic Parahyangan University, College of Technique. In 1998, he moved to the United States of America. In 2004, he earned a M.C.E. Degree in Civil and Environmental Engineering from the University of South Florida, College of Engineering. He was a Teaching Assistant and Graduate Research Assistant from 2004-2010. He has more than 18 years of experience as a civil/ structural engineer and for the last 2 years he is the Principal of the CKPE, LLC (a/k/a ARD Group). He has been responsible for the analysis and design pertaining to various projects ranging from large-scale to single family additions throughout the United States. He has extensive experience in engineering research, management, estimating, scheduling, time related claim preparation, analysis, and Business Information Modeling (BIM) design. He is a licensed Professional Engineer in civil engineering, a licensed Certified General Contractor in the State of Florida. Chandra can be reached at chandrakhoe@verizon.net.